NASA Contractor Report 185159

Microgravity Acoustic Mixing for Particle Cloud Combustors

Frederic Pla and Robert Rubinstein
Sverdrup Technology, Inc.
NASA Lewis Research Center Group
Cleveland, Ohio

March 1990

Prepared for
Lewis Research Center
Under Contract NAS3-25266

National Aeronautics and
Space Administration

TABLE OF CONTENTS

Page

Page

Page

Summary

This report describes experimental and theoretical investigations of acoustic mixing procedures designed to uniformly distribute particles in a combustion tube for application in the Particle Cloud Combustion Experiment (PCCE). Two acoustic mixing methods are investigated: mixing in a cylindrical tube using high frequency spinning modes generated by suitably phased, or "quadrature" speakers, and acoustic premixing in a sphere.

Quadrature mixing leads to rapid circumferential circulation of the powder around the tube. Good mixing is observed in the circulating regions. However, because axial inhomogeneities are necessarily present in the acoustic field, this circulation does not extend throughout the tube.

Simultaneous operation of the quadrature-speaker set and the axial-speaker was observed to produce considerably enhanced mixing compared to operation of the quadrature-speaker set alone. Mixing experiments using both types of speakers were free of the longitudinal powder drift observed using axial-speakers alone.

Vigorous powder mixing was obtained in the sphere for many normal modes; however, in no case was the powder observed to fill the sphere entirely. Theoretical analysis indicates that mixing under steady conditions cannot fill more than a hemisphere except under very unusual conditions. Premixing in a hemisphere may be satisfactory; otherwise, complete mixing in microgravity might be possible by operating the speaker in short bursts.

A general conclusion is that acoustic transients are more likely to produce good mixing than steady state conditions. The reason is that in steady conditions, flow structures like nodal planes are possible and often even unavoidable. These tend to separate the mixing region into cells across which powder cannot be transferred. In contrast, transient not only are free of such structures, they also have the characteristics, desirable for mixing, of randomness and disorder. This conclusion is corroborated by mixing experiments using axial waves.

1. Introduction

Mixing methods using steady state acoustic straming are investigated as means to achieve a uniformly dispersed particle cloud for application in the particle cloud combusion experiment. A comprehensive review of the theory of acoustic straming is given. Two specific configurations are analyzed in detail theoretically and experimentally: a "quadrature" speaker arrangement in a combustion tube designed to excite acoustic spinning modes, and premixing in a sphere. Theoretically, the spinning modes should cause a secondary streaming flow along circular streamlines throughout each tube cross-section.

Experimentally however, inhomogeneity of the acoustic field prevents establishment of this secondary flow throughout the tube. In premixing experiments, the sphere could not be filled with a uniform particle cloud. This result is confirmed by theoretical analysis which shows that secondary flow in a sphere necessarily contains a nodal plane across which particles cannot be transferred. It is concluded that acoustic transients are more likely to be successful mixing mechanisms than steady state fields.

2. Particle Motion in an Aerosol Due to an Acoustic Field

2.1. Introduction

Along the years, much work has been done on the subject of particle motion due to an acoustic field ([1] to [41]), starting with the experimental study of dust striations and figures in resonant tubes by Kundt [1] in 1866. In 1891 Koenig [3] first proposed an explanation for dust striations, which were also reported by Rayleigh [4]. However, rather than confirm Koenig's theory, further published works on the subject, such as those by Robinson [5], Thomas [6], Cook ([7] and [8]), or Irons [9], began and later fueled a controversy, with participants either supporting or refuting Koenig's theory. Only the careful experimental study of Andrade in 1931 ([10] to [13]) unveiled the complexity of most of the physical mechanisms involved, leading to an acceptable theoretical explanation of the dust striation phenomenon.

This section describes the major physical mechanisms at work when lycopodium particles are immersed in an acoustic field. The emphasis is on understanding the importance of each mechanism relative to the others as a function of such parameters as the frequency and amplitude of the acoustic vibration. How these mechanisms affect acoustic mixing is also discussed using comparisons with results obtained in PCCE experiments.

2.2. Entrainment Rate

The entrainment rate, which is a measure of the entrainment of a particle by a sound wave, is an important parameter in acoustic mixing since it can be used

to determine what the dominant mixing mechanisms are for given conditions. The entrainment rate is given by St. Clair [14] as:

$$\frac{X_p}{X_g} = \frac{1}{\sqrt{1 + (\pi \rho f d^2 / 9\mu)^2}} \tag{1}$$

$$\Phi = \tan^{-1}\left(\frac{\pi \rho f d^2}{9\mu}\right) \tag{2}$$

where X_p is the amplitude of the particle displacement, X_g is the acoustic amplitude of the gas displacement, ρ is the density of the particles, f is the frequency, d is the particle diameter, and μ is the coefficient of dynamic viscosity. Φ is the phase of the particle motion relative to the gas motion.

Equation 1 expresses the relative influence of inertia and viscous effects on mixing. At very low frequencies ($\frac{X_p}{X_g} \rightarrow 1$), the viscous term dominates and the particle is fully entrained by the gas, participating in its motion completely. At very high frequencies ($\frac{X_p}{X_g} \rightarrow 0$), the inertial effects are dominant, and the particle remains virtually stationary. At intermediate frequencies, the particle is entrained up to a certain point by the acoustic vibration of the gas.

The rate of entrainment drops rapidly with frequency as shown in Figure 1, which plots $\frac{X_p}{X_g}$ and Φ for lycopodium particles (ρ: 1020kg/m^3 and d: 22μm with a standard deviation of 1.82 μm). At frequencies for which low-frequency mixing is performed (100 Hz to 500 Hz) using low-frequency axial-speakers, the entrainment rate is fairly high (over 20%). For high-frequency mixing using quadrature-speakers, the entrainment rate is very low (2.5% at 4000 Hz).

A more detailed analysis of the forces acting on particles in a sound field is a complex task beyond the scope of this study, which is limited to

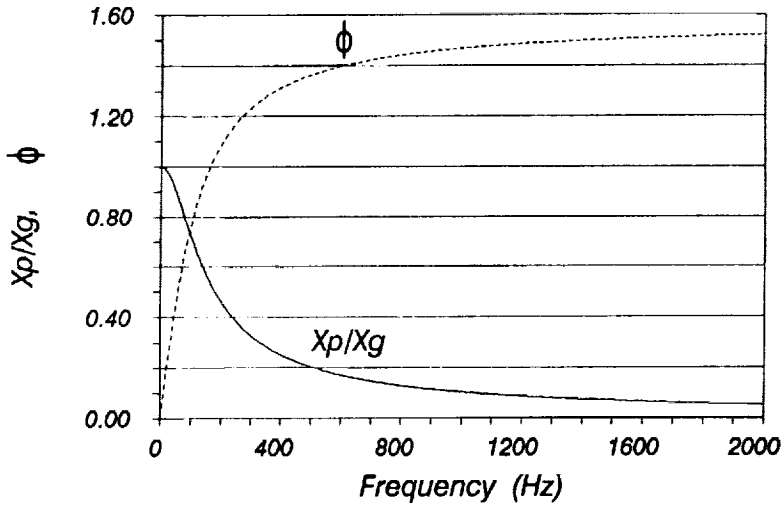

Figure 1. Entrainment Rate for Lycopodium Particles.

mechanisms relevant to acoustic mixing. Such an analysis was carried in part by Mednikov [15].

2.3. Mixing Mechanisms in an Acoustic Field

The most important mechanisms which can produce steady motion resulting in mixing in a strong acoustic field are acoustic streaming and acoustic radiation pressure. Streaming can be considered loosely as the result of the absorption of sound, while radiation pressure is a result of the scattering of sound waves by each particle. Descriptions of these mechanisms follow.

2.4. Streaming

At high sound intensity levels, stationary flows develop in fluids from acoustic streaming. These flows, also sometimes referred to as acoustic wind or quartz

wind, are particularly strong in the proximity of obstacles in the sound field. They were first observed by Faraday in 1831 [16].

Large, Medium, and Small Scale Streaming

Streaming is of several forms, as shown by Rozenberg [17]. The first type is large scale streaming (Eckart streaming), which is streaming in the bulk of the fluid as a result of viscous and thermal conduction losses.

The second kind is streaming outside a boundary-layer, which is referred to here as Rayleigh streaming. It is due to the interaction between an obstacle and an acoustic wave. Rayleigh streaming has a scale equal to the sound wavelength and is referred to in this report as "medium scale" streaming. Like Eckart streaming, Rayleigh streaming acts as a particle transport mechanism which can be used as a mixing process.

The third kind of streaming is small scale streaming, such as streaming inside a boundary-layer (Schlichting streaming), where a rotational flow develops inside the boundary-layer. As opposed to large scale and medium scale streaming, small scale streaming does not act as a transport mechanism but is responsible for interaction forces between particles which result in regular particle striation patterns.

These three types of streaming are reviewed in the next few sections, where their influence on particle motion and their effect on acoustic mixing are discussed.

Slow and Fast Streaming Solutions

Most published theoretical studies solve the streaming problem using successive approximations of the governing hydrodynamic equations. The solution for the streaming velocity obtained using this solution is limited by the following condition [17]:

$$\mathrm{Re} \ll \frac{\lambda L'}{L''^2} \tag{3}$$

where λ is the sound wavelength, L' is the scale of the sound field, L'' is the stationary streaming scale, and Re is the acoustic Reynolds number defined as:

$$\mathrm{Re} = \frac{v_0}{1.98k\nu} \tag{4}$$

where v_0 is the velocity amplitude of the sound wave, k is the wave number defined as $k = \frac{2\pi}{\lambda}$, and ν is the kinematic coefficient of viscosity.

As shown in the next section, the streaming velocity obtained using the method of successive approximations is much smaller than the acoustic velocity v_0 and corresponds to what has been referred to as the "slow streaming" solution. From Equation 3, it is clear that this solution is not valid above a certain acoustic level $v_{\max}$. Experiments have shown that at high acoustic levels, streaming velocities are greatly under predicted by the method of successive approximations. However, very little work has been published to date on this phenomenon, sometimes referred to as "fast streaming".

It is useful at this point to look at the physical meaning of the acoustic Reynolds number Re, and consider how it relates to "slow" and "fast streaming".

Re can be regarded as a measure of the strength of finite-amplitude effects versus the strength of viscous dissipation effects.

From Goldberg [18], we know that attenuation due to viscous dissipation is the dominant mechanism if $\mathrm{Re} \ll 1$. In this case, Equation 3 is usually satisfied and experimental data on streaming is in good agreement with the theoretical results.

For $\mathrm{Re} \gg 1$, the condition in Equation 3 is usually not satisfied and the theoretical streaming velocities greatly underpredict the measured data. This corresponds to the case where finite-amplitude effects, resulting in wave distortion and eventually in shock formation, dominate viscous dissipation effects. As mentioned previously, "slow streaming" is a direct result of viscous and thermal dissipation. For $\mathrm{Re} \gg 1$, the effective wave attenuation due to finite-amplitude effects is very high and replaces viscous and thermal dissipation as the major attenuation term. As discussed in greater detail in the next section, it appears that this increase in attenuation is actually responsible for the increase in streaming. Therefore, "fast streaming" is a direct result of dissipative losses, where losses due to finite-amplitude effects have replaced losses due to viscous and thermal dissipation.

2.4.1. Large Scale Streaming (Eckart Streaming)

Eckart [19] was the first to solve the problem of streaming induced by a well-collimated sound beam in a cylindrical tube. This type of streaming is caused by bulk absorption throughout the acoustic field and produces vortices having a scale determined by the volume occupied by the sound beam. Thus, it is a large scale phenomenon (larger than the wavelength).

In a practical case, Eckart streaming in a two-inch diameter PCCE combustor can only be obtained using extremely high frequencies, due to the narrowness of the sound beam required.

2.4.1.1. Slow Streaming

In the case of a cylindrical sound beam of radius r_1 travelling in an anechoically terminated tube of radius R, the streaming velocity profile is shown in Figure 2. In the direction of the tube axis z, the streaming velocity is given as a function of the tube radius r by:

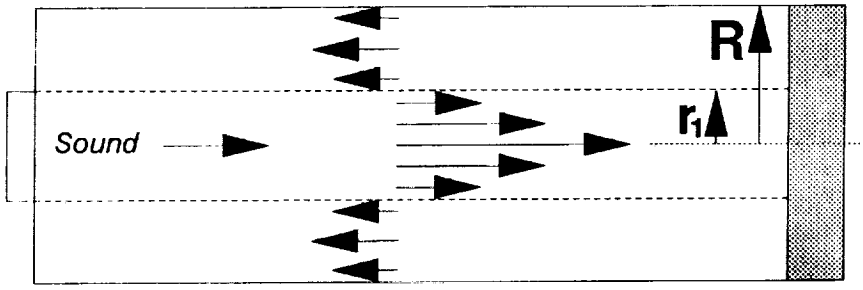

Figure 2. Eckart Streaming in a Tube.

$$u_E = U_E \left[\frac{1}{2} \left(1 - \frac{r^2}{r_1^2} \right) - \left(1 - \frac{1}{2} \frac{r_1^2}{R^2} \right) \left(1 - \frac{r^2}{R^2} \right) - \ln \left(\frac{r_1}{R} \right) \right], \quad 0 \le r \le r_1 \quad (5)$$

and

$$u_E = -U_E \left[\left(1 - \frac{1}{2} \frac{r_1^2}{R^2} \right) \left(1 - \frac{r^2}{R^2} \right) + \ln \left(\frac{r}{R} \right) \right], \qquad r_1 \le r \le R \quad (6)$$

where the main streaming velocity U_E in air is given by:

$$U_E = \frac{1.98}{4 c_0} v_0^2 (k r_1)^2 \quad (7)$$

and c_0 is the speed of sound. The ratio of the main streaming velocity to the acoustic velocity v_0 is of the order of $M_a (k r_1)^2$, where M_a is the acoustic Mach number defined as $M_a = \frac{u_0}{c_0}$.

However, from Equation 3, the "slow streaming" solution given in Equation 7 is only valid outside the practical range for acoustic mixing in a PCCE combustor, and the magnitude of the streaming velocity given by Equation 7 is usually too small to produce effective mixing.

2.4.1.2. **Fast Streaming**

The result discussed in the section above means that "fast streaming" has to be the dominant mixing mechanism if Eckart-type streaming is used in a PCCE combustor. However, little work has been done to date on this problem. Ivanovskii [20] and Statnikov [21] proposed a method valid for $M_a \ll 1$ in which they rewrite the equations of motion in a simplified form; they assume that the acoustic variables can be expressed as the sum of a time invariant term and a time variant term. Statnikov solved these equations of motion for the simplified case of a stable saw-tooth wave. Although Statnikov's solution is for a particular case, his main results are repeated here since they illustrate the differences in magnitude between "fast" and "slow streaming" velocities.

At sufficiently high sound pressure levels and at a certain distance from the source, an acoustic wave assumes a stable, saw-tooth shape if viscous losses are moderate compared to finite-amplitude effects ($\mathrm{Re} \gg 1$) (see Ref. [22] and [23]). In this limited region, most of the wave attenuation is due to the presence of the shock which arises from the finite amplitude effects, rather than from viscous and thermal conduction losses. Using this stable, saw-tooth form for the acoustic velocity in the simplified equations of motion, Statnikov showed that the "fast streaming" velocity is given by Equations 5 and 6, where U_{E} is replaced by U_{Ef}, which is given by:

$$U_{Ef} = \frac{\alpha_f}{\alpha_s} U_E \tag{8}$$

where α_s is the attenuation due to viscous and thermal conduction losses ("slow streaming"), and α_f is the attenuation due to finite amplitude effects ("fast streaming"). In air, α_f is given by:

$$\alpha_f = 1.2\,\mathrm{Re}\,\alpha_s \tag{9}$$

For $\mathrm{Re} \gg 1$, the "fast streaming" velocity U_{Ef} is proportional to v_0^3 and is much larger than the "slow streaming" velocity U_E, which is proportional to the acoustic intensity in the beam.

Again, one has to bear in mind that this solution is limited to the particular case of a stable, saw-tooth wave where finite-amplitude losses are very high. However, the point to be emphasized here is that, in both the "slow streaming" and the "fast streaming" solutions above, the magnitude of the streaming velocity is a direct function of dissipative losses, whether they are due to finite-amplitude effects or viscous and thermal conduction effects.

2.4.2. Medium Scale Streaming (Rayleigh Streaming)

Rayleigh streaming can be considered a result of the absorption of sound by viscosity at a solid boundary. Rayleigh [4] described the streaming motion in a standing wave between parallel walls, showing that a secondary flow circulation occurs between the walls in cells one-quarter wavelength long, as shown in Figure 3. In a PCCE combustor, the circulation originates in the boundary-layer vorticity generated by the no-slip condition on the tube surface and goes from antinodes to nodes along the wall, and from node to antinode along the

tube axis. This mechanism also causes recirculating regions behind solid bodies in steady flows, as demonstrated experimentally by Andrade in 1931 [10]. The scale of the vortices produced is equal to the sound wavelength.

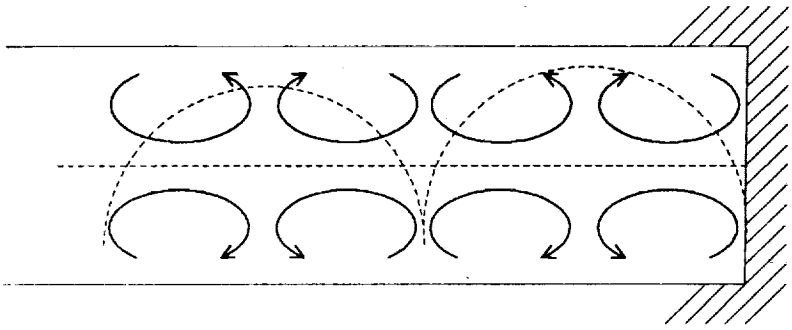

Figure 3. Rayleigh Streaming in a Tube.

The Rayleigh streaming velocities in a tube of radius R are given by Rozenberg [17]:

$$u_{Rz} = U_{Rz}\left\{1 - 2\left(\frac{r}{R}\right)^2 + \frac{e^{-\chi}}{3}\left[\left(2 + 3\frac{\delta_\nu}{r}\right)\cos\chi + \left(4 + \frac{\delta_\nu}{r}\right)\sin\chi + \left(1 + \frac{\delta_\nu}{2r}\right)e^{-\chi}\right]\right\} \tag{10}$$

and

$$u_{Rr} = U_{Rr}\left\{1 - \left(\frac{r}{R}\right)^2 + \frac{2\delta_\nu}{3r}e^{-\chi}\left(3\cos\chi + \sin\chi + \frac{1}{2}e^{-\chi}\right)\right\} \tag{11}$$

where U_{Rz} and U_{Rr} are given by:

$$U_{Rz} = -\frac{3}{8}\frac{v_0^2}{c_0}\sin(2kz) \tag{12}$$

$$U_{Rr} = -\frac{3}{8}\frac{v_0^2}{c_0}kr\cos(2kz) \tag{13}$$

$\chi = \dfrac{(R-r)}{\delta_\nu}$ and δ_ν is the acoustic boundary-layer thickness equal to:

$$\delta_\nu = \sqrt{\frac{2\nu}{\omega}} \tag{14}$$

The axial period of Rayleigh streaming is equal to $\frac{\lambda}{2}$. The ratio of Rayleigh streaming velocity to acoustic velocity is of the order of the acoustic Mach number M_a.

Medium Scale Streaming in a PCCE Combustor

From the definitions of Rayleigh streaming and Eckart streaming, it is clear that both mechanisms do not coexist in a PCCE combustor and correspond to different ranges of operations. As mentioned earlier, Eckart streaming can only be achieved at very high frequencies where U_{E} (see Equation 7) is much larger than $U_{\mathrm{R}z}$ and $U_{\mathrm{R}r}$. Rayleigh streaming, on the other hand, occurs at low frequencies when the sound completely fills the combustor tube, and when the Rayleigh streaming velocities given by Equations 12 and 13 are much higher than the Eckart streaming velocity in Equation 7.

As in the case of Eckart streaming, the solution given by Equations 11 and 12 is only valid for sound fields such that $\mathrm{Re} \ll 1$. It can be referred to as "slow Rayleigh streaming". The validity of the "slow Rayleigh streaming" theory was demonstrated by Andrade [10] in 1931. At very high sound pressure levels ($\mathrm{Re} \gg 1$), "fast Rayleigh streaming" occurs where the flow patterns remain unchanged, but the streaming velocities are much larger (up to several meters per second). Streaming velocities nearly two orders of magnitude higher than predicted by the "slow streaming" theory were obtained experimentally at high sound pressure levels in air (see Ref. [24]).

In summary, medium scale Rayleigh streaming can be used to set up a circulation in a PCCE combustor. This circulation entrains the particles, acting as a mixing mechanism.

2.4.3. Small Scale Streaming

Small scale streaming refers to streaming vortices having a scale much smaller than the sound wavelength (see Refs [15], [17], and [26] to [31]), such as the streaming which develops around each individual lycopodium particle.

As opposed to medium scale Rayleigh streaming, which acts as a particle transport mechanism, small scale streaming in particle cloud mixing is important for its effect on the interactions between lycopodium particles.

2.4.3.1. Conditions Necessary for the Presence of Small Scale Streaming

It is obvious that in order for small-scale streaming to occur around an obstacle, there must be a difference between the obstacle velocity and the velocity of the gas around it. From the previous discussion on the entrainment rate, we see that when the entrainment rate is low (high frequencies or particles with high mass), there is a large velocity difference between the particles and the gas and therefore, small scale streaming around the particles is important. When the entrainment rate is high (low frequencies or low-mass particles), the velocity difference is small and streaming around the particles is negligible.

2.4.3.2. Small Scale Streaming Inside the Boundary-Layer

The best known small scale streaming phenomenon is the streaming that develops inside the boundary-layer along an obstacle in a sound field (Schlichting

streaming [25]). This streaming is the result of the large velocity gradients inside the boundary-layer and has velocities which are of the same order as Rayleigh streaming. However, since the thickness of the boundary-layer vortex is approximately equal to $1.9\,\delta_\nu$, this streaming is confined to an area very close to the wall. In the case of a PCCE combustor, the acoustic boundary-layer δ_ν is very small (76×10^{-6} meters at 1 KHz). Therefore, small scale streaming inside the boundary-layer along a PCCE combustor tube wall is not an important mixing mechanism compared to Rayleigh streaming. However, small scale streaming around each lycopodium particle can affect the mixing process, as described in the next section.

2.4.3.3. Small Scale Streaming Around Particles

Small scale streaming around lycopodium particles results in attraction and repulsion forces between particles which can, under certain conditions, be the major contributor to the mixing process.

Due to the small radius of the particles and the large acoustic displacement amplitudes, Schlichting's streaming theory inside the boundary-layer is no longer valid (the average radius for lycopodium particles is about seven times smaller than the acoustic boundary-layer thickness at 1 KHz, and the acoustic displacement amplitude is of the order of the particle radius).

Andres and Ingard (see Refs. [29] and [30]) solved the problem of streaming around a cylinder having a radius of the order of or smaller than, the acoustic boundary-layer thickness. For conditions very close to the conditions in a PCCE combustor, they showed that the thickness of the boundary-layer vortex is much larger than the radius of the cylinder. They also revealed that the streaming

pattern resembles the pattern obtained in Rayleigh streaming on a large obstacle outside the boundary-layer [15], with the direction of rotation of the vortices reversed. A similar streaming pattern can be observed around each lycopodium particle, as shown in Figure 4.

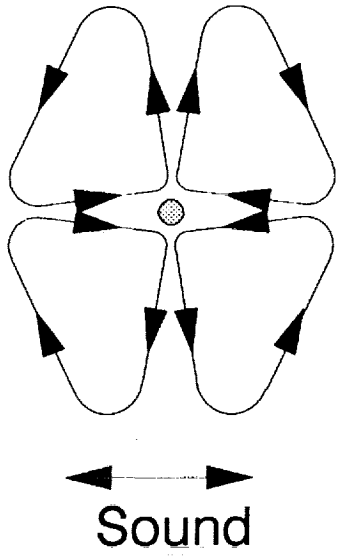

Figure 4. Streaming around a Cylinder.

2.4.3.4. Powder Striations in a PCCE Combustor

As Andrade [11] has shown, when a relative motion between particles and a gas is present ($\frac{X_p}{X_g} < 1$), small scale streaming around those particles is responsible for the dust striations observed in resonant tubes by many researchers (see Refs. [33] to [41]). The striations, caused by attraction and repulsion forces associated with the vortices, are parallel to the acoustic wave fronts, as shown in Figure 5 (reproduced from Andrade's paper [11]). A picture of similar

striations taken during PCCE mixing experiments is shown in Figure 6. In a standing acoustic wave field, the well-marked striations are sometimes separated by patches of quiescent powder indicating the acoustic nodes.

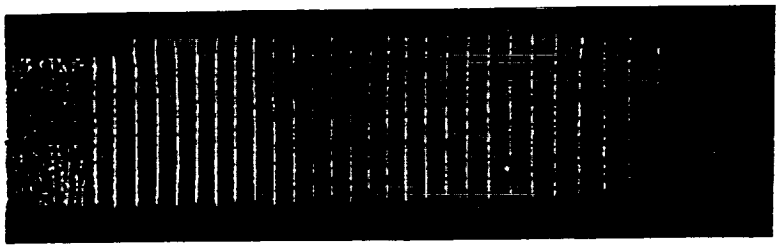

Figure 5. Dust Striations in a Resonant Pipe (from Andrade [11]).

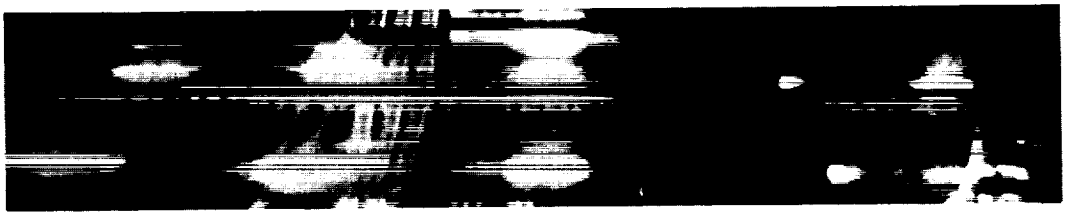

Figure 6. Lycopodium Striations in a PCCE Combustor.

The distance between striations is such that vortices from particles in adjacent striations just touch each other. Thus, spacing between striations is proportional to the size of the vortices, which in turn is proportional to the relative acoustic velocity between the particles and the gas.

Thus, according to the previous discussion on entrainment rate (see Equation 1) and because small scale streaming is directly proportional to the relative

acoustic velocity between the particles and the gas, large dense particles or high-frequency operation is associated with vigorous vortex motion, while particles having a small inertia or low-frequency operation results in little or no vortex motion.

At high frequencies (above 1 KHz), the lycopodium striations in a PCCE combustor are sharp and well-defined. As the frequency is decreased (below 1 KHz), the entrainment rate ($\frac{X_p}{X_g}$) increases and the striations become blurry and wider due to the particle motion.

2.4.3.5. Particle Motion Due to Small Scale Streaming

For a sound wave having a fixed frequency and a fixed amplitude, the position of the dust ridges is fixed. Thus no mixing can be achieved through small scale streaming in a steady state mode. However, fairly good mixing can be achieved in a transient acoustic field if the powder is originally distributed regularly over the length of the tube, as described in a later section.

2.5. Radiation Pressure

Radiation pressure due to the sound field acts on each particle inside a PCCE combustor and contributes to the overall motion and mixing of the particles. This section gives a simple estimate of the radiation pressure force on lycopodium particles, showing that this mechanism is usually small compared to streaming.

If the exact acoustic field around a spherical obstacle in a plane wave is computed, including the effects of scattering, it is found that a steady pressure on the sphere is generated by second order terms in the equation of state. In King's classic analysis (see Ref. [32]), radiation pressure is associated not so much

with steady secondary motion as with effects like the accumulation of particles in an acoustic field at nodes or antinodes (antinodal disk) or the possibility of suspending small objects against gravity (acoustic levitation).

The radiation pressure acting on a sphere having a radius a much smaller than the wavelength λ due to an incident plane wave results in a force given by [17]:

$$F_t = \frac{11\pi}{18} R^2 (kR)^4 \rho u_0^2 \tag{14}$$

For a sphere in a standing wave field given by:

$$u_1(z,t) = u_0 \sin(kz) e^{j\omega t} \quad ; \quad p_1(z,t) = \rho c_0 u_0 \cos(kz) e^{j\omega t} \tag{15}$$

the force is given by:

$$F_s = \frac{5\pi}{6} R^2 (kR) \rho u_0^2 \sin(2kz) \tag{16}$$

Thus in a standing wave field, the effect of radiation pressure is to carry the particles towards the acoustic nodes (maximum acoustic velocity), where they tend to accumulate. Although the sound field inside a PCCE combustor is dominated by the standing wave, a small traveling wave component is present due to the acoustic attenuation at the combustor walls. However, as shown by calculating the ratio $\frac{F_t}{F_s}$, the force on a particle due to a traveling wave is much smaller than the force due to a standing wave, except at a velocity node (zero velocity).

We can estimate the velocity u_{rad} of a particle under the action of radiation pressure by assuming that it is equal to the velocity determined by the balance

of radiation pressure and drag. According to Stokes' drag law, we have for a standing wave:

$$F_s = 6\pi\rho\nu R\, u_{\text{rad}} \tag{18}$$

This expression underestimates the total drag, and therefore overestimates the velocity. u_{rad} is therefore given by:

$$u_{\text{rad}} = \frac{5}{36}\frac{kR^2v_0^2}{\nu}\sin(2kz) \tag{19}$$

The ratio of radiation pressure velocity to Rayleigh streaming velocity is given by:

$$\frac{u_{\text{rad}}}{u_z} = \frac{10}{27}(kR)\frac{c_0R}{\nu} \tag{20}$$

At 100 Hz the streaming for a lycopodium particle is 530 times stronger than the radiation pressure, while at 5000 Hz, this ratio is 11. Thus radiation pressure should not be an important contributor to the motion of the particles since it only affects relatively large objects in the sound field. However, radiation pressure seems to be responsible for a tendency of the powder to accumulate rapidly at the end of the combustor, and opposite to the loudspeaker source (see Sections 3 and 4).

2.6. Summary of Acoustic Mixing Mechanisms

The motion of lycopodium particles due to a sound field in a PCCE combustor is affected by all the mechanisms described in the previous sections and is summarized here. As Andrade [11] has shown, particle motion arising from a sound field in a tube is an extremely complex phenomena mostly affected by

medium and small scale streaming, and radiation pressure. Slight changes in amplitude, frequency, particle size, or particle density result in totally different powder patterns and motions, including such striking phenomena as antinodal disk and ring, and nodal eye formation.

In the case of PCCE combustors, large scale streaming (Eckart streaming) and radiation pressure are neglected, and only medium scale Rayleigh streaming and small scale streaming are considered.

Rayleigh streaming is responsible for a circulation of the gas inside the tube which entrains the particles, therefore mixing them. Small scale streaming around lycopodium particles results in the formation of fixed powder striations.

For moderate frequencies and at a low acoustic level, "slow streaming" occurs but is too weak to affect the particles. As the acoustic level is increased, vortex motion around the particles due to small scale streaming becomes well-defined and striations appear. As the acoustic level is further increased, "fast Rayleigh streaming" become dominant, resulting in a general circulation which destroys the striations.

At high frequencies (low entrainment rate), sharp striations containing all the particles are present over a wide range of frequencies and acoustic levels. Only at very high acoustic levels does the circulation due to "fast Rayleigh streaming" becomes dominant.

At low frequencies (high entrainment rate), the circulation due to medium scale Rayleigh streaming is responsible for a node to antinode circulation and clearance of the powder at the nodes. Striations due to small scale streaming never appear or are blurred.

This blurring of the striations was observed both by Andrade [11] (see Figure 7) and during mixing experiments carried out at NASA Lewis using an air pump system (see Figure 8).

Figure 7. Blurred Dust Striations in a Resonant Pipe (from Andrade [11]).

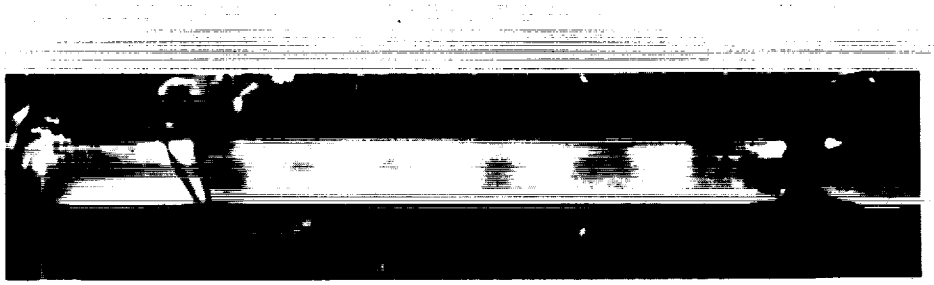

Figure 8. Blurred Lycopodium Striations in a PCCE Combustor, Air Pump Experiment.

In the pump experiment, a large amplitude acoustic wave having a frequency of 30 Hz was generated inside a PCCE combustor using an air pump. As shown in Figure 8, large widely-spaced "cells" were formed. These cells are in fact striations which are blurred due to the motion of the lycopodium particles. Similar cells are visible in Figure 7 from Andrade's paper [11].

The previous discussion also explains the differences in motion observed when particles of different size, such as smoke and lycopodium particles, are submitted to a similar acoustic field.

In the case of smoke particles, the entrainment rate is very high and the particles act as tracing points for medium scale streaming, which is the dominant mixing mechanism.

In the case of lycopodium particles, the entrainment rate can be very small (see Figure 1) and circulation and striations can be present at the same time.

2.6.1. Acoustic Mixing in a PCCE Combustor: Basic Principles

This section presents the basic principles of acoustic mixing in PCCE combustors as they can be deduced from the previous discussion on streaming. Particle mixing in a PCCE combustor using steady-state sound waves is a difficult task for the reasons which follow:

By definition, an homogeneous mixture is obtained in the PCCE combustor when the distribution of particles is uniform. Therefore, the forces acting on each particle must be of the same order everywhere in the PCCE combustor to avoid high concentrations of particles in certain areas of the combustor and low concentrations in others.

When medium scale streaming is used as the primary mixing mechanism in a steady state mode, the basic homogeneity requirement is not satisfied. This is because medium scale streaming relies on the establishment of standing waves inside the combustor. These standing waves are responsible for "structured" flow circulation cells which result in a certain amount of mixing. However, as a result of the "structured quality" of the sound field itself, a perfectly homogeneous

particle cloud cannot be obtained. Therefore, perfect mixing using steady-state acoustics is not feasible. However, "fairly good" mixing can be achieved by carefully designing the sound source and carefully selecting its operating conditions. The final crucial question is whether or not "fairly good mixing" is enough for particle cloud combustion experiments. Although the answer at this time is probably negative, indications are that sufficient mixing can be obtained by combining steady-state and transient acoustic mixing methods as described in more detail later in this report.

When small scale streaming is present in a steady state mode, it is obvious that the formation of powder striations spaced at regular intervals parallel to the wave fronts prevents good mixing from occuring.

One way to reduce the "structured quality" of the sound field would be to use a random signal such as white noise to excite the loudspeaker source connected to the combustor. However, the natural acoustic modes of the tube would still be excited, thus resulting once again in a non-homogeneous sound field. Moreover, medium scale streaming would not have time to develop because of the constantly varying sound characteristics. In addition, the circulation would be very weak because the acoustic energy in each frequency would be very small.

Pseudo-random noise such as a mono- or a multi-frequency signal randomly and slowly varying in frequency and amplitude with time could probably be used with more success than white noise for the following reason: First, the changing characteristics of the signal would provide some of the randomness and disorder needed. Next, the discrete character of the frequency spectrum of the excitation signal would allow each harmonic component to be powerful

enough to initiate a strong circulation. Finally, the slow rate of change in the signal would leave enough time for the streaming patterns to establish themselves. On the other hand, acoustic resonances in the PCCE combustor will limit the useful range of amplitude and frequency variations that can be used, unless large loudspeakers are used which can generate large acoustic levels at frequencies away from resonance, or unless the frequency is stepped from one resonance frequency to the other so as to keep the acoustic levels high.

Finally, transients have been used successfully in reducing the "structured quality" of the sound field, as discussed in a later section. In this case, the loudspeaker source is turned on and then turned off once the transient state is over and the sound field in the PCCE combustor has built up to a steady state. During the transient state, the motion of the particles results in a fairly homogeneous cloud due to the continuously changing acoustic field. The time duration of the transient can be adjusted by changing the acoustic attenuation inside the PCCE combustor.

In the next section, the basic principles and results of high-frequency steady-state mixing and low-frequency transient mixing are briefly presented. Due to the limited nature of this research effort, no experiments were carried out using random or pseudo-random excitation signals.

2.6.2. High-Frequency Steady-State Mixing

This report concentrates on high-frequency, steady-state mixing using medium scale streaming. The principle is to set up a circulatory motion of the powder perpendicular to the PCCE cylindrical combustor axis, as opposed to the circulation in the axial direction obtained in low-frequency axial wave

operation. This circulatory motion can be obtained by exciting high-frequency spinning waves inside the PCCE combustor and is due to medium scale Rayleigh streaming. If the spinning wave is excited at or just above its cut-off frequency, the axial sound wavelength in the combustor is very large (much larger than the sound wavelength), which should increase the axial homogeneity of the sound field. Striations due to small scale streaming appear perpendicular to the acoustic wavefront as a result of the high frequencies. However, if the sound pressure level in the PCCE combustor's is high enough (which is easily achieved if the sound source is operated around the cut-off frequency of one of the combustor's higher-order spinning modes), the circulation due to medium scale streaming is dominant and the striations are destroyed.

2.6.3. Low-Frequency Transient Mixing

As mentioned previously, "perfect" low-frequency mixing in a steady state mode is impossible to achieve due to the axial inhomogeneities which are necessarily present in the sound field. "Good" mixing has been achieved by NASA Lewis researchers at low frequencies in a transient mode when the powder was originally regularly distributed over the whole length of the combustor. The main results of these tests are briefly reported here and a simple explanation of their cause is given. It should be emphasized that these experiments were performed in a micro-gravity environment, as opposed to the rest of the experimental results presented in this report, which were carried out in a 1-g environment.

In this experiment, carried out in one of the drop towers at NASA Lewis, the low-frequency loudspeaker source (in the 100 Hz to 300 Hz range) is turned

on for only a fraction of a second, therefore preventing the establishment of well-defined medium scale streaming cells. Due to the low frequency of operation, blurred ridges start to form at regular intervals from each other as soon as the source is turned on (see Figure 9a). However, nearly immediately after the ridges are formed, they combine two by two to form a second set of ridges with a spacing twice the spacing of the first set of ridges (see Figure 9b). Formation of a third set is barely perceptible; afterwards, mixing appears nearly complete, which corresponds to the time when the transient state is over, and the sound field in the PCCE combustor has built up to a steady state (see Figure 9c).

The most likely explanation for this mixing process is as follows. As soon as the source is turned on, the acoustic level inside the tube starts to build up through multiple reflections at the ends of the tube (see the last section in this report on the analysis of the transient sound field in PCCE combustors). During this build up process, small scale streaming occurs around each individual particle, resulting in the formation of ridges. As the acoustic level inside the PCCE combustor increases, so does the size of the vortices around each particle. As a result, the ridges repel one another, resulting in the formation of new ridges further apart from each other. Finally, at the end of the transient state, the acoustic level and the time elapsed since the source was turned on are high enough that the circulation due to medium scale streaming takes over, destroying the ridges and creating mixing cells. Switching off the sound source just before the mixing cells due to medium scale Rayleigh streaming are well-formed results in a fairly homogeneous mixture of gas and particles.

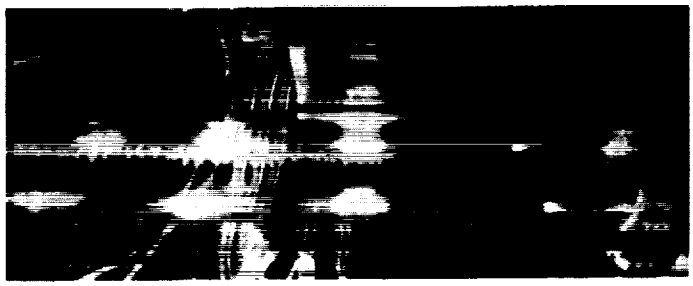

(a)

(b)

(c)

Figure 9. Low-Frequency Transient Mixing in NASA Lewis Drop Tower. (a): 0.08 seconds; (b): 0.16 seconds; (c): 0.21 seconds.

In other words, during the transient state, the motion of the particles results in a fairly homogeneous cloud due to the continuously changing acoustic field. The time duration of the transient can have an effect on the quality of the mixing and can be adjusted by changing the acoustic attenuation inside the PCCE combustor.

A similar result could be achieved at higher frequencies, where the tendency for ridges to form is strong. Another alternative which should result in very good mixing is the use of a combination of low-frequency and high-frequency sound sources both operated in a transient mode. Due to the good axial homogeneity obtained with a spinning wave at a frequency close to its cut-off frequency and an usually long transient time, it is believed that the combined use of high-frequency spinning waves and low-frequency axial waves in a transient mode would greatly enhance the mixing process.

3. Analytical Work

The goal of the analytical work supporting the particle cloud experiment was to identify the physical mechanisms which produce mixing in strong acoustic fields and, specifically, to analyze mixing due to higher acoustic modes in a cylindrical tube (quadrature-speaker mixing) and mixing in a sphere (acoustic premix). These analyses will be presented in detail. More general and qualitative discussions will also be given of some of the problems encountered during mixing experiments using steady axial modes and of the often surprising results of micro-gravity experiments using acoustic transients.

3.1. Summary of Analysis Results

3.1.1. Quadrature-Speaker Set

The quadrature-speaker set produces an acoustic progressive wave in the tube. Rayleigh streaming leads to steady circulation around the tube as observed experimentally.

The combined effect of the axial-speaker and the quadrature-speaker sets should be simultaneous longitudinal and circumferential circulation. It was difficult to assess the motion observed experimentally, but there was no doubt that the simultaneous presence of two types of circulation resulted in greatly enhanced mixing.

3.1.2. Acoustic Premix

Secondary circulation necessarily contains a nodal plane which separates the sphere into two hemispheres between which powder cannot be transferred by

steady motion. Complete mixing is only possible if the nodal plane can be so arranged that it bisects the powder. Mixing in a hemisphere might be acceptable. Otherwise, in micro-gravity, operation of the speaker in transient bursts might cause a homogeneous mixture throughout the sphere.

There is no secondary motion possible for purely radial modes. Operation of the speaker at the corresponding frequencies will result in no mixing.

3.1.3. Transient Axial Modes

The formation of blurred ridges is most probably due to small scale streaming around each individual particle.

3.2. Acoustic Streaming: Theory

Because complete and detailed derivations of the general equations governing acoustic streaming are widely available in the literature (see Ref. [42]), only a summary will be presented here.

The theory of acoustic streaming is based on the compressible Navier-Stokes equations with the linearized equation of state

$$p = c^2 \rho$$

appropriate to acoustic problems. Perturbation solutions of the form

$$\rho = \rho^{(0)} + \rho^{(1)} + \rho^{(2)}$$

$$u = u^{(1)} + u^{(2)}$$

are sought in which the superscripts indicate decreasing order of magnitude and $\rho^{(0)}$ is constant.

The first order equations for $\rho^{(1)}$ and $u^{(1)}$ are simply the equations of acoustics including corrections for viscous effects. The equations for $u^{(1)}$ are most easily solved by writing the equations for the first order compressibility and vorticity,

$$s^{(1)} = \nabla \cdot u^{(1)}$$

$$\Omega^{(1)} = \nabla \times u^{(1)}$$

which are

$$\frac{\partial^2 s^{(1)}}{\partial t^2} - c^2 \nabla^2 s^{(1)} = \left(\frac{4}{3}\nu + \nu'\right)\nabla^2 \frac{\partial s^{(1)}}{\partial t}$$

$$\frac{\partial \Omega^{(1)}}{\partial t} = \nu \nabla^2 \Omega^{(1)} \tag{1}$$

Then $u^{(1)}$ can be recovered from $s^{(1)}$ and $\Omega^{(1)}$ by solving the vector equation

$$\nabla^2 u^{(1)} = \nabla s^{(1)} - \nabla \times \Omega^{(1)} \tag{2}$$

Solutions of Equations 1 and 2 are readily expressed in terms of eigenfunctions of the scalar and vector Laplacian, that is, solutions of

$$\nabla^2 \phi = -\lambda^2 \phi$$

$$\nabla^2 A = -\mu^2 A \tag{3}$$

In fact, direct substitution shows that there are solutions of Equation 1 of the form

$$s^{(1)} = e^{i\omega t}\phi$$

$$\Omega^{(1)} = e^{i\omega t} A \tag{4}$$

and, because of the eigenfunction conditions given in Equation 3,

$$u^{(1)} = -\frac{1}{\lambda^2}\nabla s^{(1)} + \frac{1}{\mu^2}\nabla \times \Omega^{(1)} \tag{5}$$

Eigenfunctions for the scalar Laplacian are well known for a number of coordinate systems; the corresponding eigenfunctions for the vector Laplacian are less familiar, but can easily be found for the cylindrical and spherical coordinate systems.

Next consider the second order equations for $u^{(2)}$. As expected in a perturbation expansion of a quadratically nonlinear theory, the second order equations contain source terms which are quadratic in the solutions of the first order equations. Thus, if the first order terms depend on time harmonically with frequency ω, the source terms in the second order theory can have frequencies $\omega \pm \omega = 2\omega, 0$. The frequency 2ω corresponds to a higher order acoustic phenomenon; streaming is the steady phenomenon corresponding to the frequency zero.

Specifically, the perturbation method to the equation

$$\nabla^2\Omega^{(2)} = -\nabla \times \frac{(u^{(1)} \times \Omega^{(1)})}{\nu} - \left(\frac{4}{3} + \frac{\nu'}{\nu}\right)\nabla\,\rho^{(1)} \times \nabla\frac{(\partial\rho^{(1)}/\partial t)}{(\rho^{(0)})^2} - \nabla \times \frac{(\rho^{(1)}\nabla \times \Omega^{(1)})}{\rho^{(0)}} \tag{6}$$

for the second order vorticity field. Only the steady terms are to be included on the right side. Retention of only the first source term produces the theory of Rayleigh streaming (see Refs. [42] and [43]):

$$\nabla^2\,\Omega^{(2)} = -\nabla \times \frac{(u^{(1)} \times \Omega^{(1)})}{\nu}$$

and retention of only the second term produces the theory of Eckart streaming (see Refs. [19] and [42]):

$$\nabla^2\Omega^{(2)} = -\left(\frac{4}{3} + \frac{\nu'}{\nu}\right) \nabla\rho^{(1)} \times \nabla\frac{(\partial\rho^{(1)}/\partial t)}{(\rho^{(0)})^2}$$

A thorough discussion of these alternative theories appears in Ref. [42], in which the third source term in Equation 6 is also considered. Briefly, the pertinent facts are these. In Rayleigh's theory, second order vorticity requires a rotational first order acoustic field for which $\Omega^{(1)}$ is nonzero. Acoustic fields are ordinarily treated as irrotational; however, vorticity can be introduced into the acoustic field by the no-slip condition at a solid surface. In this case, although the effects of vorticity are indeed confined to a small boundary layer, this boundary layer acts as a vorticity source in the second order theory. In Eckart's theory, the source of second order vorticity is the oscillations of the first order mass density; for this reason, Eckart streaming is also called bulk streaming.

It is useful to compare the magnitudes of the source terms in Equation 6. Let u be a representative velocity in the acoustic field, and let ω be the frequency and k the wavenumber, so that $\omega = ck$. Then for the Rayleigh term, $\Omega \sim ku$ and

$$\nu^{-1}\nabla \times (u \times \Omega) \sim \frac{u^2\, k^2}{\nu}$$

To estimate the Eckart term, note that the first order continuity equation

$$\frac{\partial\rho^{(1)}}{\partial t} + \rho^{(0)}\nabla \cdot u^{(1)} = 0 \tag{7}$$

implies $\omega\rho^{(1)} \sim \rho^{(0)}ku$, or $\rho^{(1)} \sim \frac{\rho^{(0)}u}{c}$. Therefore,

$$\nabla\rho^{(1)} \times \nabla\frac{(\partial\rho^{(1)}/\partial t)}{(\rho^{(0)})^2} \sim \frac{k^3\, u^2}{c}$$

It is easy to check that the third source term in Equation 6 is also estimated by this expression. The ratio of the Rayleigh source strength to the Eckart source strength is therefore

$$\frac{k^2 v^2}{\nu} \frac{c}{k^3 u^2} = \frac{c}{\nu k}$$

For air at 15° C, $\frac{c}{\nu k} \sim 240{,}000.\ \text{cm}^{-1}$. Only for extremely short waves will the Eckart source term nearly equal the Rayleigh source term [42]. Thus, in cases in which both Rayleigh and Eckart streaming are possible, it is most likely that Rayleigh streaming will be the dominant mechanism.

3.3. Secondary Motion in Axial Wave Fields

Mixing experiments using lycopodium powder showed an undesirable tendency of the powder to accumulate rapidly at the end of the tube and only afterwards to circulate in a cell much smaller than the tube length. The results are at variance with the experiments of Andrade [10], who observed steady circulation of the type predicted by Rayleigh [43], in which the circulation cells fill the tube completely.

The differences between these observations can be attributed to radiation pressure. For spheres much smaller than the wavelength, radiation pressure in a progressive wave varies as the sixth power of the radius. Thus, if a denotes the radius of the sphere, Newton's equation takes the form

$$\rho a^3 \frac{d^2 x}{dt^2} \sim a^6 \cdot a^2$$

In Andrade's experiments, smoke particles were used to trace the secondary motion. Andrade assumed

$$\rho \sim 1 \frac{g}{\text{cm}^3} \qquad a \sim 5 \times 10^{-5}\text{cm}$$

For lycopodium powder,

$$\rho \sim 1 \frac{g}{\text{cm}^3} \qquad a \sim 2 \times 10^{-4}\text{cm}$$

Thus, if the effects of multiple scattering can be ignored, the accelerations due to radiation pressure are about 3000 times greater for lycopodium than for smoke. This difference is enhanced by a fundamental distinction between motion due to streaming and motion due to radiation pressure: in the first case, the particles follow the bulk motion of the fluid, but in the second, they are pushed through the fluid which may otherwise be at rest. Thus, viscosity will oppose the motion of smoke particles much more effectively than the motion of lycopodium particles.

It may be assumed that the speaker generates a progressive wave

$$p = p_0 \cos(\omega t - kx)$$

If sound is not absorbed by viscous dissipation and is fully reflected at the opposite end, the result is a standing wave:

$$p = p_0 \cos(\omega t - kx) + p_0 \cos(\omega t + kx) = p_0 \cos(\omega t) \cos(kx)$$

But suppose that the sound field is the result of imperfect reflection:

$$\begin{aligned} p &= p_0 \cos(\omega t - kx) + r p_0 \cos(\omega t + kx) \\ &= r p_0 \cos(\omega t) \cos(kx) + (1 - r)\, p_0 \cos(\omega t - kx), \qquad r < 1 \end{aligned} \tag{1}$$

This field contains a progressive wave component which, while possibly very small, could have a significant effect on lycopodium. It is conceivable that the radiation pressure due to this progressive wave suffices to cause the observed drift away from the speaker.

Imperfect reflection could be caused by sound being absorbed by viscosity (in this case, the pressure field should contain exponential damping). This effect is not controllable. However, imperfect reflection will certainly be increased by the presence of nonconservative boundary conditions like the impedance conditions characteristic of membrane terminations. The effect of imperfect reflection was clearly demonstrated in experiments using an anechoic termination, for which in Equation 1, $r = 0$. There was a noticeable drift away from the speaker, even in higher-order modes with presumably small axial components.

It is likely that drift can be minimized by using conservative end conditions, such as perfectly rigid or pressure release conditions, even if it cannot be eliminated entirely.

3.4. Streaming due to Higher-Order Modes in a Cylindrical Tube

The simplest acoustic mode in a finite cylinder is the axial standing wave characterized by pressure variation of the form

$$p = p_0 \cos(\omega_n t) \cos(k_n z)$$

$$\omega_n = c\, k_n$$

The values of k_n are determined by the pipe length and boundary conditions. Here and in what follows, arbitrary phase angles are understood to be permissible in the trigonometric functions, but are omitted to lighten the notation.

More complex modes, solutions of the full three-dimensional wave equation, are also possible [42]. These modes can be either progressive or standing waves in the θ coordinate. The pressure varies as

$$p = p_0 \cos(\omega_{mn} t - n\theta) \cos(kz) J_n(k_{mn} r) \qquad \text{(progressive)}$$

$$p = p_0 \cos(\omega_{mn} t) \cos(n\theta) \cos(kz)\, J_n(k_{mn} r) \qquad \text{(standing)}$$

$$\omega_{mn}^2 = c^2(k^2 + k_{mn}^2) \qquad (1)$$

The k_{mn} are roots of the equation $J_n'(k_{mn}R) = 0$, where R equals the cylinder radius. The progressive wave has a definite helicity and the standing wave can be considered the superposition of two progressive waves with opposite helicity. These modes are entirely analogous to electromagnetic waveguide modes [44] and can also be considered to arise from repeated reflections from the cylinder wall (see Refs. [44] and [45]).

The quadrature-speaker arrangement is designed to excite such modes, specifically the mode $n = 1$, $m = 0$, which has the smallest cutoff frequency [45], $\omega_{01} = c\ k_{01}$. The modes with $n = 0$ have no θ dependence or θ velocity component. These modes satisfy the no slip conditions. When $n > 0$, the exact mode shape, including viscous effects, must be determined as outlined in Section 3.2. Both standing and progressive waves will be analyzed, although the asymmetry of the quadrature-speaker arrangement and the observed streaming patterns suggest that the quadrature-speaker set excite a progressive wave, not a standing wave. It is reasonable to assume that the helicity and phase of the progressive wave are determined by the phase lag between the speakers in the quadrature-speaker set.

To compute the first order velocity field, let u_r, u_θ, u_z be cylindrical unit vectors, and note that the independence of u_z of the coordinates implies that $\phi\, u_z$ is an eigenfunction of the vector Laplacian whenever ϕ is an eigenfunction of the scalar Laplacian:

$$\nabla^2(\phi u_z) = (\nabla^2\phi)\, u_z = -\lambda^2 \phi u_z$$

Now consider a cutoff mode for which $k_z = 0$ (see Ref. [45]),

$$s = A\, e^{-i\omega t} e^{in\theta}\, J_n(l'' r) \tag{2}$$

$$\Omega = B\, e^{-i\omega t} e^{in\theta}\, J_n(l' r) uz \tag{3}$$

so that

$$\nabla^2 s = -(l'')^2 s \qquad\qquad \nabla^2 \Omega = -(l')^2 \Omega$$

Progressive waves are obtained by taking real parts of Equations 2 and 3, and standing waves result from superposition of progressive waves. The governing equation (Equation 1, Section 3.2) reduces to scalar equations relating ω, l', l'':

$$i\omega = (l')^2 \nu \tag{4}$$

$$-\omega^2 + c^2 (l'')^2 - i\omega (l'')^2 (\nu + \nu') = 0 \tag{5}$$

Equation 5 can be rewritten as

$$0 = -\omega^2 + c^2 (l'')^2 \left\{ 1 - \frac{i\omega(\nu + \nu')}{c^2} \right\} \tag{6}$$

The inviscid solution for s is defined by Equation 2 with $l'' = \frac{\omega}{c}$; Equation 6 shows that the viscous corrections to this relation are of the order of the small quantity $\frac{\omega\nu}{c^2}$. Therefore, as a first approximation, assume

$$l'' = \frac{\omega}{c}$$
$$l' = \sqrt{\frac{i\omega}{\nu}} \tag{7}$$

The second equation is exact. The first order velocity is found from

$$V^{(1)} = -\left(\frac{c}{\omega}\right)^2 \nabla s + \frac{\nu}{i\omega} \nabla \times \Omega^{(1)}$$

Explicitly, in terms of scalar components

$$V_r^{(1)} = \left[-\frac{c}{\omega} A J_n'\left(\frac{\omega r}{c}\right) + n \frac{\nu}{\omega r} B \frac{J_n\left(\sqrt{\frac{i\omega}{\nu}} r\right)}{J_n'\left(\sqrt{\frac{i\omega}{\nu}} R\right)} \right] e^{-i\omega t} e^{in\theta}$$

$$V_\theta^{(1)} = \left[-in\, A\, \frac{c^2}{\omega^2} \frac{1}{r} J_n\left(\frac{\omega r}{c}\right) - \sqrt{\frac{\nu}{i\omega}} B \frac{J_n'\left(\sqrt{\frac{i\omega}{\nu}} r\right)}{J_n'\left(\sqrt{\frac{i\omega}{\nu}} R\right)} \right] e^{-i\omega t} e^{in\theta}$$

$$\Omega_z^{(1)} = B \left[\frac{J_n\left(\sqrt{\frac{i\omega}{\nu}} r\right)}{J_n'\left(\sqrt{\frac{i\omega}{\nu}} R\right)} \right] e^{-i\omega t} e^{in\theta}$$

in which a convenient redefinition of the unknown constant B has been introduced.

The no slip boundary condition, $V_r^{(1)} = V_\theta^{(1)} = 0$ when $r = R$ leads in standard fashion to a determinant equation for ω. But it is consistent with the approximation in Equation 7 to assume that the frequencies ω are determined by the inviscid relation [45]

$$J_n'\left(\frac{\omega r}{c}\right) = 0$$

with corrections of order $\frac{\sqrt{\nu\omega}}{c}$. The no slip boundary conditions are satisfied to this order by

$$V_\theta^{(1)} = V\left[\frac{R}{r}\frac{J_n\left(\frac{\omega r}{c}\right)}{J_n\left(\frac{\omega R}{c}\right)} - \frac{J_n'\left(\sqrt{\frac{i\omega}{\nu}}r\right)}{J_n'\left(\sqrt{\frac{i\omega}{\nu}}R\right)}\right]e^{-i\omega t}e^{in\theta}$$

$$V_r^{(1)} = V\left[\frac{1}{in}\frac{\omega R}{c}\frac{J_n'\left(\frac{\omega r}{c}\right)}{J_n\left(\frac{\omega R}{c}\right)} + \sqrt{i}\frac{n}{r}\sqrt{\frac{\nu}{\omega}}\frac{J_n\left(\sqrt{\frac{i\omega}{\nu}}r\right)}{J_n'\left(\sqrt{\frac{i\omega}{\nu}}R\right)}\right]e^{-i\omega t}e^{in\theta} \qquad (8)$$

$$\Omega_z^{(1)} = V\sqrt{\frac{i\omega}{\nu}}\left[\frac{J_n\left(\sqrt{\frac{i\omega}{\nu}}r\right)}{J_n'\left(\sqrt{\frac{i\omega}{\nu}}R\right)}\right]e^{-i\omega t}e^{in\theta}$$

in which $V_\theta^{(1)} = 0$ when $r = R$ exactly, but $V_r^{(1)}$ is of the order of the small quantity $\sqrt{\frac{\nu}{\omega R^2}}$ when $r = R$.

As expected, the corrections in Equation 8 to the inviscid solution, which are given by the Bessel function ratios with complex arguments, are boundary layers significant only when r is near R. This can be seen from the asymptotic expansions for the Bessel functions [46], which imply

$$\frac{J_n'\left(\sqrt{\frac{i\omega}{\nu}}r\right)}{J_n'\left(\sqrt{\frac{i\omega}{\nu}}R\right)} \sim e^{\sqrt{\frac{\omega}{2\nu}}(R-r)(1-i)}$$

$$\frac{J_n\left(\sqrt{\frac{i\omega}{\nu}}r\right)}{J_n'\left(\sqrt{\frac{i\omega}{\nu}}R\right)} \sim \frac{1}{i}e^{\sqrt{\frac{\omega}{2\nu}}(R-r)(1-i)} \qquad (9)$$

Since $R\sqrt{\frac{\omega}{\nu}}$ is quite large, these approximations are numerically quite accurate.

Progressive waves are found by taking the real or imaginary parts in Equation 8. It is convenient at the same time to substitute the asymptotic expansions given in Equation 9. The result is

$$
\begin{aligned}
V_\theta^{(1)} \sim & V\left\{\frac{R}{r}\frac{J_n(\frac{\omega r}{c})}{J_n(\frac{\omega R}{c})}\cos(-\omega t+n\theta)\right. \\
& \left. - e^{\sqrt{\frac{\omega}{\nu}}(R-r)}\cos(-\omega t+n\theta-\sqrt{\frac{\omega}{\nu}}(R-r))\right\} \\
V_r^{(1)} \sim & V\left\{\frac{\omega R}{nc}\frac{J_n'(\frac{\omega r}{c})}{J_n(\frac{\omega R}{c})}\sin(-\omega t+n\theta)\right. \\
& \left. + \sqrt{\frac{\nu}{\omega}}\,\frac{n}{r}\,e^{\sqrt{\frac{\omega}{\nu}}(R-r)}\sin(-\omega t+n\theta+\frac{\pi}{4}-\sqrt{\frac{\omega}{\nu}}(R-r))\right\} \qquad (10) \\
\Omega_z^{(1)} \sim & V\sqrt{\frac{\omega}{\nu}}\,e^{\sqrt{\frac{\omega}{\nu}}(R-r)}\sin(-\omega t+n\theta+\frac{\pi}{4}-\sqrt{\frac{\omega}{\nu}}(R-r))
\end{aligned}
$$

Analogous results for standing waves are obtained by first adding the solutions in Equation 8 with the values $\pm n$. This operation corresponds to superposing progressive waves with opposite helicities. Then, taking real parts,

$$
\begin{aligned}
V_\theta^{(1)} \sim & V\left\{\frac{R}{r}\frac{J_n(\frac{\omega r}{c})}{J_n(\frac{\omega R}{c})}\cos(\omega t)\,\cos(n\theta)\right. \\
& \left. - e^{\sqrt{\frac{\omega}{\nu}}(R-r)}\cos(n\theta)\,\cos(\omega t+\sqrt{\frac{\omega}{\nu}}(R-r))\right\} \\
V_r^{(1)} \sim & V\left\{\frac{\omega R}{nc}\frac{J_n'(\frac{\omega r}{c})}{J_n(\frac{\omega R}{c})}\cos(\omega t)\,\sin(n\theta)\right. \\
& \left. + ne^{\sqrt{\frac{\omega}{\nu}}(R-r)}\sin(n\theta)\,\cos(\omega t+\frac{\pi}{4}+\sqrt{\frac{\omega}{\nu}}(R-r))\right\} \qquad (11) \\
\Omega_z^{(1)} \sim & V\sqrt{\frac{\omega}{\nu}}\,e^{\sqrt{\frac{\omega}{\nu}}(R-r)}\,\cos(n\theta)\,\cos(\omega t+\frac{\pi}{4}+\sqrt{\frac{\omega}{\nu}}(R-r))
\end{aligned}
$$

The source strength for Rayleigh streaming is given by

$$
\nabla\times V^{(1)}\times\Omega^{(1)} = -\left\{\frac{1}{r}\,\frac{\partial}{\partial r}(rV_r^{(1)}\Omega_z^{(1)})+\frac{1}{r}\,\frac{\partial}{\partial\theta}(V_\theta^{(1)}\Omega_z^{(1)})\right\}u_z
$$

Only steady terms are retained in evaluating the products. Thus, for the progressive waves

$$\nabla \times V^{(1)} \times \Omega^{(1)} = V^2 \sqrt{\frac{\omega}{\nu}}\, e^{\sqrt{\frac{\omega}{\nu}}(R-r)}\, F(r) u_z$$

and for the standing waves

$$\nabla \times V^{(1)} \times \Omega^{(1)} = V^2 \sqrt{\frac{\omega}{\nu}}\, e^{\sqrt{\frac{\omega}{\nu}}(R-r)}\, G(r) \sin(2n\theta) u_z$$

The explicit expressions for F and G are bulky and unilluminating; the exponential factors which obviously persist throughout the calculation have been retained to emphasize the fact that both source terms are boundary layers.

The secondary vorticity is found by solving the Rayleigh streaming equation,

$$\nabla^2 \Omega^{(2)} = -\frac{1}{\nu} \nabla \times \left(V^{(1)} \times \Omega^{(1)} \right) \tag{14}$$

derived in Section 3.2. Substituting Equation 12 into Equation 14, the secondary vorticity for progressive waves has the form

$$\Omega^{(2)} = A(r)\, e^{\sqrt{\frac{\omega}{\nu}}(R-r)}\, u_z + C\, u_z \tag{15}$$

in which the first term represents a particular solution of Equation 14 and the second term is the part of the homogeneous solution which will be required to satisfy the no slip boundary condition on $V^{(2)}$. Similarly, for standing waves,

$$\Omega^{(2)} = B(r)\, e^{\sqrt{\frac{\omega}{\nu}}(R-r)} \sin(2n\theta)\, u_z + D r^{2n} \sin(2n\theta)\, u_z \tag{16}$$

The secondary flow corresponding to Equations 15 and 16 can be evaluated as follows. Since the secondary flow is incompressible, there is a vector potential A such that

$$V^{(2)} = \nabla \times A \tag{17}$$

where A satisfies

$$\Omega^{(2)} = \nabla \times V^{(2)}$$

$$= -\nabla^2 A$$

In view of Equation 15, $\Omega^{(2)}$ has the form

$$\Omega^{(2)} = a(r)\, u_z + C\, u_z$$

in which $a(r)$ is a boundary layer. Therefore,

$$A = b(r)\, u_z - \frac{1}{4} C\, r^2\, u_z$$

where $b(r)$ satisfies

$$\frac{1}{r}\frac{d}{dr} r \frac{db}{dr} = -a$$

This equation can be solved by quadratures. Write the general solution as

$$b = c(r) + c_0 \ln(r) + c_1$$

The logarithmic term would introduce a singularity and the constant term disappears when the curl is taken in Equation 14. It is therefore sufficient to assume $c_0 = c_1 = 0$. Thus,

$$V^{(2)} = \left[-b'(r) + \frac{1}{2} C_r\right] u_\theta \tag{18}$$

and defining C by

$$C = 2\,\frac{b'(R)}{R}$$

the no slip boundary condition is satisfied.

Except for the boundary layer correction represented by the term $b(r)$, the secondary motion is simply a rigid rotation about the center of the tube. This

is not a laminar flow of the familiar type because it is produced by the body forces generated by the acoustic field. The qualitatively important feature of this secondary flow is that it spins the particles around circular paths throughout the tube.

The secondary motion due to standing waves is quite different. Without insisting on details, it is clear that in the analysis leading to Equation 18, the trigonometric factor persists. It produces a secondary flow of the form

$$V^{(2)} = \left[\frac{c(r)}{r} + \frac{nD}{2(n+1)}\, r^{2n+1}\right] \cos(2n\theta)\, u_r - \left[c'(r) + \frac{1}{2}\, D\, r^{2n+1}\right] \sin(2n\theta)\, u_\theta$$

In this case, the θ velocity component vanishes along the $4n$ symmetrically spaced rays through the origin defined by $\sin(2n\theta) = 0$. The tube is therefore partitioned by nodal planes into regions across which powder cannot be transferred. This secondary motion would obviously be extremely unfavorable for mixing.

There is no doubt that the quadrature-speaker arrangement produced secondary motion of the type associated with progressive waves. Indeed, it is difficult to imagine how the asymmetric quadrature-speaker arrangement could produce standing waves. Extremely carefully adjusted dual quadrature-speaker sets might produce standing waves through interference of progressive waves of opposite helicity, but it is much more likely that only symmetric sources, like a line source along the top of the tube, could actually produce standing waves.

The analysis includes as a special case the purely radial acoustic modes in which the particles oscillate along lines through the center of the tube. The inviscid forms of these modes automatically satisfy the no slip boundary

conditions and therefore require no viscous corrections. They are obtained analytically by setting $n = 0$ throughout. In particular, Equation 13 shows, as expected, that there is no secondary vorticity. Therefore, Rayleigh streaming is not possible, but Eckart streaming is also impossible. Consider the Eckart streaming source term, Equation 6 (Section 3.2) for any mode in which the time and space dependence separate; for example,

$$\rho^{(1)} = \cos(\omega t)\, F$$

with F a function of the space variables only. Then, necessarily,

$$\nabla\rho^{(1)} \times \nabla \frac{\partial \rho^{(1)}}{\partial t} = -\omega \cos(\omega t) \sin(\omega t)\, \nabla F \times \nabla F$$
$$= 0$$

Thus Eckart streaming is possible only in progressive modes. The radial acoustic modes necessarily have the separated form $\cos(\omega t)\, F(r)$ of standing waves, so that Eckart streaming is impossible. Moreover, since $\Omega^{(1)} = 0$, the third term in Equation 6 (Section 3.2) is also zero.

The conclusion is that there is no secondary motion associated with these modes. However, the extremely high frequencies required to excite them ruled out experimental investigation of this prediction.

This analysis has assumed that a cut-off mode is excited. The acoustic field in these modes, and hence the secondary motion, is the same in every axial cross-section of the tube. Experimentally, modes with frequencies slightly higher than the cutoff are excited. These modes are not axially homogeneous; this is expressed analytically by axial sinusoidal variation of the acoustic field. The effect of this variation on the secondary motion is easily assessed; the particles move along the same circular paths in a progressive wave field, but the velocity

varies with axial position. In particular, regions of low velocity can develop so that the circulation may not extend throughout the tube. Axial nodes may even develop. The circulation will be in opposite directions on both sides of such a node. Both effects have been observed experimentally; in particular, circulation throughout the entire tube was never achieved.

3.5. Mixing due to Combined Axial and Spinning Modes

The vorticity source term in the Rayleigh streaming theory is quadratically nonlinear in the first order field quantities:

$$\nabla^2\Omega^{(2)} \sim \nabla \times (v^{(1)} \times \Omega^{(1)}) \tag{1}$$

Suppose that the first order field is a superposition:

$$V^{(1)} = V_a^{(1)} + V_b^{(1)}$$
$$\Omega^{(1)} = \Omega_a^{(1)} + \Omega_b^{(1)}$$

Such equations describe the field due to simultaneous operations of an axial-speaker and a quadrature-speaker set. Then the vorticity source is proportional to the curl of the steady part of

$$V_a^{(1)} \times \Omega_a^{(1)} + V_b^{(1)} \times \Omega_b^{(1)} + V_a^{(1)} \times \Omega_b^{(1)} + V_b^{(1)} \times \Omega_a^{(1)}$$

The first two terms are produced by each first order field acting separately, and the second two are interaction terms. But these interaction terms are retained only if they have the same frequency; otherwise, they do not contribute to the steady part. Thus, the difference between streaming due to progressive waves and standing waves can be described as an interaction effect: a standing

wave is the superposition of two progressive waves at the same frequency, and a progressive wave is the superposition of two standing waves at the same frequency. On the other hand, the frequencies of the axial-speaker and the quadrature-speaker set are quite different. Interaction would only be possible between the spinning mode and a very high order harmonic of the axial mode. This interaction seems unlikely.

The conclusion is that, if the first order fields superpose linearly due to the axial-speaker and the quadrature-speaker set, the secondary vorticity sources also superpose linearly. The result of this superposition would be an helical secondary velocity field in which the particles simultaneously rotate around the tube circumference and move along axial circulation cells. This simultaneous motion should produce greatly enhanced mixing. This was observed experimentally, although the complexity of the particle motions precluded even qualitative statements about the particle paths.

A possibility which perhaps deserves further consideration is that the first order acoustic fields interact nonlinearly to produce a more complex first order field. Nonlinear self-interaction of a finite amplitude sound wave is a well known phenomenon which leads to steepening of the waveform. The corresponding problem for finite amplitude spinning modes is addressed in Ref. [47]. However, the interaction between finite amplitude axial and spinning modes does not appear to have been studied, and may be important for this case of particle cloud mixing.

3.6. Acoustic Streaming in a Sphere

The analysis of streaming in a sphere presents no conceptually new features; naturally however, the details are somewhat more elaborate. Explicit formulas in the streaming calculation will necessarily be bulky and somewhat opaque. Nevertheless, it will be possible to use these expressions to answer several questions about streaming in a sphere.

1. Does a streaming velocity field exist with θ component everywhere negative? Such a streaming field would fill the sphere with powder even if all the powder began at the bottom of the sphere.
2. Experiments showed that for some modes, the powder was active when the speaker was 180° away, the normal configuration, but quiescent when it was 90° away. For other modes, this relationship was reversed. This suggests the possibility of a streaming velocity field in which the r component of streaming changes sign from $\theta = 180°$ to $\theta = 90°$. Do streaming modes with this property exist?
3. Is the sphere divided into circulation cells by planes through the lines of longitude? Alternatively, could a streaming field exist with ϕ component everywhere of one sign?

The analysis begins as usual with the evaluation of the exact first order velocity field. Eigenfunctions of the scalar Laplacian are expressed in standard notation [45] as

$$\Phi = j_m(kr)\ P_m^n(\cos\theta)\ e^{in\phi} \tag{1}$$

so that

$$\nabla^2\Phi = -k^2\Phi$$

Irrotational progressive and standing waves in a sphere are defined by

$$p = p_0 \cos(\omega t - n\phi)\, j_m(kr)\, P_m^n(\cos\theta) \qquad \text{(progressive)}$$

$$p = p_0 \cos(\omega t)\cos(n\theta)\, j_m(kr)\, P_m^n(\cos\theta) \qquad \text{(standing)}$$

Eigenfunctions of the vector Laplacian can be found as follows. Let

$$R_x = y\frac{\partial}{\partial z} - z\frac{\partial}{\partial y}, \qquad R_y = z\frac{\partial}{\partial x} - x\frac{\partial}{\partial z}, \qquad R_z = x\frac{\partial}{\partial y} - y\frac{\partial}{\partial x}$$

denote the infinitesimal operators for rotations about the coordinate axes. Then $R_x\Phi$, $R_y\Phi$, and $R_z\Phi$ are obviously eigenfunctions of the scalar Laplacian whenever Φ is. The vector

$$B = (R_x i + R_y j + R_z k)\Phi$$

is spherically symmetric and is obviously an eigenfunction of the vector Laplacian. But a simple computation shows

$$B = \nabla \times (x\Phi i + y\phi j + z\Phi k) = \nabla \times (r\Phi u_r)$$

With Φ defined by Equation 1,

$$\nabla^2 B = -k^2 B$$

Therefore also

$$\nabla^2 \nabla \times B = -k^2 \nabla \times B$$

It follows that $\nabla \times (r\Phi)u_r$ and $\nabla \times \nabla \times (r\Phi)u_r$ are both eigenfunctions of the vector Laplacian [44].

The evaluation of modes satisfying the no slip boundary conditions closely follows the analogous computation in the cylindrical coordinate system. Define the functions

$$\Phi = j_m\left(\frac{\omega r}{c}\right) P_m^n(\cos\theta)\, e^{i\omega t} e^{in\phi}$$

$$\Psi = j_m\left(\sqrt{\frac{i\omega}{\nu}} r\right) P_m^n(\cos\theta)\, e^{i\omega t} e^{in\phi}$$

and set

$$s^{(1)} = A\Phi$$

$$\Omega^{(1)} = B\nabla \times (r\Psi u_r)$$

Then

$$V^{(1)} = -A\frac{c^2}{\omega^2}\nabla s^{(1)} + B\frac{\nu}{i\omega}\nabla \times \Omega^{(1)}$$

As in the calculation in cylindrical coordinates, viscous corrections to the frequencies will be ignored; the frequencies are therefore roots of the equation

$$j_m'\left(\frac{\omega R}{c}\right) = 0$$

Modes which approximately satisfy the no slip boundary conditions are

$$V_\theta^{(1)} = V\left[\frac{R}{r}\,\frac{j(\frac{\omega r}{c})}{j(\frac{\omega R}{c})} - \frac{\sqrt{\frac{i\omega}{\nu}}\, j'\left(\sqrt{\frac{i\omega}{\nu}} r\right) + \frac{1}{r}\, j\left(\sqrt{\frac{i\omega}{\nu}} r\right)}{\sqrt{\frac{i\omega}{\nu}}\, j'\left(\sqrt{\frac{i\omega}{\nu}} R\right) + \frac{1}{R}\, j\left(\sqrt{\frac{i\omega}{\nu}} R\right)}\right]\frac{dP}{d\theta}\, e^{i\omega t} e^{in\phi}$$

$$V_\phi^{(1)} = iV\left[\frac{R}{r}\,\frac{j(\frac{\omega r}{c})}{j(\frac{\omega R}{c})} - \frac{\sqrt{\frac{i\omega}{\nu}}\, j'\left(\sqrt{\frac{i\omega}{\nu}} r\right) + \frac{1}{r}\, j\left(\sqrt{\frac{i\omega}{\nu}} r\right)}{\sqrt{\frac{i\omega}{\nu}}\, j'\left(\sqrt{\frac{i\omega}{\nu}} R\right) + \frac{1}{R}\, j\left(\sqrt{\frac{i\omega}{\nu}} R\right)}\right]\frac{nP}{\sin\theta}\, e^{i\omega t} e^{in\phi}$$

$$V_r^{(1)} = V\left[\frac{cR}{\omega}\,\frac{j'(\frac{\omega r}{c})}{j(\frac{\omega R}{c})} + \frac{n(n+1)}{r}\,\frac{j\left(\sqrt{\frac{i\omega}{\nu}} r\right)}{\sqrt{\frac{i\omega}{\nu}}\, j'\left(\sqrt{\frac{i\omega}{\nu}} R\right) + \frac{1}{R}\, j\left(\sqrt{\frac{i\omega}{\nu}} R\right)}\right] P\, e^{i\omega t} e^{in\phi}$$

$$\Omega_\theta^{(1)} = V\,\frac{\omega}{\nu}\,\frac{j\left(\sqrt{\frac{i\omega}{\nu}} r\right)}{\sqrt{\frac{i\omega}{\nu}}\, j'\left(\sqrt{\frac{i\omega}{\nu}} R\right) + \frac{1}{R}\, j\left(\sqrt{\frac{i\omega}{\nu}} R\right)}\,\frac{P}{\sin\theta}\, e^{i\omega t} e^{in\phi} \qquad (2)$$

$$\Omega_{\phi}^{(1)} = iV\frac{\omega}{\nu}\frac{j\left(\sqrt{\frac{i\omega}{\nu}}r\right)}{\sqrt{\frac{i\omega}{\nu}}j'\left(\sqrt{\frac{i\omega}{\nu}}R\right)+\frac{1}{R}j\left(\sqrt{\frac{i\omega}{\nu}}R\right)}\frac{dP}{d\theta}e^{i\omega t}e^{in\phi}$$

In order to lighten the notation, the indices on the spherical Bessel functions, Legendre polynomials, and frequencies have been omitted. Since $R\sqrt{\frac{\nu}{\omega}}$ is small, the Bessel function ratios with complex arguments can be approximated by

$$\frac{\sqrt{\frac{i\omega}{\nu}}\,j'\left(\sqrt{\frac{i\omega}{\nu}}r\right)+\frac{1}{r}j\left(\sqrt{\frac{i\omega}{\nu}}r\right)}{\sqrt{\frac{i\omega}{\nu}}\,j'\left(\sqrt{\frac{i\omega}{\nu}}R\right)+\frac{1}{R}j\left(\sqrt{\frac{i\omega}{\nu}}R\right)} \sim e^{\sqrt{\frac{\omega}{\nu}}(R-r)(1-i)}$$

$$\frac{\sqrt{\frac{i\omega}{\nu}}\,j\left(\sqrt{\frac{i\omega}{\nu}}r\right)}{\sqrt{\frac{i\omega}{\nu}}j'\left(\sqrt{\frac{i\omega}{\nu}}R\right)+\frac{1}{R}j\left(\sqrt{\frac{i\omega}{\nu}}R\right)} \sim \frac{1}{i}\,e^{\sqrt{\frac{\omega}{\nu}}(R-r)(1-i)}$$

The progressive waves are found by taking real and imaginary parts in Equation 2:

$$\begin{aligned}
V_{\theta}^{(1)} \sim & V\left[\frac{R}{r}\frac{j\left(\frac{\omega r}{c}\right)}{j\left(\frac{\omega R}{c}\right)}\cos(\omega t+n\phi)\right. \\
& \left. - e^{\sqrt{\frac{\omega}{\nu}}(R-r)}\cos\left(\omega t+n\phi-\sqrt{\frac{\omega}{\nu}}(R-r)\right)\right]\frac{dP}{d\theta} \\
V_{\phi}^{(1)} \sim & -V\left[\frac{R}{r}\frac{j\left(\frac{\omega r}{c}\right)}{j\left(\frac{\omega R}{c}\right)}\sin(\omega t+n\phi)\right. \\
& \left. - e^{\sqrt{\frac{\omega}{\nu}}(R-r)}\sin\left(\omega t_n\phi-\sqrt{\frac{\omega}{\nu}}(R-r)\right)\right]\frac{nP}{\sin\theta} \qquad (3) \\
V_{r}^{(1)} \sim & V\left[\frac{\omega R}{c}\frac{j_m'\left(\frac{\omega r}{c}\right)}{j_m\left(\frac{\omega R}{c}\right)}\cos(\omega t+n\phi)\right. \\
& \left. + \frac{n(n+1)}{r}\sqrt{\frac{\nu}{\omega}}\,e^{\sqrt{\frac{\omega}{\nu}}(R-r)}\sin\left(\omega t+n\phi-\frac{\pi}{4}-\sqrt{\frac{\omega}{\nu}}(R-r)\right)\right]P
\end{aligned}$$

$$\Omega_\theta^{(1)} \sim V\sqrt{\frac{\omega}{\nu}}\, e^{\sqrt{\frac{\omega}{\nu}}(R-r)} \sin(\omega t + n\phi - \frac{\pi}{4} - \sqrt{\frac{\omega}{\nu}}(R-r))\, \frac{nP}{\sin\theta}$$

$$\Omega_\phi^{(1)} \sim V\sqrt{\frac{\omega}{\nu}}\, e^{\sqrt{\frac{\omega}{\nu}}(R-r)} \sin(\omega t + n\phi + \frac{\pi}{4} - \sqrt{\frac{\omega}{\nu}}(R-r))\, \frac{dP}{d\theta}$$

Standing waves are found by superposing solutions in Equation 2 with values $\pm n$ and taking real and imaginary parts:

$$V_\theta^{(1)} \sim V\left[\frac{R}{r}\,\frac{j\left(\frac{\omega r}{c}\right)}{j\left(\frac{\omega R}{c}\right)}\cos(\omega t)\cos(n\phi)\right.$$
$$\left. - e^{\sqrt{\frac{\omega}{\nu}}(R-r)}\cos(\omega t - \sqrt{\frac{\omega}{\nu}}(R-r))\cos(n\phi)\right]\frac{dP}{d\theta}$$

$$V_\phi^{(1)} \sim -V\left[\frac{R}{r}\,\frac{j\left(\frac{\omega r}{c}\right)}{j\left(\frac{\omega R}{c}\right)}\cos(\omega t)\sin(n\phi)\right.$$
$$\left. - e^{\sqrt{\frac{\omega}{\nu}}(R-r)}\cos(\omega t - \sqrt{\frac{\omega}{\nu}}(R-r))\sin(n\phi)\right]\frac{nP}{\sin\theta} \qquad (4)$$

$$V_r^{(1)} \sim V\left[\frac{\omega R}{c}\,\frac{j_m'\left(\frac{\omega r}{c}\right)}{j_m\left(\frac{\omega R}{c}\right)} + \right.$$
$$n^2\sqrt{\frac{\nu}{\omega}}\,\frac{1}{r}\cos(n\phi)\, e^{\sqrt{\frac{\omega}{\nu}}(R-r)}\sin(\omega t - \frac{\pi}{4} - \sqrt{\frac{\omega}{\nu}}(R-r))$$
$$\left. + n\sqrt{\frac{\nu}{\omega}}\,\frac{1}{r}\sin(n\phi)\, e^{\sqrt{\frac{\omega}{\nu}}(R-r)}\cos(\omega t - \frac{\pi}{4} - \sqrt{\frac{\omega}{\nu}}(R-r))\right] P$$

$$\Omega_\theta^{(1)} \sim V\sqrt{\frac{\omega}{\nu}}\sin(n\phi)\, e^{\sqrt{\frac{\omega}{\nu}}(R-r)}\cos(\omega t - \frac{\pi}{4} - \sqrt{\frac{\omega}{\nu}}(R-r))\, \frac{nP}{\sin\theta}$$

$$\Omega_\phi^{(1)} \sim V\sqrt{\frac{\omega}{\nu}}\cos(n\phi)\, e^{\sqrt{\frac{\omega}{\nu}}(R-r)}\sin(\omega t + \frac{\pi}{4} - \sqrt{\frac{\omega}{\nu}}(R-r))\, \frac{dP}{d\theta}$$

In computing the secondary velocity, the second order compressibility will be ignored. This approximation can be justified by Rayleigh's calculation for axial standing waves [43], which showed that the second order compressibility was indeed negligible compared to the second order vorticity components, but it

also seems reasonable *a priori* in any case. Thus, taking the curl of Rayleigh's Equation 6, (Section 3.2),

$$\nabla^4 V^{(2)} = -\frac{\nabla \times \nabla \times (V^{(1)} \times \Omega^{(1)})}{\nu} \tag{5}$$

Consider the modes with $n = 0$. Explicit calculation using Equation 4 shows that the source term in Equation 5 has the form

$$u_r \left[A(r) \frac{1}{\sin\theta} \frac{d}{d\theta} \left(P \frac{dP}{d\theta} \sin\theta \right) + B(r) \frac{d}{d\theta} \left(\frac{dP}{d\theta} \frac{d^2P}{d\theta^2} \sin\theta \right) \right]$$
$$+ u_\theta \left[C(r) P \frac{dP}{d\theta} + D(r) \frac{dP}{d\theta} \frac{d^2P}{d\theta^2} \right] \tag{6}$$

As in cylindrical coordinates, the functions $A(r), \cdots D(r)$ are boundary layers, but their exact dependence on r will have no importance in the analysis.

The Legendre polynomials are alternately odd and even functions of $\theta - \frac{\pi}{2}$:

$$P_0^0 = 1 \qquad P_1^0 = \cos\theta \qquad P_2^0 = 3\cos^2\theta - 1, \cdots$$

The source strength for secondary motion vanishes for P_0 as expected: such acoustic modes are purely radial, they satisfy the no slip conditions exactly, and they therefore require no viscous corrections. For the nonradial modes which contain P_m, $m \geq 1$, the θ component of the source strength is always an odd function of $\theta - \frac{\pi}{2}$; it is the product of consecutive order derivatives one of which must be odd and the other even, regardless of the parity of P_m. In fact, it is easy to check that this component always contains the factor $\sin\theta \cos\theta$, which vanishes on the equatorial plane $\theta = \frac{\pi}{2}$. It follows that both the particular and homogeneous solutions for $V^{(2)}$ required by Equation 5 must also vanish on the equatorial plane; in particular, the homogeneous solution is a superposition of modes of the form

$$\nabla \times \nabla \times [r P_{2k}^{0}(\cos\theta)\, j(r)\, u_r]$$

The secondary velocity field therefore has ∂ vanishing θ component on the equatorial plane $\theta = \frac{\pi}{2}$, along which u_θ is the normal vector. The secondary velocity is tangential to this plane; therefore, the secondary streamlines remain either in the northern or the southern hemisphere. Steady streaming could not move powder between them.

The next question is whether this behavior also occurs in the modes $n \geq 1$. In the first place, it is obvious from Equations 3 and 4 that progressive and standing waves do not differ in this respect since their θ dependence is identical. The θ component of the source term in Equation 5 is given by

$$\frac{1}{r\sin\theta}\frac{\partial}{\partial\phi}\frac{1}{r\sin\theta}\left\{\frac{\partial}{\partial\theta}(\sin\theta V_r\Omega_\theta)+\frac{\partial}{\partial\theta}(V_r\Omega_\phi)\right\}$$
$$+\frac{1}{r}\frac{\partial}{\partial r}\left\{\frac{\partial}{\partial r}(rV_r\Omega_\phi)+\frac{\partial}{\partial\theta}(V_\theta\Omega_\phi - V_\phi\Omega_\theta)\right\}$$

Evaluating the θ dependence of these terms separately,

$$\frac{1}{r^2\sin^2\theta}\frac{\partial^2}{\partial\phi\partial\theta}(\sin\theta V_r\Omega_\theta) \sim \frac{1}{\sin^2\theta}\, P\,\frac{dP}{d\theta}$$
$$\frac{1}{r^2\sin^2\theta}\frac{\partial^2}{\partial\phi^2}(V_r\Omega_\phi) \sim \frac{1}{\sin^2\theta}\, P\,\frac{dP}{d\theta}$$
$$\frac{1}{r}\frac{\partial^2}{\partial r^2}(rV_r\Omega_\phi) \sim \frac{1}{\sin^2\theta}\, P\,\frac{dP}{d\theta}$$
$$\frac{1}{r}\frac{\partial^2}{\partial r\partial\theta}(V_\theta\Omega_\phi - V_\phi\Omega_\theta) \sim \frac{\partial}{\partial\theta}\left[\left(\frac{dP}{d\theta}\right)^2 - \left(\frac{P}{\sin\theta}\right)^2\right]$$

Since $\sin^2\theta$ is an even function, all of these terms are obviously odd, except for the last one. But $P_m^n(\cos\theta)$ is the product of $\sin\theta$ and an odd or an even function; therefore, the last term is necessarily odd as well.

This discussion answers the first question negatively. Steady Rayleigh streaming in a sphere, whether due to standing or to progressive waves, necessarily separates the sphere into noncommunicating hemispheres. The addition of a second speaker would only change the position of the nodal plane. Unless the speakers and powder can be arranged so that the nodal plane bisects the powder, complete mixing throughout the sphere by steady Rayleigh streaming is not possible.

It must not be concluded, however, that mixing in a sphere is unsuitable for particle cloud experiment. In the first place, in micro-gravity, the particles will continue in straight lines along their instantaneous velocity vectors if the speaker is turned off. By operating the speaker in bursts, the particles could certainly be made to migrate from the southern to the northern hemisphere. Second, powder must be removed from the sphere to the combustion tube in any case. Well-mixed powder occupying only half the sphere could therefore be entirely satisfactory.

A related question concerns the possible existence of radial circulation cells. As in the analysis of streaming in a cylinder, the preliminary conclusion is that such cells will not occur because the secondary vorticity source $\Omega^{(2)}$ is concentrated at the surface of the sphere.

The analysis also answers the second question. Namely, consider the acoustic modes $m = 1$, $n = 0$ containing the function P_1^0. For these modes, the particular and homogeneous solutions for $V^{(2)}$ contain contributions from the mode

$$\nabla \times \nabla \times (rjP_2^0 u_r) = u_r A(r)(3\cos^2\theta - 1) + u_\theta B(r)\sin(2\theta)$$

in which the r component changes sign from $\theta = 180°$ to $\theta = 90°$. Clearly, if the r component of secondary velocity is positive, the powder is pushed toward the

wall, and if it is negative, the powder is drawn into the sphere. In the first case, the powder is quiescent; in the second case, it is active. Thus, depending on the sign of A(r), it is possible for the powder to be active when it is 180° from the speaker and quiescent at 90° from the speaker, or for the behavior at these two angles to be interchanged. Naturally, this sign change in the r component occurs more generally. It can be checked, for example, for the acoustic modes $m = 3$, $n = 0$.

Comparison of Equations 3 and 4 at once answers the third question. It is evident that dependence of the first order quantities on the angle ϕ in spherical coordinates resembles in every respect their dependence on the angle θ in cylindrical coordinates. Thus, progressive acoustic modes generate secondary flows which circulate around parallels of latitude, whereas standing waves cause the familiar quarter-wavelength behavior which partitions the sphere into $4m$ circulation cells. Provided that each cell contains the same amount of powder initially, this partitioning will not prevent satisfactory mixing. This condition appears to be satisfied by the experimental set up with the speaker and powder at antinodal points so that the cell boundaries are planes through the line connecting these points.

Left partially unanswered was the question of whether steady streaming could fill the sphere if the nodal plane could be made to bisect the powder initially. The second and third questions are both relevant to the possible success of such an attempt. First, it would be preferable to arrange a negative r component of secondary velocity around the powder. Second, a nonzero ϕ component free of circulation cells is necessary. This completely rules out using any of the modes

$n = 0$ and also requires the use of progressive waves. Symmetry considerations strongly suggest that a single speaker generates standing waves, so that a dual speaker arrangement could be mandatory. But it is not obvious in advance where the corresponding nodal equatorial plane will be located; this would have to be determined either analytically or experimentally.

4. Experimental Work

Several experiments were conducted in a two-inch diameter cylindrical Lexan combustor to investigate the feasibility of acoustic mixing of lycopodium powder in a micro-gravity environment. Smoke was used to visualize the flow patterns due to acoustic streaming for different frequencies, amplitudes, phase angles between loudspeakers, and combustor terminations. These experiments were also repeated using lycopodium particles to test the effectiveness of the mixing process.

This study mainly concentrates on the effect of high-frequency, higher-order modes (i.e., where sound wavelength is shorter than the radius of the combustor pipe) on the mixing process. All of the tests were carried out at 1-g.

A quadrature-speaker arrangement was used first. This set up consists of a rudimentary spinning mode synthesizer designed to excite non-axial high-frequency spinning waves in the combustor. It results in a fairly homogeneous sound field in the combustor axial direction.

Next, several configurations were tested, including two opposite sets of quadrature-speaker; an axial-speaker and quadrature-speaker set combination; and anechoic, reflecting, and pressure release terminations.

Finally, mixing experiments were conducted in a seven-inch diameter sphere to study the effect of several higher-order modes on the mixing process and to examine the feasibility of using a sphere for the pre-mixing of particles. This test was also used to give us better insight into the physics of the acoustic mixing process.

4.1. Experimental Setup

4.1.1. Quadrature-Speaker Experiments

The first experimental setup is shown in Figure 10. The quadrature-speaker set consists of two 908-8B Altec Lansing compression driver loudspeakers mounted at a 90° angle from each other. The high efficiency and high power rating of these drivers (30 to 100 Watts) allow sound pressure levels of up to 150 dB inside the combustor in the 1 KHz to 10 KHz frequency range. This provides enough acoustic energy to induce the relatively large lycopodium particles to move within an 1-g environment. Each loudspeaker is driven by a wave generator and an amplifier. Voltages across the drivers are monitored by two digital voltmeters (DVM) to ensure that no excessive loads are applied to the loudspeakers. The relative phase between loudspeakers is controlled by a phase-lock wave generator.

The sound field inside the combustor is monitored using several flush-mounted Endevco Model 8510 five-psi pressure transducers connected to a set of signal conditioners, filters, and amplifiers. An FFT analyzer, an oscilloscope, a frequency counter, and a DVM are used to analyze the amplitude and phase characteristics of the transducers signals.

A radial and an axial microphone probe were designed to measure the three-dimensional sound field in the combustor two-inch pipe. The 35-inch axial probe can be moved along the combustor centerline to measure the axial sound pressure distribution, the axial wavelength, and the magnitude of the axial standing wave. The $2\frac{1}{2}$-inch radial probe can be moved along one of the

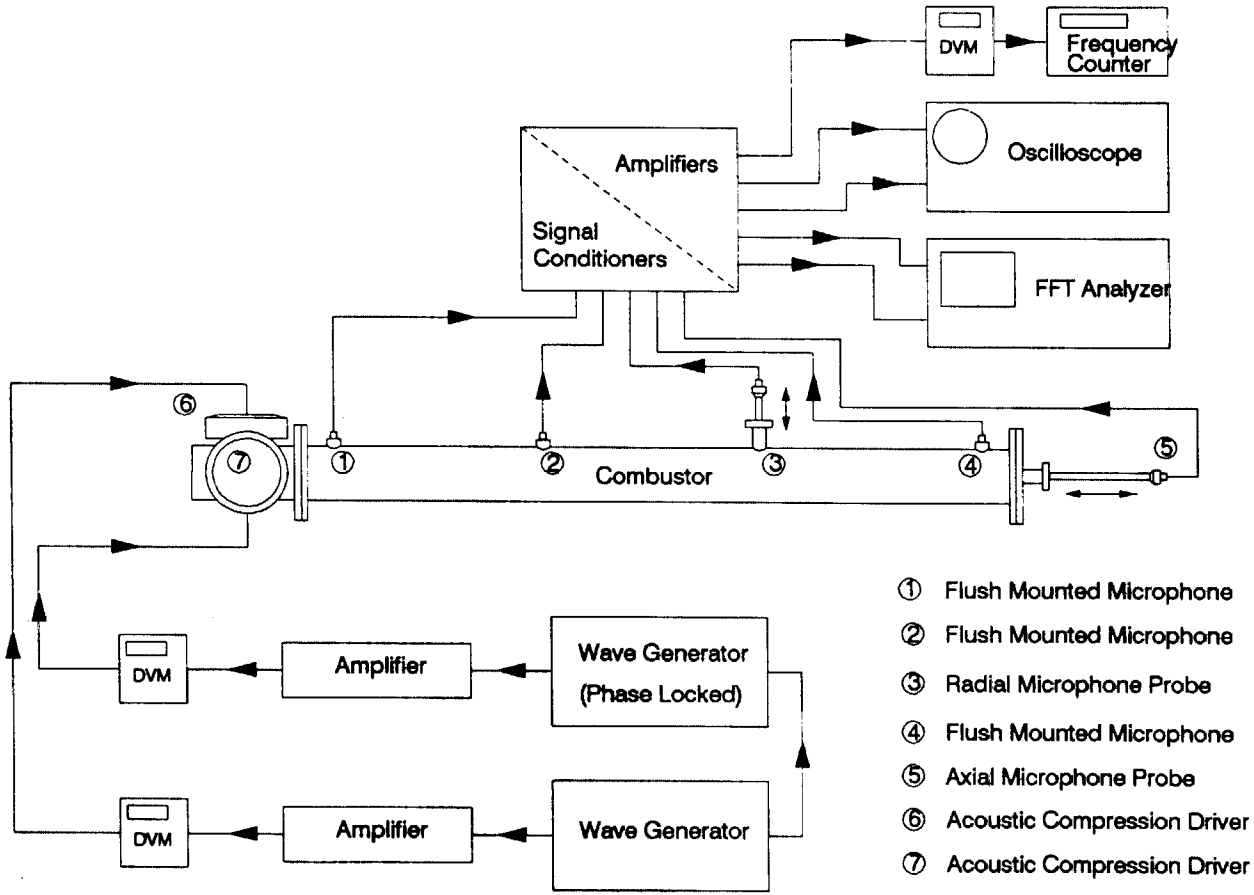

Figure 10. Quadrature Speaker Experiment

combustor radial lines (i.e., in the cross sectional plane and through the pipe center) to measure the radial sound pressure distribution. The radial probe is used for modal identification of the sound field, thus allowing us to distinguish among spinning, radial, and plane-wave modes. Accurate measurement of the combustor resonance frequencies can be made using the microphone probes and the frequency counter.

In the case of the smoke experiments, cigarette smoke was introduced using ports located near microphones 1, 2, and 4.

Another experiment was performed using two sets of quadrature-speaker mounted at each end of the combustor (see Figure 11, Part 2).

4.1.2. Axial-Speaker and Quadrature-Speaker Experiment

The third experimental set up is shown in Figure 12. It is similar to the quadrature-speaker experiment except for the addition of a low frequency axial-speaker mounted behind the quadrature-speaker set. The axial-speaker used was a modified 4C10PA QUAM four-inch eight-ohm loudspeaker driven in the 10- to 15-Watts range. The "axial-speaker alone" configuration was tested as shown in Figure 11, Part 3. In the design frequency range, the efficiency of the loudspeaker is very low compared to the Altec Lansing compression drivers used for the quadrature-speaker set. However, the QUAM driver was used most of the time at very low frequencies (100 Hz to 200 Hz) around its mechanical resonance frequency, thereby boosting its efficiency to a level equal to or higher than the efficiency of the Altec Lansing drivers.

In another experiment, the low frequency axial-speaker was mounted at the combustor end opposite to the quadrature-speaker set (see Figure 11, Part 5).

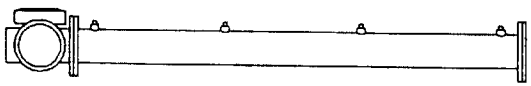

1. Quadrature-Speaker

2. Double Quadrature-Speaker Set

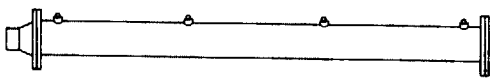

3. Axial-Speaker

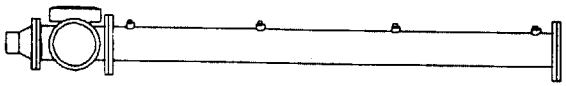

4. Axial-Speaker and Quadrature-Speaker (a)

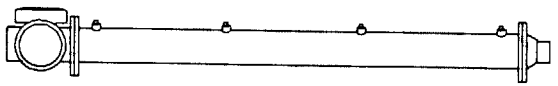

5. Axial-Speaker and Quadrature-Speaker (b)

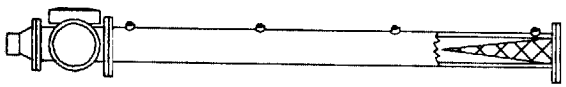

6. Anechoic Termination

Figure 11. Experimental Configurations

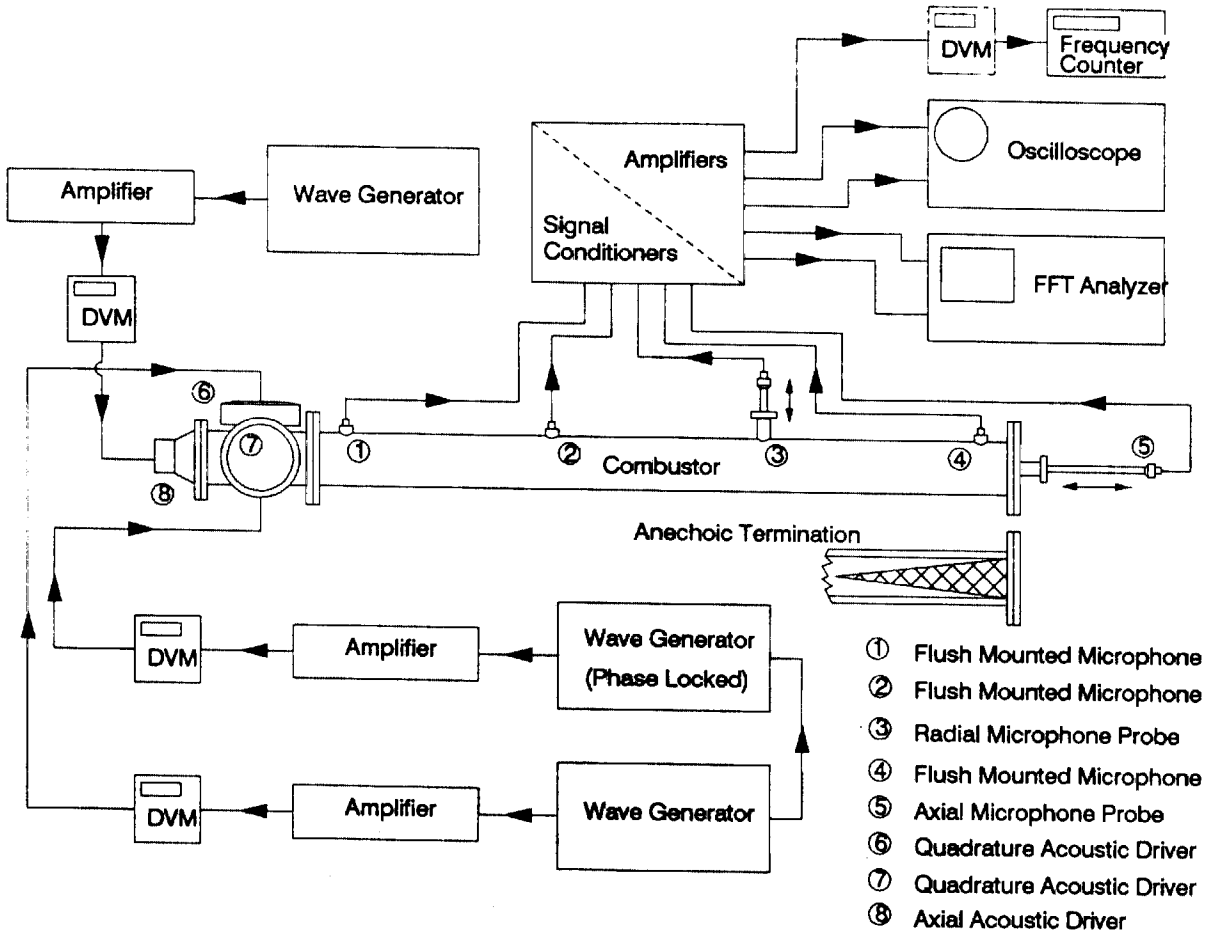

Figure 12. Axial-Speaker and Quadrature-Speaker Experiment

The fifth test performed is shown in Figure 11, Part 6. The set up is similar to the first axial-speaker and quadrature-speaker combination with the addition of an anechoic termination. This type of termination is designed to absorb sound waves incident on its surface, thereby preventing sound reflection and axial standing waves inside the combustor pipe. The termination used consisted of an eight-inch long cone made of a thin lightweight plastic mesh filled with fiberglass material. Tests showed that the termination performed extremely well at high frequencies (quadrature-speaker frequency range) and well at lower frequencies (axial-speaker frequency range), thus allowing an homogeneous axial sound distribution.

4.1.3. Sphere Acoustic Premix Experiment

Figure 13 is a schematic of the sphere acoustic premix experimental set up. A seven-inch diameter, transparent plastic sphere is mounted in a support frame. A 290-8K Altec Lansing Compression Driver Loudspeaker mounted vertically on top of the sphere through a $1\frac{1}{2}$-inch hole provides the acoustic power required for this experiment in the 500 Hz to 10 KHz frequency range. Again, the high efficiency and high power rating (120 Watts) of the acoustic driver allow for a high enough sound pressure level in the sphere for this experiment. A radial microphone probe was designed to measure the three-dimensional sound field inside the sphere. The probe can be moved across one of the sphere radial lines (i.e., in the cross sectional plane and through the sphere center) to measure the spatial distribution of the sound field. This gives the modal characteristics of the sound field, thus allowing us to distinguish between radial and circumferential modes, and to measure the sphere resonance frequencies accurately.

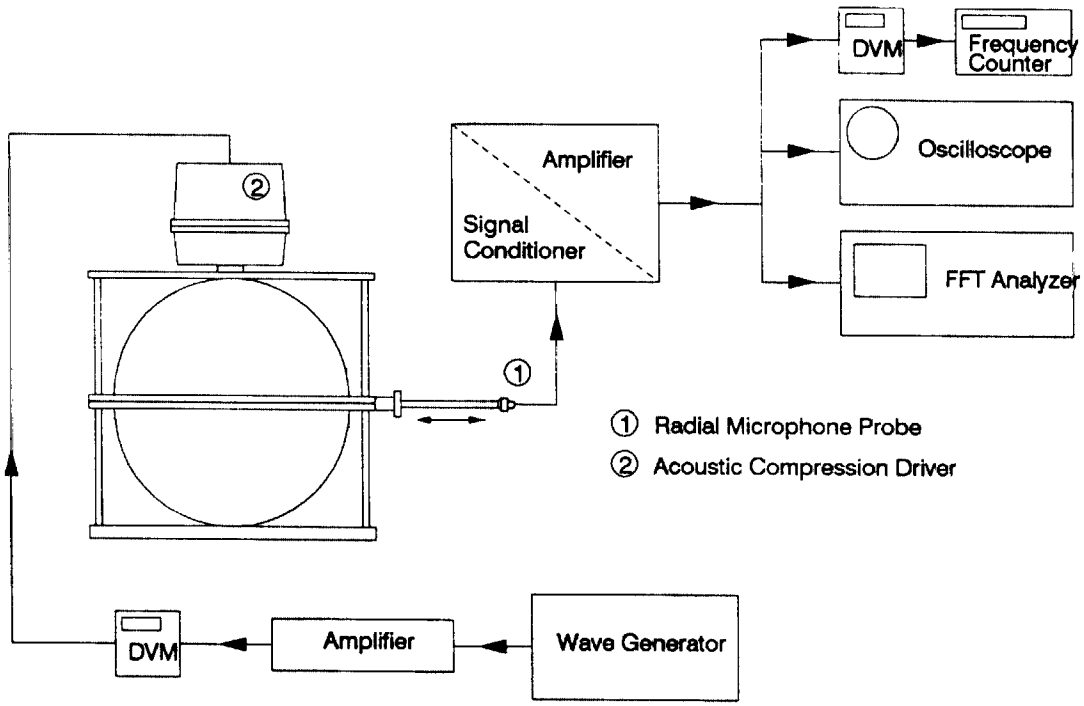

Figure 13. Sphere Experiment

4.2. Results

With each of the experimental set ups described previously, cigarette smoke and lycopodium powder were used to investigate the mixing process.

Smoke particles which have a diameter on the order of less than one micron have an entrainment rate very close to unity in the frequency range of interest. The motion of smoke particles is thus representative of the acoustic velocities and of the steady flow in the system. It can be used to visualize the acoustic streaming (such as medium scale streaming) for different frequencies, amplitudes, and phase angles between loudspeakers.

Lycopodium particles, on the other hand, are relatively large, having a mean diameter of 22 microns, and a density of 1020 kg/m^3. Thus at high frequencies, the particles are not entrained by the sound wave and their motion is not representative of the acoustic velocities. However, streaming and steady flows still affect the particles.

4.2.1. Quadrature-Speaker Experiment

4.2.1.1. Smoke Particles

Tests were first carried out using smoke particles. When the first spinning mode is excited (lowest non-plane wave mode: cutoff frequency of 3920 Hz) the smoke particles are violently entrained, spinning inside the tube. Good mixing is obtained over axial distances equal to several sound wavelengths, as opposed to 1/4 wavelength in the case of low frequency mixing using an axial-speaker. The particle motion is very dependent on frequency, with no motion below the cut-off frequency. The best mixing is obtained right above the cut-off frequency

of the first spinning mode and for frequencies as far apart as possible from the axial resonance frequencies (the axial resonance frequencies for a plane wave in the combustor are 220 Hz apart from each other).

The mixing process is limited in part due to the inefficiencies and the large losses inherent in the high frequency of operation needed to excite the first spinning mode.

Effect of the Relative Phase Difference Between Speakers

Changes in relative phase between the two loudspeakers does not seem to affect the mixing of smoke significantly. Intuitively, the first spinning mode should be best excited for a relative phase difference of 90°, whereas a 0° relative phase angle should favor the plane wave component. However, as evidenced by the probe measurements, the effect of phasing on the sound field in the combustor is not as important as was first expected. This is mainly due to the non-symmetry in the two-speaker array used. A larger array of speakers regularly spaced along the combustor cicumference would allow much better control of the modal content of the sound field inside the pipe.

Axial Standing Waves

Some axial inhomogeneities were observed due mainly to the presence of axial standing waves as a result of the non-anechoic end termination.

As discussed earlier in this report, the main reason for the use of high-frequency spinning modes for mixing is the vorticity generated, which moves the particles in a circumferential motion in the combustor cross-sectional plane

rather than in the combustor axial plane. However, as in the case of the low-frequency axial-speaker, axial standing waves are still present in the system above the cut-off frequency of the first spinning mode, due to the rigid termination at the combustor end. Previous experimental work carried out with a low-frequency axial-speaker has shown that mixing in a plane (axial) standing wave acoustic field occurs in cells that are 1/4 wavelength long each. Perfect mixing would require the size of the cells to fill the combustor completely, therefore requiring a very low frequency of operation. This low frequency of operation is in practical using conventional acoustic drivers, and results in strong inhomogeneities in the axial particle distribution. However, in the case of high-frequency spinning-modes, the acoustic wavelength along the combustor centerline goes from infinity at the cut-off frequency of the mode to its plane wave value at an infinite frequency. Thus the use of a spinning mode at or very close to its cut-off frequency allows axial standing waves that have nodes much farther apart than if a plane wave mode having the same frequency were excited. This results in larger "mixing cells" and better overall mixing. This effect can be optimized by using a cylindrical combustor having a diameter no smaller than about 5 to 10 times the combustor length.

Other Higher-Order Modes

The effect of other higher-order modes on the acoustic mixing was not investigated because their cut-off frequencies are outside the frequency range required for the effective mixing of lycopodium particles.

4.2.1.2. Lycopodium Particles

The results obtained with lycopodium are fairly similar to the smoke tests, except for a much stronger dependence of the particle motion on the relative phase difference between the two loudspeakers, and the increased effect of gravity. Again, the mixing was shown to be very dependent on frequency, and did not fill the combustor completely due to sound inhomogeneities in the axial direction. Due to the sharpness of the resonances, the proper setting of the excitation frequency was critical in reaching optimum mixing. This was clearly demonstrated by the fact that introducing a $\frac{1}{4}$ inch probe at the center of the combustor completely stopped the mixing process, which started again when the frequency was shifted a few Hertzs.

The difference in mixing between smoke and lycopodium is due to the varying magnitude of the small scale streaming around each particle, which depends on size and density, as discussed in the first section of this report.

4.2.2. Double Quadrature-Speaker Set Experiment

Some tests were carried out with a second set of quadrature-speakers mounted at the combustor end, opposite to the first loudspeaker set (see Figure 11, Part 2).

The purpose of this experiment was to increase the sound pressure level inside the combustor in order to enhance the mixing process.

Very little mixing is obtained with this configuration with either smoke or lycopodium particles. This is due to destructive interferences between the two spinning waves generated by each quadrature-speaker set, as well as to strong reflections from the tube's rigid ends. Better mixing is possible by properly phasing the four loudspeakers together to prevent destructive interferences, and by using anechoic end terminations to remove the reflections from the rigid terminations. However, no further work was done with this set up because the potential mixing improvements are small and do not seem to justify the greatly increased complexity of the system.

4.2.3. Axial-Speaker Alone Experiment

The aim of this experiment was to briefly investigate the effect of the first few axial resonances of the combustor on the mixing process so that it could be separated from the effect of the quadrature-speaker set in further tests (see Figure 11, Part 3).

Smoke Particles

Very little smoke movement was observed, although the amplitude of the acoustic vibration was much higher than with the quadrature-speaker set up. A very slow moving pattern seemed to develop which was similar to the one obtained by Andrade [10] in previous experiments.

Lycopodium Particles

Tests done with lycopodium particles found large powder concentrations at the antinodes of the standing wave as a result of the circulation from to medium scale streaming. Tests done with lycopodium particles also found smaller concentrations in fine striations a few millimeters apart from each other that were moving in a direction perpendicular to the sound wave as a result of small scale streaming. Some rotational particle motion was apparent in each 1/4-wavelength cell, as well as a general migration of the particles toward the end opposite to the loudspeaker.

No further work was done with this set up because this study concentrates mainly on the effect of non-plane wave modes on the mixing process.

4.2.4. Axial-Speaker and Quadrature-Speaker Experiment

The fourth configuration tested included the low frequency axial-speaker and the quadrature-speaker arrangements mounted at one end of the combustor tube (see Figure 11, Part 4).

Smoke Particles

The use of both configurations together greatly enhances the mixing process, producing tremendous smoke agitation in the pipe. This set up seems to produce the best results of all those tested so far.

Small axial inhomogeneities still exist, preventing perfect mixing. However, the mixing obtained might still be good enough for combustion purposes, especially if the axial sound source is turned on only for a short period of time

(transient mode of operation). In addition, axial inhomogeneities develop at a much slower pace using the high frequency quadrature-speaker set up than using the low frequency axial-speaker arrangement. Partly because the low frequency axial-speaker setup operates at resonance and depends on standing waves, i.e., axial inhomogeneities, to generate high sound pressure levels.

Lycopodium Particles

With lycopodium particles, mixing is greatly increased occurred compared to the quadrature-speaker or axial-speaker alone configurations. Again, this is due to the mutual reinforcement of both mixing processes. Also, as in previous experiments with lycopodium, mixing was much more sensitive to relative phase differences between the quadrature speakers than in the case of smoke mixing.

In a fifth configuration (see Figure 11, Part 5), the axial-speaker was mounted opposite to the quadrature-speaker set. No noticeable difference was observed between this set up and the previous one, which had used both speaker sets mounted at the same end.

4.2.5. Anechoic Termination

As mentioned in the previous section, the combination of axial and spinning waves results in poor axial homogeneity in the powder distribution. This poor homogeneity is due to the strong axial standing wave present in the combustor. Although this standing wave seems to be the major factor responsible for the mixing at low frequencies, its presence prevents "perfect mixing".

The standing wave is generated by the interaction between incident sound waves from the loudspeakers and sound waves reflected from the rigid termination

at the end of the combustor. Thus the rigid plate terminating the combustor was replaced by an anechoic (no echo) termination. This type of termination is designed to absorb sound waves incident on its surface, thus preventing the formation of standing waves.

The experiments run were disappointing although not surprising. When the loudspeakers were turned on, the lycopodium powder was very quickly blown towards the anechoic termination by the axial component of the traveling sound wave. Although the sound pressure level was constant in the axial direction, the sound propagated away from the loudspeakers, entraining the particles as a result of radiation pressure and streaming in the bulk of the fluid.

To ensure that the particle motion was not caused by air leaks in the system, the experiment was repeated using a carefully sealed combustor and loudspeaker arrangement without microphone ports. When the sound source was turned on and streaming appeared, the particles were blown towards the rigid termination as in previous experiments.

This experiment clearly illustrates one of the fundamental problems inherent in steady state acoustic mixing: unless the sound field has no axial component, such as at the cut-off frequency of the first spinning mode, standing waves are necessary to prevent particles from being blown away from the sound source. However, by definition, the presence of standing waves means axial inhomogeneities, which prevent perfect mixing.

4.2.6. Sphere Acoustic Premix Experiment

One of the main motivations for the sphere experiment was to investigate the influence of several acoustic modes on the mixing process, especially radial

modes. A seven-inch diameter sphere was used for this test, as opposed to the two-inch diameter cylindrical combustor. The large diameter of the sphere allows at least seven modes (starting at 1260 Hz) to be excited using available acoustic drivers, as opposed to only one mode in the case of the cylindrical combustor. The first few acoustic modes inside the sphere are shown in Figure 14 along with the radial pressure distributions.

Little smoke particle motion is observed in the sphere at most frequencies and sound pressure levels. With lycopodium, no motion is recorded for purely radial modes (n = 0). Large powder motions are present when circumferential modes are excited (n > 0). However, due to the standing wave nature of the sound field, particle motion seems to occur in cells whose shape is dictated by the circumferential order of the mode excited (n) and by the source boundary condition. This is clearly illustrated by the fact that no motion occurs opposite the loudspeaker at certain frequencies, while violent motion occurs at the same frequencies and at a 90° angle from the loudspeaker (with the sphere lying on its side and the speaker axis horizontal). The opposite effect occurs at other frequencies, with violent motion opposite the loudspeaker, and no motion at a 90° angle from the loudspeaker.

To eliminate the "mixing cell effect" and obtain better mixing, a traveling spinning wave should be excited in the sphere. Although this might be achieved by using a properly phased loudspeaker array, it would greatly increase the complexity of the system.

Instad of a traveling wave a standing wave field similar to the field in the sphere could be obtained in the cylindrical combustor if the loudspeaker sources

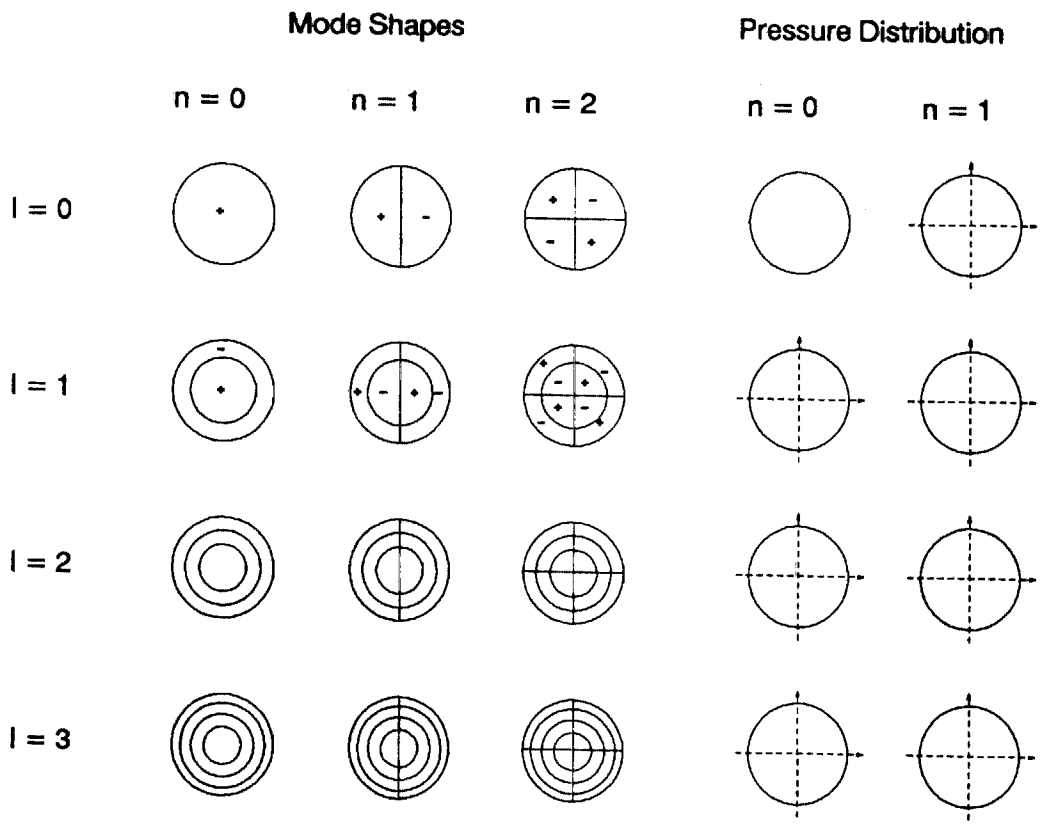

Figure 14. Sphere Experiment, Mode Shapes

were replaced by line sources running along the pipe wall parallel to the pipe axis. However, the effect on the mixing would be detrimental due to the "mixing cell effect" discussed above.

The main anticipated result for this experiment was that the dominant streaming mechanism in the acoustic mixing process arises from the interaction between the sound field and the boundary-layer at the combustor wall. Indeed, very little mixing was obtained when purely radial modes were excited. This corresponds to the case when the acoustic velocity is perpendicular to the wall and the interactions between the sound-field and the wall boundary-layer are very small. Inversely, large particle motions were recorded for circumferential modes when the interactions between the acoustic field and the sphere wall are large.

4.3. Conclusions

There does not seem to be a practical way to obtain perfect mixing under steady state conditions using sound waves. Particle concentrations due to axial inhomogeneities are unavoidable unless a pure spinning mode having an infinite phase velocity (i.e., no axial component) is excited at the cut-off frequency of the combustor, which is impossible to realize practically. However, the mixing obtained using a combination of low-frequency axial waves and high-frequency spinning waves, with a rigid termination might be sufficient for our purposes. The mixing process could also be improved by running the loudspeakers under transient conditions. This would prevent a strong build-up of the standing waves which are responsible for the inhomogeneities in the sound field.

5. Low-Frequency Acoustic Theory for PCCE Combustors

5.1. Introduction

This section describes the tools needed to study and predict the acoustic field in PCCE combustors at low frequencies. This knowledge is required to predict the resonance frequencies at which the system must operate, and to minimize the detrimental effect on the mixing process of such elements as instrument ports or diaphragms. The analysis is one-dimensional and assumes that only plane waves propagate in the system. The PCCE combustor studied consists of a cylindrical waveguide having a length several times its diameter. Although the theory presented here is for a tube (i.e., cylindrical cross-section), it is directly applicable to ducts of any cross-section as long as the low-frequency condition is satisfied.

5.2. Low-Frequency Condition

This section defines the term "low-frequency" as it applies to the analysis presented in this section. First, let's look at the definition of the sound wavelength λ:

$$\lambda = cT = \frac{c}{f} \tag{2.1}$$

where c is the speed of sound, T is the period, and f is the frequency of the sound wave. It is clear from Equation 2.1 that the higher the frequency, the shorter the sound wavelength.

When sound produced by a loudspeaker propagates in a waveguide, such as in a tube, several types of acoustic waves can exist, depending on the size of the sound wavelength.

- For short wavelengths (i.e., high frequency) compared to the typical cross-sectional dimension, the sound can "bounce" back and forth against the tube walls as it propagates along its axis. In this high-frequency mode of propagation, the sound pressure level in the tube cross-section is non-uniform (higher-order modes).
- For long wavelengths (i.e., low-frequency) compared to the typical cross-sectional dimension, the sound can only move along the tube axis, and the sound pressure level in the tube cross-section is uniform. The wave fronts are planar and the sound field is one-dimensional (zero-order mode or plane wave propagation).

The transition between the low-frequency and the high-frequency modes of propagation occurs at the cut-off frequency of the first non-planar mode for the particular waveguide used. This is the lowest frequency for which the first higher-order mode can exist.

For a rectangular waveguide (duct), the first mode occurs when the half-wavelength is equal to the shortest width a of the duct. Thus, the cutoff frequency of first mode f_{Crec} is given by:

$$f_{\mathrm{Crec}} = \frac{c}{2a} \tag{2.2}$$

Similarly, for a cylindrical waveguide such as the one used in the PCCE experiments, the first mode starts propagating when the half-wavelength is approximately equal to the duct diameter. The exact value is given by the root of the derivative of the Bessel function [45] and corresponds to the frequency f_{Ccyl} given by:

$$f_{\text{Ccyl}} = 0.584 \frac{c}{D} \tag{2.3}$$

where D is the tube diameter.

Theoretically, depending on the source type and the frequency spectrum of the excitation signal, non-plane waves, plane waves, or a combination of both can be generated in a waveguide. In practical cases, due to non-homogeneous source boundary conditions, acoustic attenuation, and the boundary-layer at the tube walls, a combination of both waves is always present. However, by using an excitation signal having frequencies much lower than the tube first cut-off frequency, it is possible to minimize the non-planar component in the sound field.

5.3. Wave Equation

The acoustic field in a combustor of arbitrary cross-section can be described at low frequency and moderate amplitude by the first order inviscid wave equation in one dimension:

$$\frac{d^2p}{dx^2} = \frac{1}{c^2}\frac{d^2p}{dt^2} \tag{3.1}$$

where p is the acoustic pressure, x is the axial distance along the combustor axis, and t is the time.

This equation is the basis of all the tools presented in this section and its solutions are presented for a variety of cases relevant to the acoustics of PCCE combustors.

The relationship between the acoustic velocity v and the acoustic pressure p is also needed to solve the wave equation. In one dimension, it is given by the momentum equation:

$$\rho_0 \frac{dv}{dt} = -\frac{dp}{dx} \tag{3.2}$$

where ρ_0 is the static density of the medium.

Assuming a harmonic pressure variation, Equation 3.2 can be rewritten in a more direct form as:

$$v = -\frac{1}{j\omega\rho_0}\frac{dp}{dx} \tag{3.3}$$

where ω is the radial frequency ($\omega = 2\pi f$).

5.4. Axial-Speaker in a Closed Tube

This simple configuration is representative of the case when an axial-speaker is mounted at one end of a tube of length L, with the other end closed by a rigid termination such as shown in the figure below.

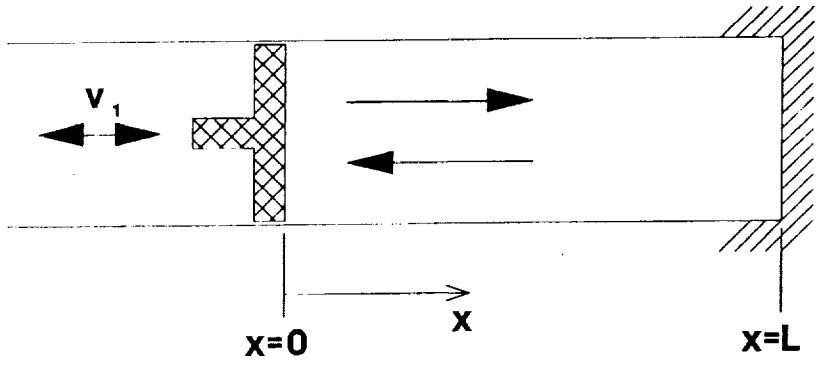

The sound field inside the tube can be characterized as a steady state or a transient sound field depending on the time history of the source (i.e., whether or not it is stable). Both types of sound field have been used in acoustic mixing

experiments, resulting in very different mixing characteristics. When using a steady state sound field, mixing is obtained in streaming cells; while when using a transient sound field, such as a short duration loudspeaker signal, mixing is due to thin particle striations forming and coming together inside the tube.

5.4.1. Steady State Sound Field

A steady state is reached when the variables characterizing the sound field have constant averaged values. In other words, a steady state is reached when the source signal is constant, and the sound field is stable.

5.4.1.1. Steady State Sound Field Equations

The boundary conditions on the acoustic velocity are velocity of zero at the rigid end of the combustor, and the loudspeaker diaphragm velocity at the other end:

$$v(x=0,t) = v_1\, e^{j\omega t} \qquad ; \qquad v(x=L,t) = 0 \tag{4.1}$$

Solving the wave equation for these conditions yields:

$$v(x,t) = v_1 \frac{\sin\left[k(L-x)\right]}{\sin\left(kL\right)} e^{j\omega t} \tag{4.2}$$

where k is the wave number ($k = \frac{\omega}{c}$). Using the relationship between pressure and velocity given in Equation 3.3, we get:

$$p(x,t) = -jv_1\rho_0 c \frac{\cos\left[k(L-x)\right]}{\sin\left(kL\right)} e^{j\omega t} \tag{4.3}$$

The acoustic impedance is defined as

$$Z(x,t) = \frac{p(x,t)}{V(x,t)} \tag{4.4}$$

$V(x,t)$ is the acoustic volume velocity defined as $V(x,t) = v(x,t)\,S$, where S is the tube cross-section.

Using Equations 4.2 and 4.3, the acoustic impedance can be rewritten as:

$$Z(x,t) = -j\frac{\rho_0 c}{S}\cot\left[k(L-x)\right] \tag{4.5}$$

5.4.1.2. Steady State Sound Field Characteristics

The sound field inside the tube is a standing wave, as shown in the next figure (including some attenuation).

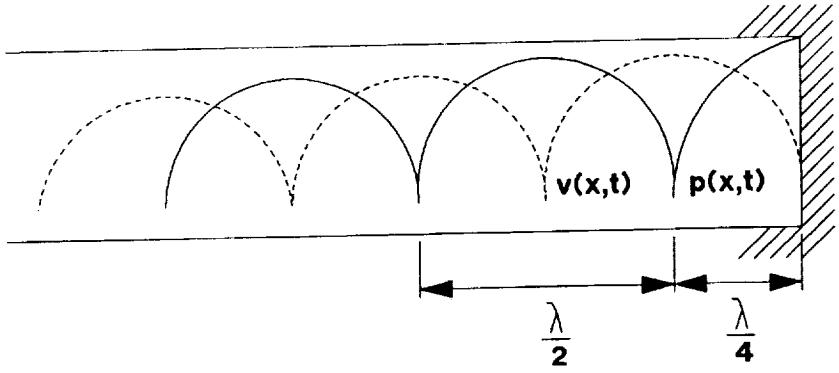

At the rigid end of the tube, the acoustic velocity is zero (velocity node) and the acoustic pressure is at the maximum (pressure antinode). Note that the velocity and the pressure are out of phase; each pressure minimum corresponds to a velocity maximum and vice versa; and the standing wave pattern repeats itself every $\frac{\lambda}{2}$. The decrease in amplitude of the maximum pressure and velocity is due to the attenuation of the sound wave in the tube.

5.4.1.2.1. Streaming patterns

Streaming patterns in the tube as a result of such a standing wave sound field are shown below (from Ref. [31]).

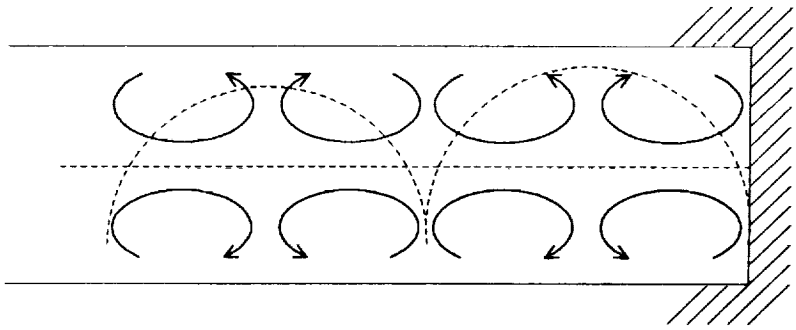

5.4.1.2.2. Resonances

Resonances occur at frequencies $f_r(n)$ for which the acoustic pressure and the acoustic velocity reach a maximum in the tube at their respective antinodes ($Z(x=0,t)=\infty$):

$$f_r(n) = n\,\frac{c}{2L} \qquad ; \qquad n > 0 \tag{4.6}$$

$f_r(n)$ corresponds to frequencies for which the length of the tube L is equal to an integer number of half-wavelengths $\frac{\lambda}{2}$. Also note that in a practical situation, viscosity limits the amplitude of the acoustic pressure and velocity at resonance.

5.4.1.2.3. Antiresonances

Antiresonances occur when the acoustic pressure and velocity are at a minimum at the antinodes. Therefore,

$$f_a(n) = (2n+1)\frac{c}{4L} \tag{4.7}$$

Experience has shown that to get any significant mixing in a zero-gravity environment using low-frequency axial-speakers, the combustor system must be excited at one of its resonance frequencies.

5.4.1.2.4. Acoustic Pressure at Resonance

At resonance, the acoustic pressure given by Equation 4.3 goes to infinity. In reality, viscous dissipation and the compliance of the tube wall limit the build up of energy inside the tube. An upper limit for the pressure can be obtained by replacing the wave number k by a complex number k_c:

$$k_c = k + j\alpha \tag{4.8}$$

where α is an attenuation coefficient.

It can be shown both experimentally and theoretically that replacing k in the expression for the acoustic velocity and pressure (Equations 4.2 and 4.3) by k_c satisfies the wave equation, including attenuation due to molecular, viscous, and thermal effects in the bulk of the fluid and in the tube wall boundary-layer. Using Equation 4.8 and assuming that the attenuation is small ($\alpha \ll k$), the denominator in Equation 4.3 can be rewritten as:

$$\begin{aligned} \sin(k_c L) &= \sin[(k + j\alpha)L] \\ &\approx \sin(kL) + j\,\alpha L \cos(kL) \\ &= \sqrt{\sin^2(kL) + [\alpha L \cos(kL)]^2}\; e^{j\Phi} \end{aligned} \tag{4.9}$$

where

$$\Phi = \tan^{-1}\left[\alpha L \cot\left(kL\right)\right] \tag{4.10}$$

Therefore, the steady state acoustic pressure can be approximated by:

$$p(x,t) \approx -jv_1\rho_0 c \frac{\cos\left[k(L-x)\right]}{\sqrt{\sin^2\left(kL\right) + \left[\alpha L \cos\left(kL\right)\right]^2}} e^{j(\omega t - \Phi)} \tag{4.11}$$

At resonance, the acoustic pressure amplitude in the tube is:

$$|p_{res}(x,t)| = \rho_0 c \frac{v_1}{\alpha L} \cos\left[k(L-x)\right] \tag{4.12}$$

5.4.1.2.5. **Attenuation Coefficient** α

The main acoustic attenuation mechanisms in a tube are the regular and the boundary-layer absorptions. Regular absorption consists of the attenuation due to viscous and heat-conduction effects in the bulk of the fluid, as well as the attenuation due to the rotational and vibrational molecular relaxation. Boundary-layer absorption due to viscous and heat-conduction effects is the main attenuation mechanism in the tube at the frequencies of interest. It is best described by the Helmholtz-Kirchhoff wide-tube attenuation coefficient:

$$\alpha_w = \frac{2}{cD}\sqrt{\frac{\omega\nu}{2}}\left(1 + \frac{\gamma - 1}{\sqrt{P_r}}\right) \tag{4.13}$$

where ν is the kinematic viscosity, γ is the ratio of specific heats, and P_r is the Prandtl number. For a 2-inch diameter tube, $\alpha_w = 0.037$ Np/m at $f = 1000$ Hz, and $\alpha_w = 0.016$ Np/m at $f = 200$ Hz.

5.4.1.3. Steady State Energy Balance Equations

This section defines acoustic energy and acoustic intensity, both of which are widely used in the characterization of sound fields. Expressions are given for the case of a traveling plane wave and a standing wave in a tube.

5.4.1.3.1. General Relationships

The energy balance for a volume V of area A can be written as:

$$\frac{\partial}{\partial t}\int_V \left(\frac{1}{2}\rho_0\, v\cdot v + \frac{1}{2}\frac{c^2}{\rho_0}\rho^2\right) dV = -\int_A p\, v\cdot n\, dA \tag{4.14}$$

where ρ is the acoustic density.

The left hand side of Equation 4.13 represents the rate of energy variation in V. Therefore, the energy density ϵ inside V is given by:

$$\begin{aligned}\epsilon &= \epsilon_k + \epsilon_p \\ &= \frac{1}{2}\rho_0\, v\cdot v + \frac{p^2}{2\rho_0 c^2}\end{aligned} \tag{4.15}$$

The first term on the right hand side represents the kinetic energy density ϵ_k and the second term the potential energy density ϵ_p of the fluid in the volume. The total energy inside V is:

$$E_a = \int_V \epsilon\, dV \tag{4.16}$$

The right hand side of Equation 4.14 represents the rate at which the energy leaves V through A. We can define the acoustic intensity vector $\vec{I}$ as the time average of the energy flux $p\,v$:

$$\vec{I} = < p\, v^* > \tag{4.17}$$

The acoustic power crossing the surface A is given by:

$$W = \int_A \vec{I}\, dA \tag{4.18}$$

5.4.1.3.2. **Traveling Plane Wave**

In a traveling plane wave, the acoustic pressure and velocity are in phase and related by:

$$\frac{p}{v} = \pm \rho_0 c \tag{4.19}$$

Therefore, the energy density is equal to:

$$\epsilon = \frac{p^2}{\rho_0 c^2} \tag{4.20}$$

The energy flux vector and the acoustic intensity are given by:

$$p\, v = \epsilon c \tag{4.21}$$

$$\vec{I} = \frac{p_{\text{rms}}^2}{\rho_0 c} \tag{4.22}$$

where p_{rms} is the RMS acoustic pressure.

For a plane wave, acoustic intensity and energy density are real and directly related to the squared RMS pressure.

5.4.1.3.3. **Standing Wave in a Closed Tube**

For a standing wave in a closed tube, the energy density ϵ can be calculated using the results from Section 5.4.1.1:

$$\epsilon = \epsilon_k + \epsilon_p$$
$$= \frac{\rho_0 v_1^2}{4}\left[\frac{\sin\left[k(L-x)\right]}{\sin\left(kL\right)}\right]^2\left(1+e^{j2\omega t}\right) + \frac{\rho_0 v_1^2}{4}\left[\frac{\cos\left[k(L-x)\right]}{\sin\left(kL\right)}\right]^2\left(1-e^{j2\omega t}\right)$$
$$= \frac{\rho_0 v_1^2}{4\sin^2\left(kL\right)}\left(1-\cos\left[2k(L-x)\right]e^{j2\omega t}\right) \tag{4.23}$$

The energy flux vector and the acoustic intensity are given by:

$$p\,v = \frac{v_1^2\rho_0 c}{4}\frac{\sin[2k(L-x)]}{\sin^2(kL)}\sin(2\omega t) \tag{4.24}$$

$$\vec{I} = 0 \tag{4.25}$$

The total acoustic energy inside the tube can be calculated using Equation 4.16:

$$E_a = < E_a > \left[1 - \frac{\sin\left(2kL\right)}{2kL}e^{j2\omega t}\right] \tag{4.26}$$

where the time averaged acoustic energy $< E_a >$ is equal to:

$$< E_a >= \frac{\rho_0 v_1^2}{4} S \frac{L}{\sin^2\left(kL\right)} \tag{4.27}$$

Finally, the rate at which the loudspeaker does work on the fluid is given by:

$$W_p = p(0,t)v(0,t)S$$
$$= -jv_1^2\rho_0 c\,\cot\left(kL\right)\,\cos\left(2\omega t\right) \tag{4.28}$$

Therefore, when only standing waves are present in the tube, there is no average net flow of energy inside the tube ($\vec{I} = 0$). The averaged rate at which the loudspeaker does work on the fluid $< W_p >$ is also equal to zero, which is

typical of the steady state condition. Finally, as expected from Section 5.4.1.1, the averaged energy inside the tube is infinite at resonance.

5.4.2. Transient Sound Field

A transient occurs when the variables characterizing the sound field do not have constant averaged values. In other words, transients are present when the source is unstable, such as when it is switched on or off.

Good mixing has been obtained in a micro-gravity environment using an axial-speaker operated in a transient mode. In this experiment, the source is turned on for a brief period of time. As the loudspeaker is first turned on, thin striations formed of groups of particles arranged perpendicular to the tube axis rise vertically in a "finger"-like fashion. As time goes on, the "fingers" join and mix with each other, completing the mixing process. The loudspeaker is turned off before streaming cells fully develop to prevent the steady state mixing process studied in the previous section from developing.

5.4.2.1. Transient Sound Field Equations

The transient response of the tube is studied here for a loudspeaker generating a sinusoidal signal starting at $t = 0$.

In a practical case, the assumption of a sinusoidal signal is valid because of when the transient has a long duration. For short transients, the sinusoidal assumption might not be valid because the ringing effect caused by the inertia and stiffness of the loudspeaker voice-coil and membrane assembly. In any

C-2

case, the sinusoidal assumption gives a good insight into the transient response characteristics, and the energy build up in the tube.

The transient response of a closed tube can be obtained by taking the Laplace transform of the wave equation using the following boundary and initial conditions:

$$\begin{aligned} v(x=0,t) &= v_1 \cos(\omega t) \quad ; \quad v(x=L,t) = 0 \\ p(x,t=0) &= 0 \quad ; \quad v(x,t=0) = 0 \end{aligned} \tag{4.29}$$

The acoustic pressure solution of the wave equation is:

$$\begin{aligned} p(x,t) = j\rho_0 c v_1 \sum_{m=0}^{\infty} & \sin\left[\omega\left(t - \frac{2mL+x}{c}\right)\right] H\left[t - \frac{2mL+x}{c}\right] \\ & + \sin\left[\omega\left(t - \frac{2(m+1)L-x}{c}\right)\right] H\left[t - \frac{2(m+1)L-x}{c}\right] \end{aligned} \tag{4.30}$$

where $H(t)$ is the Heaviside function defined by:

$$H(t) = \begin{cases} 0 & t < 0 \\ 1/2 & t = 0 \\ 1 & t > 0 \end{cases}$$

The solution for the acoustic pressure given in Equation 4.30 consists of a sum of reflections from the wall and the loudspeaker diaphragm, with each reflection starting to contribute to the total pressure after a time delay equal to its propagation time.

5.4.2.2. Transient Sound Field Characteristics

5.4.2.2.1. Pressure and Velocity Build up at Resonance

At resonance, $\omega = 2\pi f_r(n)$ where $f_r(n)$ is given by Equation 4.6. Therefore, $p_{res}(x,t)$ can be written as:

$$p_{res}(x,t) = j\rho_0 c v_1 \sum_{m=0}^{\infty} \sin\left[\omega\left(t-\frac{x}{c}\right)\right] H\left[t-\frac{2mL+x}{c}\right] + \sin\left[\omega\left(t+\frac{x}{c}\right)\right] H\left[t-\frac{2(m+1)L-x}{c}\right] \quad (4.31)$$

As expected, the reflections are in phase and reinforce each other, resulting in the acoustic pressure building to infinity. The normalized acoustic pressure is shown in the figure below for an excitation frequency such that the tube length is equal to one wavelength (i.e., $n = 2$ in Equation 4.6).

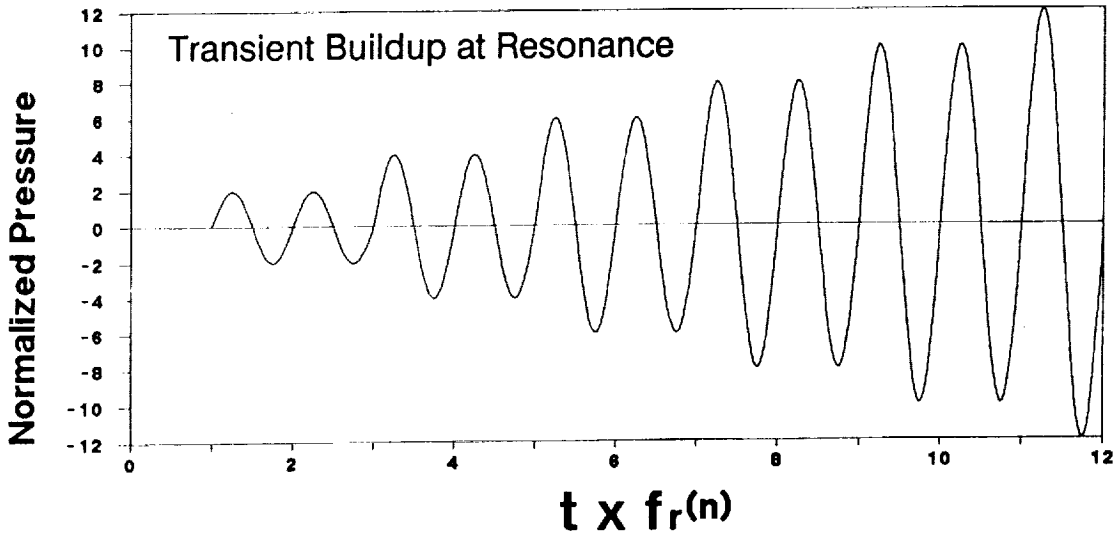

However, the formulation for the acoustic pressure given by Equation 4.31 is not very practical and is simplified below.

From the previous Figure and Equation 4.31, the acoustic pressure amplitude at resonance can be approximated by:

$$|p_{res}(x,t)| = \rho_0 c v_1 \, 2 \, \frac{t f_r(n)}{n}$$
$$= \rho_0 c^2 \, \frac{v_1}{L} \, t \qquad (4.32)$$

The harmonic time dependence of the acoustic pressure is readily evaluated from the momentum equation and the velocity boundary condition at the source (Equations 3.2 and 4.29). The axial dependence is obtained by analogy with the steady state case. Combining these and Equation 4.32, we get the simplified expression for the acoustic pressure at resonance:

$$p_{res}(x,t) = \rho_0 c^2 \, \frac{v_1}{L} \, t \, \cos\left[k(L-x)\right] \, \sin\left(\omega t\right) \qquad (4.33)$$

The approximate expression for the acoustic velocity is obtained using Equations 4.33 and 3.2:

$$v_{res}(x,t) = c \, \frac{v_1}{L} \, t \, \sin\left[k(L-x)\right] \, \cos\left(\omega t\right) \qquad (4.34)$$

5.4.2.2.2. **Transient Duration**

The time t_s needed for the sound field to reach a steady state from the moment the loudspeaker is turned on can be evaluated simply by equating the acoustic pressure amplitude at resonance in the case of a transient (Equation 4.33) with the steady state acoustic pressure amplitude (Equation 4.12), and solving for the time variable:

$$t_s = \frac{1}{\alpha c} \qquad (4.35)$$

When the acoustic attenuation is high, the transient has a short duration as the high dissipation rate rapidly catches up with the energy growth rate. For low attenuation, the transient is long because the acoustic pressure builds up in the pipe for a longer period of time.

For a 2-inch tube having a perfectly rigid end, $t_s = 0.08$ sec at $f = 1000$ Hz, and $t_s = 0.18$ sec at $f = 200$ Hz. In reality, the value for t_s will be somewhat different. This is due to the higher "perceived" sound attenuation as a result of the non-perfectly rigid end (i.e., shorter t_s), and the non-sinusoidal input signal which results from of the loudspeaker ringing (i.e., longer t_s).

5.4.2.3. Transient Energy Balance Equations

Energy formulations can also be used to evaluate the transient duration t_s, or the acoustic pressure amplitude at resonance. The transient duration is readily obtained by equating the total energy growth rate inside the tube with the energy dissipation rate.

5.4.2.3.1. Energy Growth at Resonance

Using Equations 4.15, 4.33, and 4.34, the energy density at resonance ϵ_{res} is given by:

$$\epsilon_{res} = \frac{\rho_0 c^2}{2}\left(\frac{v_1 t}{L}\right)^2 \left[\sin^2(k[L-x])\cos^2(\omega t) + \cos^2(k[L-x])\sin^2(\omega t)\right] \quad (4.36)$$

The total energy in the tube at resonance is obtained from Equation 4.16:

$$E_a(t) = \frac{\rho_0 c^2}{4}\left(\frac{v_1 t}{L}\right)^2 V \quad (4.37)$$

where V is the tube volume ($V = LS$).

5.4.2.3.2. Energy Dissipation at Resonance

It can be easily shown by solving the wave equation, including attenuation in the case of a standing wave, that the decay of the pressure and the velocity amplitudes with time is exponential. Thus the energy decay due to dissipation is of the form:

$$E_d(t) = E(t=0)\, e^{-2\alpha c t} \tag{4.38}$$

5.4.2.3.3. Transient Duration

Steady state is reached when the energy dissipation rate $\frac{dE_d(t)}{dt}$ is equal to the total energy growth rate inside the tube $\frac{dE_a(t)}{dt}$:

$$\frac{dE_a(t)}{dt} = -\frac{dE_d(t)}{dt}$$

$$\frac{\rho_0 c^2}{2}\left(\frac{v_1}{L}\right)^2 t\, V = 2\,\alpha c\,\frac{\rho_0 c^2}{4}\left(\frac{v_1 t}{L}\right)^2 V \tag{4.39}$$

Solving for the transient duration t_s, we get:

$$t_s = \frac{1}{\alpha c}$$

which is the value previously obtained (see Equation 4.35).

5.5. Axial-Speaker in an Open Tube

The study of the open tube configuration helps us understand the acoustics of combustors because it represents one of two extreme cases encountered in

resonating tubes (the other extreme case being the closed tube configuration). The open end of the tube can be modeled as a pressure release boundary condition, i.e., the acoustic pressure at the tube end is zero, instead of the acoustic velocity being zero (as in the case of a closed tube). The following figure describes the open tube configuration.

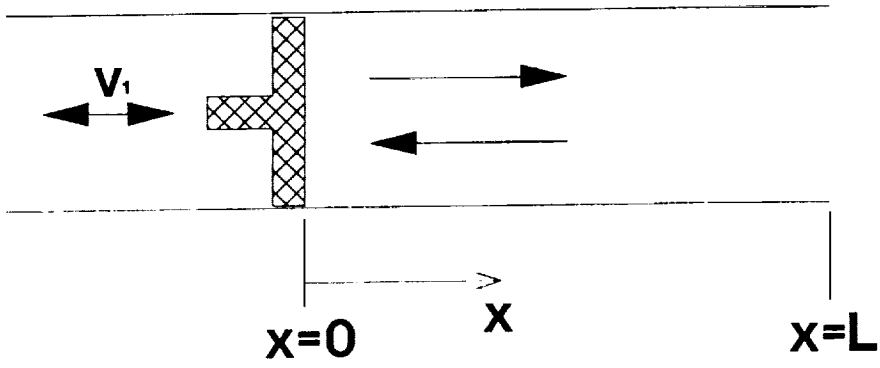

5.5.1. Sound Field Equations

The boundary conditions are an acoustic pressure of zero at the open end of the combustor, and the loudspeaker diaphragm velocity at the other end:

$$v(x=0,t) = v_1\, e^{j\omega t} \qquad ; \qquad p(x=L,t) = 0 \tag{5.1}$$

Solving the wave equation for these conditions yields:

$$v(x,t) = v_1\, \frac{\cos\left[k(L-x)\right]}{\cos\left(kL\right)}\, e^{j\omega t} \tag{5.2}$$

$$p(x,t) = -jv_1\rho_0 c\, \frac{\sin\left[k(L-x)\right]}{\cos\left(kL\right)}\, e^{j\omega t} \tag{5.3}$$

$$Z(x,t) = -j\frac{\rho_0 c}{S} \tan\left[k(L-x)\right] \tag{5.4}$$

5.5.2. Sound Field Characteristics

As shown in the figure below, the position of the nodes and antinodes is shifted by $\frac{\lambda}{4}$ compared to the closed tube case.

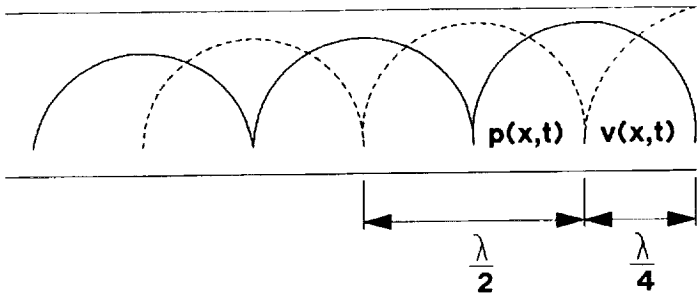

The streaming patterns are also reversed as shown below:

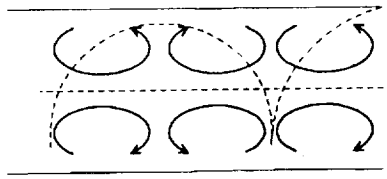

The resonance frequencies are given by:

$$f_r(n) = (2n+1)\frac{c}{4L} \qquad n \geq 0 \tag{5.5}$$

Therefore, the first resonance occurs at half the frequency of the first resonance of the closed tube.

5.6. Axial-Speaker in a Tube having a Termination of Impedance Z_l

The acoustical characteristics of a tube termination can be expressed by its acoustic impedance. From the definition of the impedance given in Equation 4.4,

we can calculate the termination impedance Z_l at resonance for a closed and an open tube as:

$$Z_l = -j \times \infty \qquad \text{for a closed tube} \tag{6.1}$$

$$Z_l = -j \times 0 \qquad \text{for an open tube} \tag{6.2}$$

In both cases, a pure standing wave is set up in the tube and the acoustic impedance is imaginary (see Equations 4.5 and 5.4). Any other termination impedance will have a value somewhere between ∞ and 0, resulting in the tube having resonance frequencies between the resonance frequencies obtained for the closed and open ended cases, as well as some attenuation at the boundary.

5.6.1. Sound Field Equations

The case of an axial-speaker in a tube having a termination Impedance Z_l is shown below:

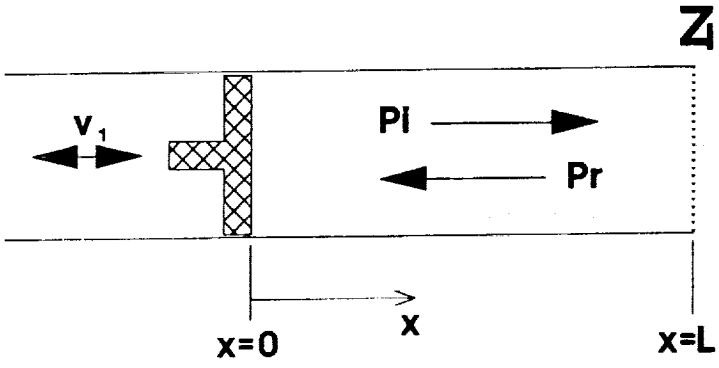

The acoustic field inside the tube can be described as follows:

$$v(x,t) = v_1 \left[\cos(kx) - \left[\frac{j(\rho_0 c/S)\tan(kL) + Z_l}{Z_l \tan(kL) - j(\rho_0 c/S)} \right] \sin(kx) \right] e^{j\omega t} \tag{6.3}$$

$$p(x,t) = -jv_1\rho_0 c\left[\sin(kx) - \left[\frac{j(\rho_0 c/S)\tan(kL) + Z_l}{Z_l\tan(kL) - j(\rho_0 c/S)}\right]\cos(kx)\right]e^{j\omega t} \tag{6.4}$$

$$Z(x=0,t) = \frac{\rho_0 c}{S}\left[\frac{Z_l + j(\rho_0 c/S)\tan(kL)}{(\rho_0 c/S) + jZ_l\tan(kL)}\right] \tag{6.5}$$

5.6.2. Measurement of the Termination Impedance Z_l

The complex termination impedance Z_l required to characterize the sound field inside the tube is usually determined experimentally. Z_l can be rewritten as:

$$Z_l = \beta e^{j\phi} \tag{6.6}$$

where β and ϕ are the modulus and the phase of the impedance.

Solving for β and ϕ we get:

$$\beta = \frac{\rho_0 c}{S}\frac{\sqrt{1 + (P_i/P_r)^4 - 2(P_i/P_r)^2 + 4(P_i/P_r)^2\sin^2\theta}}{1 + (P_i/P_r)^2 - 2(P_i/P_r)\cos\theta} \tag{6.7}$$

$$\phi = \tan^{-1}\left[\frac{2(P_i/P_r)\sin\theta}{(P_i/P_r)^2 - 1}\right] \tag{6.8}$$

where

$$\theta = 2ka - \pi \tag{6.9}$$

and

$$\frac{P_i}{P_r} = \frac{\mathrm{SWR} + 1}{\mathrm{SWR} - 1} \tag{6.10}$$

a is the distance between the termination and the first pressure minimum in the standing wave as shown in the next figure. SWR is the Standing Wave Ratio, P_i is the amplitude of the wave incident on the termination, and P_r is the amplitude of the wave reflected by the termination. SWR is equal to the ratio of the maximum to the minimum measured acoustic pressure in the tube, as shown in the figure below.

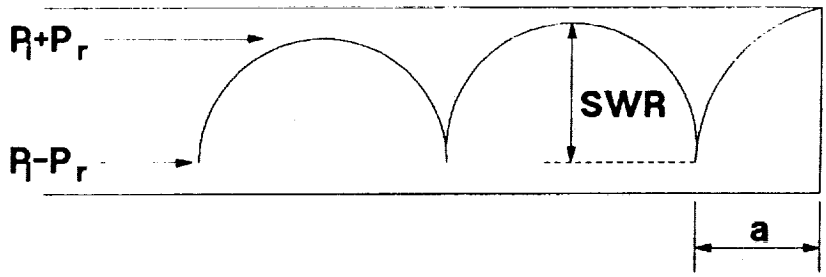

5.7. Acoustic Elements

This section describes the acoustical properties of various simple acoustic elements which are found in PCCE tubes. The equations describing these elements can be combined together to build a complete acoustic model of the PCCE tube, or used as simple guidelines during the design of an acoustic mixing system for a PCCE combustor.

5.7.1. Variable Area Sections

Short variable area sections are used in the PCCE set up, such as to connect the large diameter loudspeaker diaphragms (9.5 cm) to the small diameter PCCE tube (5 cm), or between the ignition (6 cm diameter) and the combustor (5 cm

diameter) sections of the PCCE tube. Although these area variations are gradual, the acoustic losses generated can be estimated by treating the gradual variations as sudden transitions. This is justified because the wavelength at the frequencies of interest is much longer than the length of the area variations for a substantial change in area. In other words, the sound wave is too large to see the change of area as gradual, and perceives it as a sudden change in cross-section.

The transmission coefficient α_t for a sound wave going through a sudden transition is defined as the ratio of the power in the transmitted wave to the power in the incident wave:

$$\alpha_t = \left|\frac{P_t}{P_i}\right|^2 \tag{7.1}$$

$$= \frac{4S_0S_1}{(S_0 + S_1)^2} \tag{7.2}$$

where P_t and P_i are the RMS amplitudes of the transmitted and incident acoustic pressures, and S_0 and S_1 are the areas on each side of the transition, as shown in the figure below.

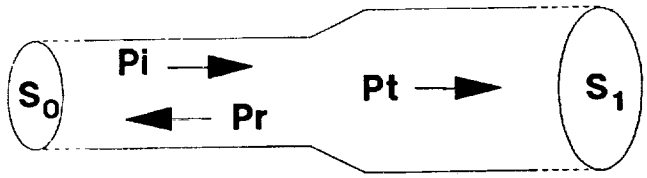

The acoustic loss due to the area change between the axial-speaker and the PCCE tube is $\alpha_t = -1.61$ dB. The loss due to the area change between the ignition and the combustor sections of the PCCE tube is $\alpha_t = -0.14$ dB.

5.7.2. Side Branch Sections

Side branches are frequently used in PCCE configurations to inject fuel into the combustor or as instrument ports. This section first presents the general relationships for a side branch having arbitrary acoustic impedances and then looks more closely at two simple cases which illustrate the effect of a side branch on an acoustic system such as a PCCE tube.

5.7.2.1. General Relationships

The figure below represents a side branch

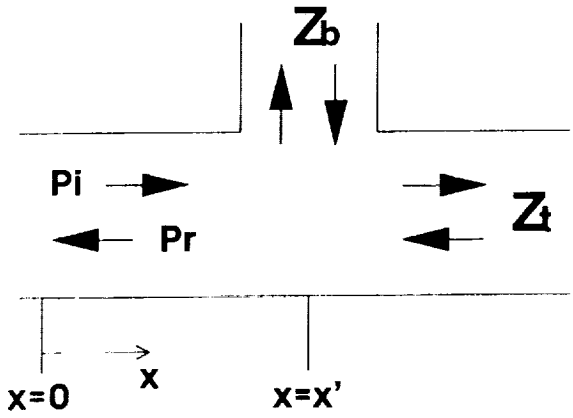

Z_t is the complex acoustic impedance of the main tube at the point where the branch is connected to the main tube ($x = x'$). Z_t is defined as:

$$Z_t = \frac{P_t(x = x', t)}{S_t\, v_t(x = x', t)} = R_t + jX_t \qquad (7.3)$$

where S_t is the area of the main tube for $x > x'$.

Z_b is the complex acoustic impedance of the branch and is defined as:

$$Z_b = \frac{P_b(x = x', t)}{S_b\, v_b(x = x', t)} = R_b + jX_b \tag{7.4}$$

where S_b is the area of the branch.

The reflection coefficient α_r is defined as the ratio of the power in the reflected wave to the power in the incident wave:

$$\alpha_r = \frac{|Z_t|^2|Z_b|^2 + {Z_a}^2\left[(R_t + R_b)^2 + (X_t + X_b)^2\right] - 2Z_a\left[R_t|Z_b|^2 + R_b|Z_t|^2\right]}{|Z_t|^2|Z_b|^2 + {Z_a}^2\left[(R_t + R_b)^2 + (X_t + X_b)^2\right] + 2Z_a\left[R_t|Z_b|^2 + R_b|Z_t|^2\right]} \tag{7.5}$$

where $Z_a = \frac{\rho_0 c}{S}$, and S is the area of the main tube for $x < x'$.

The transmission coefficient is given by:

$$\alpha_t = \frac{4|Z_t|^2|Z_b|^2}{|Z_t|^2|Z_b|^2 + {Z_a}^2\left[(R_t + R_b)^2 + (X_t + X_b)^2\right] + 2Z_a\left[R_t|Z_b|^2 + R_b|Z_t|^2\right]} \tag{7.6}$$

The impedance of the whole acoustic system at $x = 0$ is given by:

$$Z(x = 0) = \frac{Z_a^2 R\left[1 + \tan^2(kx')\right]}{\left[Z_a - X\tan(kx')\right]^2 + \left[R\tan(kx')\right]^2} + jZ_a\frac{\left[X + Z_a\tan(kx')\right]\left[Z_a - X\tan(kx')\right] - \left[R\tan(kx')\right]^2}{\left[Z_a - X\tan(kx')\right]^2 + \left[R\tan(kx')\right]^2} \tag{7.7}$$

where R and X are the real and imaginary parts of the combined impedance Z_c of the side branch and the main tube.

$$Z_c = R + jX \tag{7.8}$$

and

$$R = \frac{R_t|Z_b|^2 + R_b|Z_t|^2}{(R_t + R_b)^2 + (X_t + X_b)^2} \quad ; \quad X = \frac{X_t|Z_b|^2 + X_b|Z_t|^2}{(R_t + R_b)^2 + (X_t + X_b)^2} \tag{7.9}$$

5.7.2.2. Side Branch in an Infinite Tube

In the case of an infinite tube, the acoustic wave traveling down the tube is never reflected back and the sound field inside the tube is purely real (see Section 5.4.1.3.2).

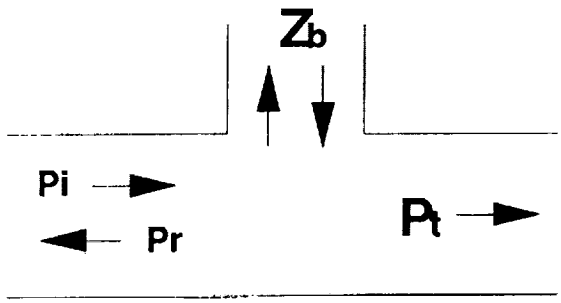

The impedance Z_t is given by:

$$Z_t = \frac{\rho_0 c}{S_t} \tag{7.10}$$

If the main tube diameter stays constant ($S_t = S$), the reflection and transmission coefficients can be calculated using Equations 7.5, 7.6, and 7.10:

$$\alpha_r = \frac{(\rho_0 c/2S)^2}{[R_b + (\rho_0 c/2S)]^2 + X_b^2} \tag{7.11}$$

$$\alpha_t = \frac{R_b^2 + X_b^2}{[R_b + (\rho_0 c/2S)]^2 + X_b^2} \tag{7.12}$$

5.7.2.2.1. Infinite Y-Section

An infinite Y-section can be looked at as an infinite side branch in an infinite tube.

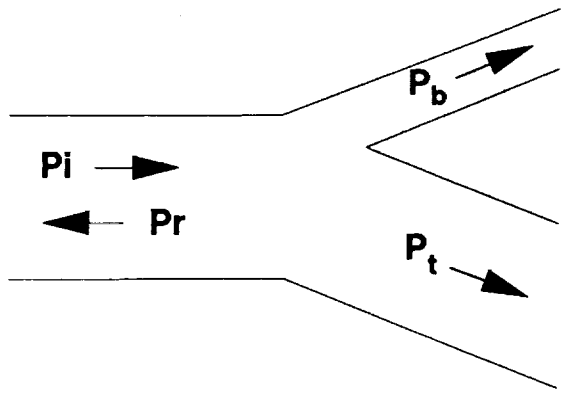

The reflection and transmission coefficients are given by:

$$\alpha_r = \frac{(S_b/S)^2}{[2 + (S_b/S)]^2} \tag{7.13}$$

$$\alpha_t = \frac{4}{[2 + (S_b/S)]^2} \tag{7.14}$$

For a 2-inch diameter main tube and a 1/4-inch diameter instrument port, $\alpha_r = -42$ dB and $\alpha_t = -0.07$ dB. Nearly all of the energy in the acoustic wave is transmitted past the 1/4-inch branch. Thus instrument ports or small openings have very little effect on the acoustics of the main tube if no reflections are present.

For a 2-inch diameter main tube and a 2-inch diameter injection port, $\alpha_r = \frac{1}{9} = -9.5$ dB and $\alpha_t = \frac{4}{9} = -3.5$ dB. In this case, nearly half of the energy in the sound wave is lost to the side branch while about 1/10 is reflected back to the loudspeaker.

5.7.2.2.2. Closed Side Branch in an Infinite Tube

In practical cases, the assumption that the side branch is infinite is difficult to justify. Reflections can be minimized by placing an anechoic termination in the side branch, or by replacing it with a long, small diameter tube that attenuates most of the acoustic wave. In most cases, a closed pipe is more representative of the true behavior of the type of side branch found in PCCE tubes.

A closed side branch in an infinite tube is shown in the figure below next to an infinite side branch in a closed tube.

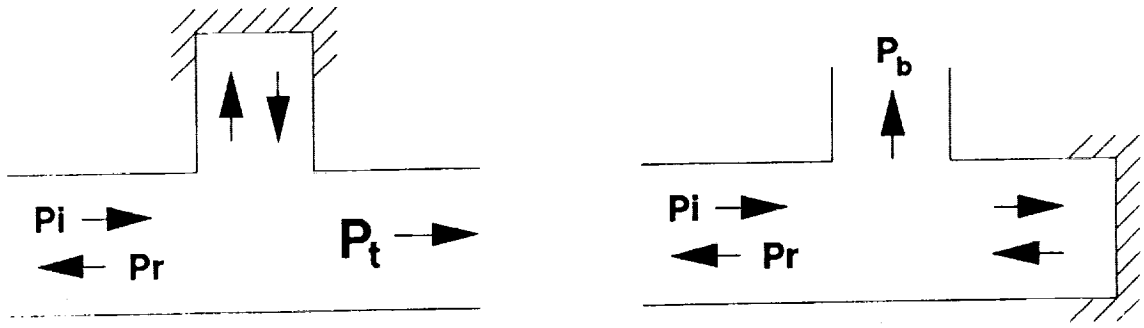

It is clear from the symmetry in the equations in Section 5.7.2.1 that the main tube and the side branch act in the same way on the sound wave. Thus both representations in the figure above can be studied using the same set of equations.

Let's consider the case of the closed side branch. The acoustic impedance for the side branch is given by Equation 4.5:

$$Z_b = -j\frac{\rho_0 c}{S_b}\cot(kL) \tag{7.15}$$

Replacing Z_b in Equations 7.11 and 7.12 by its value above, we get:

$$\alpha_r = \frac{1}{1 + (2S/S_b)^2 \cot(kL)^2} \tag{7.16}$$

$$\alpha_t = \frac{1}{1 + (S_b/2S)^2 \tan(kL)^2} \tag{7.17}$$

When $\tan(kL) = 0$ $(\cot(kL) = \infty)$, $\alpha_r = 0$ and $\alpha_t = 1$. From Section 5.4.1.2.2, we know that this corresponds to the resonances of the closed side branch. In this case, whatever the diameter of the side branch is, its impedance at the junction with the main tube is infinity. In other words, the side branch imposes a zero velocity boundary condition and acts as a rigid wall. All of the acoustic energy is transmitted to the main tube and the side branch is invisible to the sound wave.

When $\tan(kL) = \infty$ $(\cot(kL) = 0)$, $\alpha_r = 1$ and $\alpha_t = 0$. This corresponds to the antiresonance of the side branch. No energy is transmitted through the main pipe, and the sound wave is reflected back to the loudspeaker in its entirety. This configuration can be used as a "tuned" acoustic absorber (or filter) to remove unwanted frequency components from piping systems. In the case of PCCE tubes, such a set up is detrimental because it prevents the sound from filling the whole tube.

In conclusion, care must be taken when introducing closed side branches into the PCCE tube. Tuning the side branch can minimize its effect, although this not always possible at low frequencies because of the long length required. For instance, at 250 Hz, the minimum length required for the side branch to be tuned is equal to $\frac{\lambda}{2} = 27$ inches, which is too long for practical purposes. However,

it is critical to stay away from the side branch antiresonances, the first of which occurs for a branch length of $\frac{\lambda}{4} = 13.5$ inches.

5.7.2.2.3. Open-Ended Side Branch in an Infinite Tube

The case of an open-ended side branch can be studied in the same way.

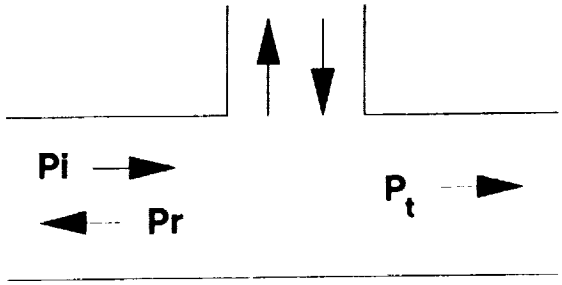

From the previous results and Section 5.5, it is obvious that the effect of the open-ended side branch will be null when its length is equal to $(2n+1)\frac{\lambda}{4}$, which corresponds to a minimum length of 13.5 inches at 250 Hz. The losses due to the side branch will be very strong when its length is a multiple of the half-wavelength. This result is the opposite of the closed side branch case and emphasizes the importance of knowing the acoustic termination impedance of the branch. In the case of a termination of impedance Z_l, a precise tuning of the branch can also be obtained by varying its minimum length between $\frac{\lambda}{4}$ and $\frac{\lambda}{2}$ until resonance occurs.

5.7.3. Diaphragms

Diaphragms are used to separate various sections in PCCE tubes, such as the ignitor from the combustion chamber. This section looks at how the presence of

diaphragms affects the sound field inside a PCCE tube.

The diaphragms used are made of 0.5/1000-inch thick silvered Mylar. They are mounted on support rings with several grades of tightness. The tightness is evaluated by measuring the diaphragm deflection due to the weight of a 1/2-inch diameter steel ball placed at its center. The various degrees of tightness are roughly categorized into three classes as follows:

Tight:	50/1000-inch deflection $\pm$ 10/1000-inch
Medium:	100/1000-inch deflection $\pm$ 20/1000-inch
Loose:	150/1000-inch deflection $\pm$ 30/1000-inch

Diaphragms have widely varying effects on the sound field inside a tube depending on their mechanical properties. For instance, the stretching properties might be most important in the response of a rubber diaphragm, while the bending stiffness might dominate the response of a stiff plate-like diaphragm. In these two cases, the acoustic transmission characteristics are different, resulting in different, sound fields inside the tube.

The PCCE diaphragms are assumed to be loose and non-stretchable. By "loose" we mean that a diaphragm "flaps" back and forth with the acoustic wave. By "non-stretchable" because it is loosely mounted we mean that, at very high sound pressure level when the acoustic air displacement exceeds the diaphragm displacement, the diaphragm bottoms-out, thus clipping the acoustic pressure waveform transmitted through it. In reality, the diaphragm does stretch a little, allowing an extra displacement of the air molecules. However, this stretching is limited and contributes little to the overall sound pressure level transmitted through the diaphragm. Moreover, as shown in Section 5.7.3.2.2, diaphragm

motion is minimized and bottoming-out does not occur in a properly designed system.

5.7.3.1. Non-Stretchable Loose Diaphragm Having Zero Mass and Zero Stiffness

The study of a non-stretchable loose diaphragm having zero mass and zero stiffness helps define the relationship between the diaphragm measured deflection and the maximum acoustic pressure that can be "passed" through the diaphragm before it bottoms-out.

The assumption of zero-mass and zero-stiffness means that the diaphragm is completely entrained by the sound wave in the tube and does not disturb the sound field until it bottoms-out.

5.7.3.1.1. Deflection of a Loose Diaphragm Due to an Acoustic Pressure Load

The acoustic pressure load on a PCCE diaphragm due to a plane wave can be assumed to be constant over the whole diaphragm area. This is justified by looking at the properties of the acoustic boundary-layer in the tube.

Viscous and Thermal Boundary-Layer Thicknesses in a PCCE Tube

For a plane wave in a tube, the acoustic thermal and viscous boundary-layer thicknesses δ_ν and δ_κ are given by:

$$\delta_\nu = \sqrt{\frac{2\nu}{\omega}} \quad ; \quad \delta_\kappa = \sqrt{\frac{2\kappa}{\omega}} \tag{7.18}$$

where κ is the thermal conductivity of the air in the tube.

The ratio of thermal and viscous boundary-layer thicknesses is given by

$$\frac{\delta_\nu}{\delta_\kappa} = \sqrt{\mathrm{P_r}} \tag{7.19}$$

For air at ambient temperature, $\mathrm{P_r} = 0.73$. Thus, δ_ν and δ_κ are approximately equal.

The higher the frequency, the smaller the thermal and viscous boundary-layer thicknesses. For a low frequency of 100 Hz, $\delta_\nu = 0.02$ cm which is over a hundred times smaller than the PCCE tube radius (2.5 cm). Thus it is safe to assume that the wave is truly planar and that the acoustic pressure load is constant over the whole diaphragm area.

Deflection of a Loose Diaphragm Due to a Pressure Load

The displacement $z(r)$ of a circular diaphragm due to a pressure load is shown in the following figure on the right.

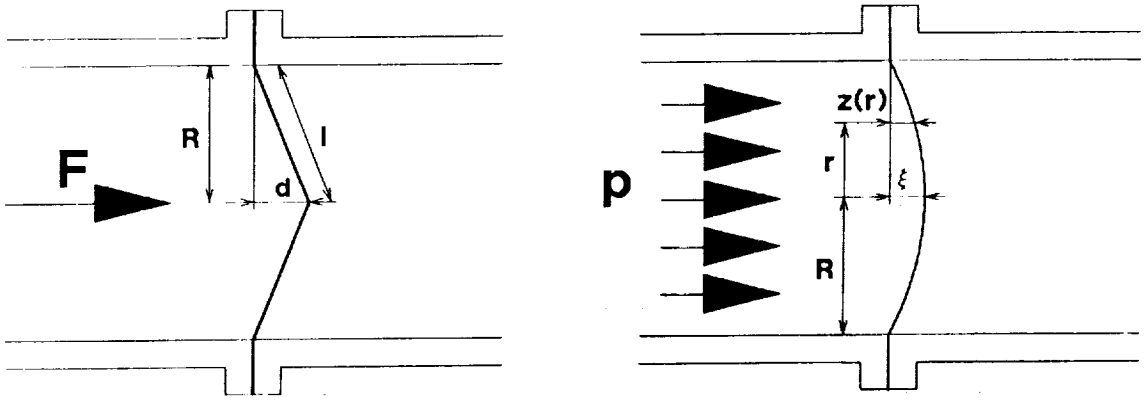

It can easily be shown that $z(r)$ must satisfy the following equation:

$$\nabla_{\mathrm{r}}^2 z(r) = \frac{f}{T} \tag{7.20}$$

where ∇_r^2 is the Laplacian operator in cylindrical coordinates, r is the radial coordinate, f is the acoustic pressure, and T is the tension of the diaphragm.

For a diaphragm of radius R fixed at its edges and having a maximum deflection ξ at its center, the boundary conditions are given by:

$$z(r=0) = \frac{\partial z(r=0)}{\partial r} = 0 \qquad \text{and} \qquad z(r=R) = \xi \tag{7.21}$$

Thus the solution for the diaphragm displacement is:

$$z(r) = \frac{\xi}{R^2} r^2 \tag{7.22}$$

The diaphragm diameter $2l$ is easily calculated:

$$2l = 2\xi \left(\sqrt{1 + \left(\frac{R}{2\xi}\right)^2} + \left(\frac{R}{2\xi}\right)^2 + \ln \left[\frac{2\xi}{R} \left(1 + \sqrt{1 + \left(\frac{R}{2\xi}\right)^2} \right) \right] \right) \tag{7.23}$$

5.7.3.1.2. Deflection of a Loose Diaphragm Due to a Concentrated Force

The displacement d of a diaphragm due to the weight of a steel ball is shown in the previous figure on the left. For the sake of simplicity, the ball weight is assumed to act as a point force rather than a distributed force. The diaphragm diameter can be approximated by:

$$2l = 2\sqrt{R^2 + d^2} \tag{7.24}$$

Therefore, if R and d are measured, and $2l$ is known, we can solve for ξ using Equation 7.23. In the range of displacement measured (50/1000-inch to 200/1000-inch), ξ is only between 13% and 13.5% smaller than d.

5.7.3.1.3. Maximum Sound Pressure Level Through a Loose Diaphragm

Using the adiabatic gas law, the perfect gas law, and the definition of the speed of sound, the acoustic pressure p can be related to a volume variation dV as follows:

$$p = -c^2 \rho_0 \frac{dV}{V} \tag{7.25}$$

For an acoustically transparent diaphragm in an infinite tube and for a diaphragm displacement that is small compared to the sound wavelength, the acoustic pressure amplitude at the diaphragm p_d is equal to the acoustic pressure amplitude of a plane wave p_p at any point in the tube. Therefore, from Equation 7.25 we get,

$$dV_d = dV_p \tag{7.26}$$

where the volume variation dV_d due to the diaphragm motion is obtained by integrating Equation 7.22:

$$dV_d = \frac{\pi R^2 \xi}{2} \tag{7.27}$$

and the volume variation dV_p associated with a plane wave generating a displacement of the air of amplitude y is given by:

$$dV_p = \pi R^2 y \tag{7.28}$$

Thus the maximum diaphragm displacement ξ can be related to the maximum air displacement amplitude y due to a plane wave at any point in the tube by:

$$y = \frac{\xi}{2} \tag{7.29}$$

For a sinusoidal plane traveling wave, the maximum acoustic pressure amplitude through the diaphragm p_{max} is easily calculated by integrating Equation 7.29 with respect to time to get the acoustic velocity, and relating it to the acoustic pressure using the momentum equation (see Equations 3.3 and 4.19):

$$p_{max} = \frac{\rho_0 c \omega \xi}{2} \tag{7.30}$$

The following table lists the diaphragm displacement d measured using the steel ball for various degrees of tightness, and the corresponding displacement ξ for the same diaphragm due to an acoustic pressure load (solution of the coupled Equations 7.23 and 7.24). Also shown are the corresponding maximum sound pressure levels at two frequencies (Equation 7.30) before stretching occurs.

d (inches × 1000)	ξ (inches × 1000)	SPL Max (dB)	
		200 Hz	1000 Hz
50	43	143	157
90	78	148	162
100	87	149	163
150	130	153	167
200	174	155	169

5.7.3.2. Non-Stretchable Loose Diaphragm Having Non-Zero Mass and Non-Zero Stiffness

The more realistic case of a non-stretchable loose diaphragm having non-zero mass, non-zero stiffness, and non-zero damping illustrates the way a diaphragm acts as a partition and how to minimize its effect on the sound field. The diaphragm studied here is assumed to be non-flexible. In other words, the motion of every point of the diaphragm is the same. This assumption is a poor one, for in reality, the diaphragm motion varies along its cross section and the restoring force on the diaphragm is due mainly to its bending stiffness. However, the partition model helps draw some basic conclusions about sound transmission through a PCCE diaphragm, which can then be used as a set of guidelines for basic designs.

5.7.3.2.1. Acoustic Impedance Equations

The figure below is a schematic of a diaphragm in a tube having a termination impedance Z_l at $x = L$. The diaphragm is assumed to have a mass, a stiffness, and a damping coefficient per unit area of m, s, and r, respectively.

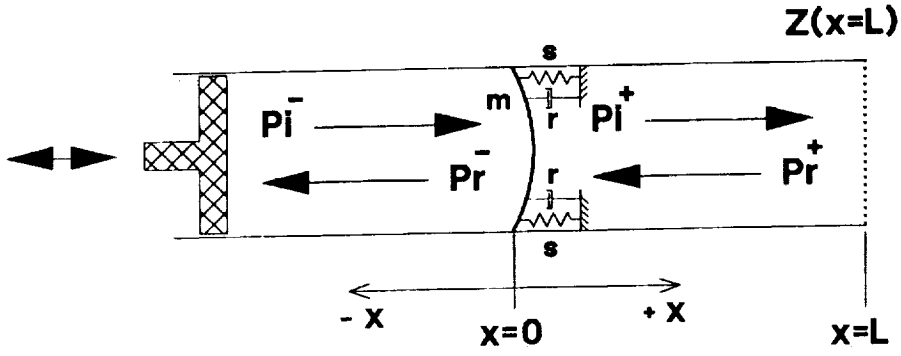

Assuming that all points on the diaphragm are in phase and moving with the same amplitude (i.e., the diaphragm is regarded as a rigid partition), the total acoustic pressure and velocity on both sides of the diaphragm are given by:

$$p^{\pm}(x,t) = p_{\mathrm{i}}^{\pm}\, e^{j(\omega t - kx)} + p_{\mathrm{r}}^{\pm}\, e^{j(\omega t + kx)} \tag{7.31}$$

$$v^{\pm}(x,t) = \frac{v_{\mathrm{i}}^{\pm}}{\rho_0 c}\, e^{j(\omega t - kx)} - \frac{v_{\mathrm{r}}^{\pm}}{\rho_0 c}\, e^{j(\omega t + kx)} \tag{7.32}$$

where the acoustic velocities are readily obtained from the momentum equation.

The boundary conditions on the velocity are:

$$v^{\pm}(x=0,t) = |v| e^{j\omega t} \qquad ; \qquad v^{+}(x=L,t) = \frac{p^{+}(x=L,t)}{Z_l\, S} \tag{7.33}$$

where $|v|$ is the velocity amplitude of the diaphragm and Z_l is the acoustic impedance of the tube termination.

Solving for the acoustic pressure after the diaphragm we get:

$$p^{+}(x,t) = \frac{\rho_0 c |v|}{1 - e^{-j2kL}\dfrac{(Z_l - \rho_0 c/S)}{(Z_l + \rho_0 c/S)}} \left[e^{-jkx} + e^{jk(x-2L)} \left(\frac{Z_l - \rho_0 c/S}{Z_l + \rho_0 c/S} \right) \right] e^{j\omega t} \tag{7.34}$$

The acoustic pressure before the diaphragm is given by:

$$p^{-}(x,t) = \left(2\, p_{\mathrm{i}}^{-} \cos(kx) - \rho_0 c |v| e^{jkx} \right) e^{j\omega t} \tag{7.35}$$

The first term on the right-hand side represents the "blocked pressure", which is the pressure that would exist if the diaphragm were fixed. The second term on the right-hand side represents the contribution to the pressure field due to the diaphragm motion.

The equation of motion for the diaphragm can be written as:

$$\left[j\left(\omega m - \frac{s}{\omega}\right) + r\right] |v| e^{j\omega t} = p^{-}(x=0,t) - p^{+}(x=0,t) \qquad (7.36)$$

Using Equations 7.34, 7.35, and 7.36, the incident acoustic pressure amplitude is given by:

$$p_i^{-} = \frac{|v|}{2}\left(\rho_0 c\left[1 + \frac{Z_l + j\,(\rho_0 c/S)\,\tan(kL)}{(\rho_0 c/S) + j\,Z_l\,\tan(kL)}\right] + \left[j\left(\omega m - \frac{s}{\omega}\right) + r\right]\right) \qquad (7.37)$$

The acoustic impedance at the diaphragm on the source side is obtained from Equations 4.4, 7.35, and 7.37:

$$\begin{aligned} Z(x=0^{-},t) &= \frac{2\,p_i^{-}}{S|v|} - \frac{\rho_0 c}{S} \\ &= \frac{\rho_0 c}{S}\left[\frac{Z_l + j\,(\rho_0 c/S)\,\tan(kL)}{(\rho_0 c/S) + j\,Z_l\,\tan(kL)}\right] + \frac{[j\,(\omega m - s/\omega) + r]}{S} \\ &= Z_a + Z_m \end{aligned} \qquad (7.38)$$

Z_a is the acoustic impedance of a tube having a termination impedance Z_l (see Equation 6.5), and Z_m is the mechanical impedance of the diaphragm.

5.7.3.2.2. Effect of Diaphragm Properties on the Sound Field as a Function of Frequency

Inspecting Equation 7.38 helps us understand how the diaphragm affects the sound field inside the tube. It is clear that in order to minimize its impact on the sound field, the total impedance Z of the system must be dominated by the acoustic impedance Z_a ($Z_a \gg Z_m$), which can be insured by a proper design and placement of the diaphragm.

Next we can look at the frequency response of Z_m, by first taking the simple case of a plane wave traveling in an infinitely long or an anechoically terminated tube. The total acoustic impedance at the diaphragm is given by:

$$Z(x = 0^-, t) = \frac{\rho_0 c}{S} + \frac{1}{S}\left[j\left(\omega m - \frac{s}{\omega}\right) + r\right] \tag{7.39}$$

At very low frequencies ($\omega \ll \omega_r$, where $\omega_r = \sqrt{\frac{s}{m}}$) the total impedance Z is controlled by the diaphragm stiffness, while at high frequencies ($\omega \gg \omega_r$), the diaphragm mass is dominant. In either case, the diaphragm greatly affects the sound field, limiting the amount of acoustic energy that can pass through it. At a frequency ω_r, the diaphragm is at resonance and its effect on the sound field is minimal (Z_m is at the minimum). In other words, the diaphragm acts as a band-pass filter.

For a small damping compared to the acoustic impedance ($r \ll \rho_0 c$), the diaphragm is essentially acoustically transparent until it bottoms-out (see Section 5.7.3.1.3). For a light-weight, low-stiffness diaphragm, the stiffness and inertia only become dominant at very low and very high frequencies, respectively, well outside the operating frequency range of the system.

As mentioned above, proper design and placement of the diaphragm can minimize its effect on the sound field.

For instance, in the case of a closed tube, the system impedance becomes:

$$Z(x = 0^-, t) = -j\frac{\rho_0 c}{S}\cot(kL) + \frac{1}{S}\left[j\left(\omega m - \frac{s}{\omega}\right) + r\right] \tag{7.40}$$

For a diaphragm placed at a distance L from the closed end such that $L = n\frac{\lambda}{2}$, the acoustic impedance Z_a goes to infinity and the diaphragm effect is negligible whatever its impedance is. In other words, placing the diaphragm at

a velocity node (i.e., zero acoustic velocity) minimizes its effect. Another reason for placing the diaphragm at a velocity node is that it will not move and therefore will not bottom-out, thus allowing the use of a tight diaphragm.

Similarly, for an open-ended tube, the diaphragm should be placed at a distance L from the end such that $L = (2n+1)\frac{\lambda}{4}$.

5.7.3.2.3. Generalization to Any Diaphragm

The results from the previous section can be generalized and used for any tube and diaphragm arrangement by replacing Z_a and Z_m in Equation 7.38. This generalization is most useful in presenting some design guidelines on how to minimize the effect of "real-life" diaphragms on the sound field in PCCE tubes.

The silvered Mylar diaphragms used have physical characteristics which differ from the "rigid partition" assumption of the preceding section. These differences, as well as their effect on the previous results, are listed below:

- The amplitude of the diaphragm motion is not constant over the whole diaphragm area. However, this has no effect on the equations in Section 5.7.3.2.1 since the acoustic velocity $|v|$ is equal to the diaphragm velocity averaged over the whole diaphragm area.
- The mass per unit area m of the diaphragm is about 0.0178 kg/m^2. Neglecting stiffness and damping, and using the previous filter analogy, the diaphragm can be looked at as a low-pass filter. The 3-dB point occurs when $Z_m = \frac{\omega m}{S}$ is equal to $Z_a = \frac{\rho_0 c}{S}$, which corresponds to a frequency of 3710 Hz. Therefore, at the low frequencies of interest in this study ($\approx$ 200 Hz), the transmission loss due to the diaphragm inertia is negligible (-0.005 dB at 200 Hz).

- The stiffness term is a complex function of the bending stiffness and the Young's modulus of the diaphragm material. Due to diaphragm construction and mounting, this term is most probably highly non-linear and varies widely from one diaphragm to another. No simple theoretical estimate can be found for the stiffness term and experiments should be carried out to determine its magnitude versus degree of tightness and displacement. However, the basic conclusion from the previous section is still valid: the diaphragm is stiffness-controlled at low frequencies (stiffness acts as a high-pass filter). The frequency range of the stiffness-controlled region should be determined experimentally.
- The damping term is also different in the case of a PCCE diaphragm. However, it is probably negligible compared to the inertia and stiffness terms.

5.7.3.2.4. Conclusions

The inertia of diaphragms used in PCCE tubes acts as a low-pass filter. For Mylar, the 3-dB point of the filter is equal to 3710 Hz. Thus inertia is only important for high-frequency mixing using quadrature speakers.

The stiffness of diaphragms acts as a high-pass filter and might have an effect on the sound transmission at low frequencies depending on its magnitude. The easier the diaphragm can "flap" back and forth, the less it will affect the sound field.

Finally, when diaphragms are in a standing wave field, their effect can be minimized by mounting them where the acoustic impedance is at a maximum (i.e., where the acoustic velocity is at a minimum). In the case of a closed tube at very low frequencies, this might not be possible, and the diaphragms should be placed as close as possible to the tube terminations, where the acoustic velocity

is very small. In any case, mounting diaphragms at velocity antinodes should be avoided at all costs, because the diaphragms' contribution to the total impedance is then maximized and they might stretch (bottom-out).

5.8. Two-Speaker Configuration

The two-speaker configuration has been used in PCCE tubes as a means to better control the mixing process. The use of two low frequency opposite loudspeakers allows better control of the standing wave pattern inside the combustor tube, and therefore of the mixing process. The next two sections review the two most common two-speaker configurations.

5.8.1. Non-Reflecting Two-Speaker Configuration

The non-reflecting two-speaker configuration is the simplest one. Although it is unachievable with the present design of PCCE tubes due to the low acoustic attenuation, it represents an ideal situation which best explains the concept of the two-speaker set up.

In this configuration, the two loudspeakers are facing each other and the sound field on the loudspeakers' axis is assumed to be only a combination of the two incident waves coming from each loudspeaker. In other words, no sound from one loudspeaker is reflected by the other. This configuration is typical of a large anechoic chamber, or of the case when the acoustic attenuation is so high that reflected and incident waves do not interfere with each other. For instance, such an acoustic system is a good model for the multi-speaker acoustic levitation devices designed for use in a zero-gravity environment.

A non-reflecting two-speaker configuration for acoustic mixing is shown in the figure below.

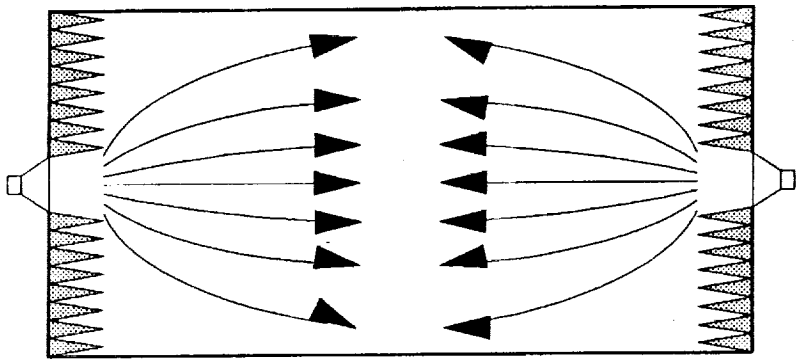

The two loudspeakers are mounted facing each other in an anechoic chamber. Most of the sound radiated by each loudspeaker is absorbed by the anechoic area surrounding the opposite loudspeaker so that the interactions between incident and reflected waves are negligible. However, this set up is bulky and the desired standing wave and strongest mixing only occur on the loudspeakers' axis.

The boundary conditions on the diaphragm velocity for the left and the right loudspeakers are as follows:

$$v_l(t) = v_1 \cos\left(-\frac{\phi}{2}\right) e^{j\omega t} \tag{8.1}$$

$$v_r(t) = v_2 \cos\left(+\frac{\phi}{2}\right) e^{j\omega t} \tag{8.2}$$

Thus, the acoustic velocity on the loudspeakers' axis is given by:

$$v(x,t) = v_1(x) \cos\left(-kx - \frac{\phi}{2}\right) e^{j\omega t} + v_2(x) \cos\left(kx + \frac{\phi}{2}\right) e^{j\omega t} \tag{8.3}$$

The x dependence of the acoustic velocities $v_1(x)$ and $v_2(x)$ takes into account the spreading of the acoustic beam radiated from the loudspeaker.

For instance, $v_1(x) = v_1\sqrt{\frac{S_0}{S(x)}}$ where S_0 is the area of the left loudspeaker diaphragm and $S(x)$ is the area of the beam cross-section from that loudspeaker at x. The shape of the beam depends on the shape and size of the diaphragm as well as the sound wavelength. For the sake of simplicity, we assume here that the waves from each loudspeaker are planar and that $v = v_1(x) = v_2(x)$. Using Equation 3.2 for a traveling plane wave, the acoustic pressure amplitude on the loudspeakers' axis can be written as:

$$p(x,t) = 2\rho_0 c\, v \cos\left(kx + \frac{\phi}{2}\right) e^{j\omega t} \tag{8.4}$$

$p(x,t)$ is characteristic of a standing wave pattern having a normalized amplitude $\cos\left(kx + \frac{\phi}{2}\right)$. For a zero phase shift between loudspeakers ($\phi =$ 0 degrees), the sound amplitude is maximum at the center ($x = 0$). For a 180 degrees phase shift between loudspeakers ($\phi =$ 180 degrees), the sound amplitude is zero at the center. Thus the standing wave pattern and the position of the mixing cells can be shifted by changing ϕ.

It is possible to move the nodes of the standing wave continuously and thus also move the mixing cells by continuously changing the phase shift between each source. This is best achieved by using slightly different excitation frequencies for each loudspeaker. Rewriting the boundary conditions on the diaphragm velocity of the left and right loudspeakers as follows:

$$v_l(t) = v_1 \cos\left(-\frac{\phi}{2}\right) e^{j\omega_1 t} \tag{8.5}$$

$$v_r(t) = v_2 \cos\left(+\frac{\phi}{2}\right) e^{j\omega_2 t} \tag{8.6}$$

we get the acoustic pressure:

$$p(x,t) = 2\rho_0 c\, v \cos\left[kx + \frac{\phi}{2} + \Delta\omega\left(t + \frac{x}{c}\right)\right] e^{j\omega t} \qquad (8.7)$$

where $\omega = \frac{\omega_1 + \omega_2}{2}$ and $\Delta\omega = \frac{\omega_1 - \omega_2}{2}$. $\Delta\omega$ controls the speed of the motion of the mixing cells.

5.8.2. **Reflecting Two-Speaker Configuration**

The reflecting two-speaker configuration shown in the figure below is a good approximation of the two-speaker set up tested in the 2-inch diameter PCCE

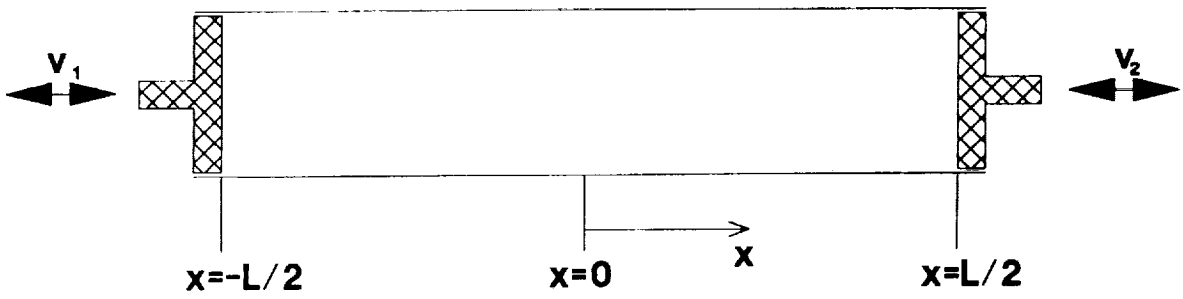

tube.

In this configuration, sound waves are reflected by the diaphragms from each loudspeaker, imposing two non-zero boundary conditions on the acoustic velocity in the tube. It is assumed that the operation of each loudspeaker is unaffected by the sound field inside the tube. In other words, the combined mechanical-electrical impedance of the loudspeakers is much higher than the acoustic impedance of the tube. This assumption is usually valid for most loudspeakers except around the tube resonance frequency.

5.8.2.1. General Relationships

Solving for the acoustic pressure using the boundary conditions given by Equations 8.1 and 8.2, we get:

$$p(x,t) = \frac{\rho_0 c}{\sin(kL)} \left[-\sin\left(\frac{\phi}{2}\right) \left(v_1 \cos\left[k\left(x - L/2\right)\right] + v_2 \cos\left[k\left(x + L/2\right)\right] \right) + j \cos\left(\frac{\phi}{2}\right) \left(-v_1 \cos\left[k\left(x - L/2\right)\right] + v_2 \cos\left[k\left(x + L/2\right)\right] \right) \right] \quad (8.8)$$

or, if $p(x,t) = \beta e^{j\varphi}$:

$$\beta = \frac{\rho_0 c}{|\sin(kL)|} \left[\left(v_1 \cos\left[k\left(x - L/2\right)\right]\right)^2 + \left(v_2 \cos\left[k\left(x + L/2\right)\right]\right)^2 - 2 v_1 v_2 \cos\left[k\left(x - L/2\right)\right] \cos\left[k\left(x + L/2\right)\right] \cos(\phi) \right]^{1/2} \quad (8.9)$$

and

$$\tan^{-1}(\varphi) = \tan\left(\frac{\phi}{2}\right) \left(\frac{v_1 \cos\left[k\left(x - L/2\right)\right] + v_2 \cos\left[k\left(x + L/2\right)\right]}{v_1 \cos\left[k\left(x - L/2\right)\right] - v_2 \cos\left[k\left(x + L/2\right)\right]} \right) \quad (8.10)$$

Equation 8.9 characterizes a standing wave of period $\frac{\lambda}{2}$.

5.8.2.2. Moving the Standing Wave Pattern

The expression for the magnitude of the pressure amplitude β is much more complex than in the case of two non-reflecting loudspeakers, and the control of the standing wave pattern in the tube is not as straightforward. The two parameters that can be used to move the standing wave around are the relative phase ϕ and the relative amplitude $\frac{v_1}{v_2}$ between loudspeakers.

5.8.2.2.1. Changing the Relative Phase between Loudspeakers

The effect of changing the relative phase between loudspeakers is given by looking at the rate of variation of β with ϕ while holding the other parameters constant. From inspection of Equation 8.9, the result is obvious and given by:

$$\left[\frac{\partial \beta^2}{\partial \phi}\right]_{(v_1/v_2)} = \text{Constant} \times \sin(\phi) \tag{8.11}$$

Therefore, the minimums and maximums in the standing wave pattern occur for $\phi = n\pi$ and are independent of frequency (or wavenumber). In other words, as opposed to the previous case, the standing wave pattern cannot be moved on the loudspeakers' axis by changing the relative phase alone. This is illustrated in the next figure showing the normalized magnitude of the acoustic pressure in the tube for several relative phase angles between loudspeakers. The loudspeakers' amplitudes are kept constant and equal ($v_1 = v_2 = 1$), and the frequency is such that $L = 1.5\,\frac{\lambda}{2}$, which is halfway between the resonance frequencies for $\phi = 0$ and for $\phi = \pi$ (see Section 5.8.2.3).

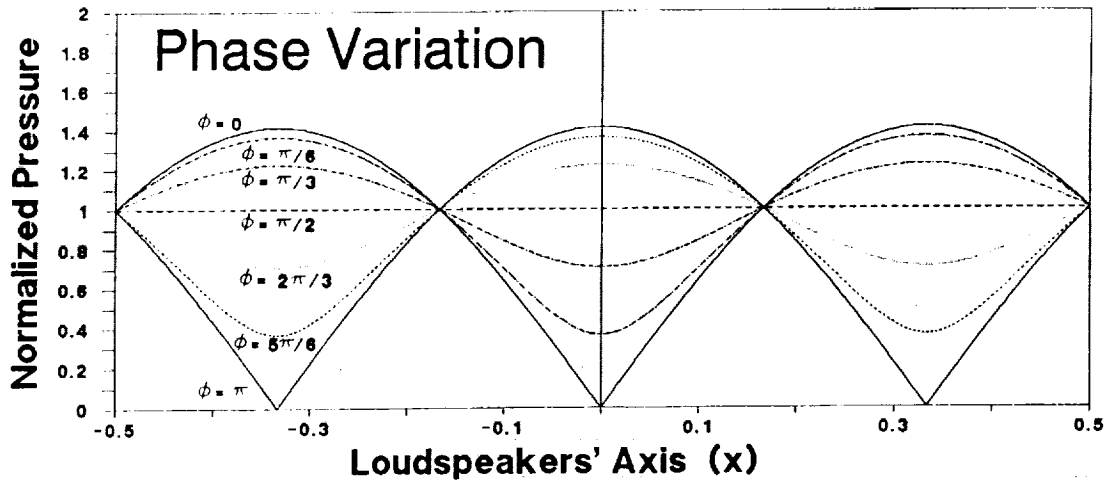

For $\phi = 0$, the acoustic pressure magnitude β is zero at the center of the tube due to the symmetrical motion of the loudspeaker diaphragms. At very low frequencies, the air moves back and forth in the tube in an incompressible fashion (β is very small). For $\phi = \frac{\pi}{2}$, β is constant through the pipe and no standing waves are present (this is only true when $v_1 = v_2$). For $\phi = \pi$, β is maximum at the center of the tube due to the opposite motion of the loudspeakers' diaphragms.

The variation of the pressure magnitude β as a function of the relative phase angle ϕ in the middle of the tube is displayed in the next picture.

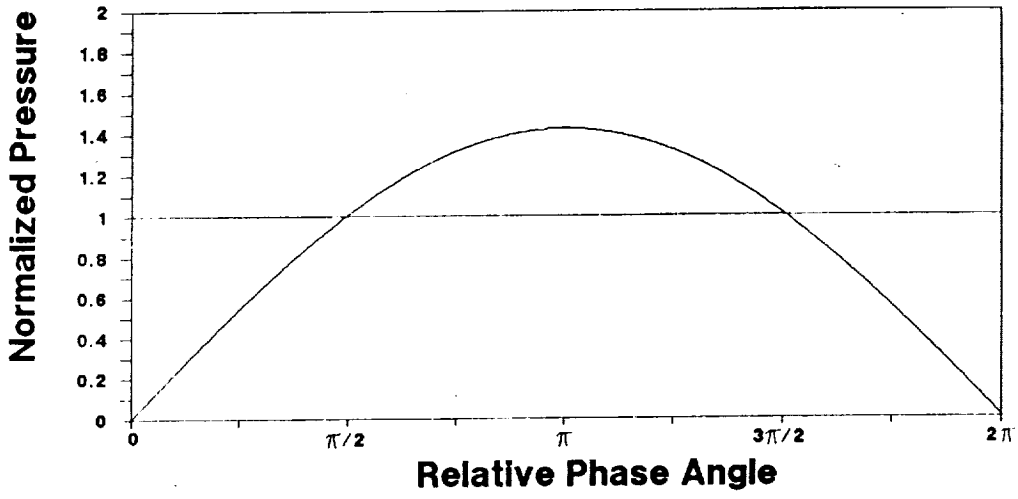

In effect, changing the relative phase between loudspeakers changes the direction of rotation of the streaming vortices.

5.8.2.2.2. Changing the Loudspeakers' Amplitudes

The effect of changing the amplitudes of the loudspeakers while holding the other parameters constant is given by:

$$\left[\frac{\partial\beta^2}{\partial(v_1/v_2)}\right]_\phi = \text{Constant}' \times \left[\left(\frac{v_1}{v_2}\right)\cos\left[k(x-L/2)\right] - \cos\left[k(x+L/2)\right]\cos\phi\right] \tag{8.12}$$

The minimum of the pressure magnitude β occurs for:

$$\frac{v_1}{v_2} = \frac{1-\tan(kx)\tan(kL/2)}{1+\tan(kx)\tan(kL/2)}\cos\phi \tag{8.13}$$

or

$$\tan(kx) = \cot\left(\frac{kL}{2}\right)\left[\frac{1-v_1/(v_2\cos\phi)}{1+v_1/(v_2\cos\phi)}\right] \tag{8.14}$$

This equation can be satisfied for any value of x by a proper combination of the loudspeakers' relative phase angle and amplitudes.

The figure below shows the solution of Equation 8.13 as a function of x for a relative phase angle $\phi = 0$, and a frequency such that $L = 2.15\,\frac{\lambda}{2}$. For each x, the relative amplitude $\frac{v_1}{v_2}$ is obtained from Equation 8.13. Next, v_1 and v_2 are normalized so that the pressure magnitude β in the tube at a node is equal to ρc.

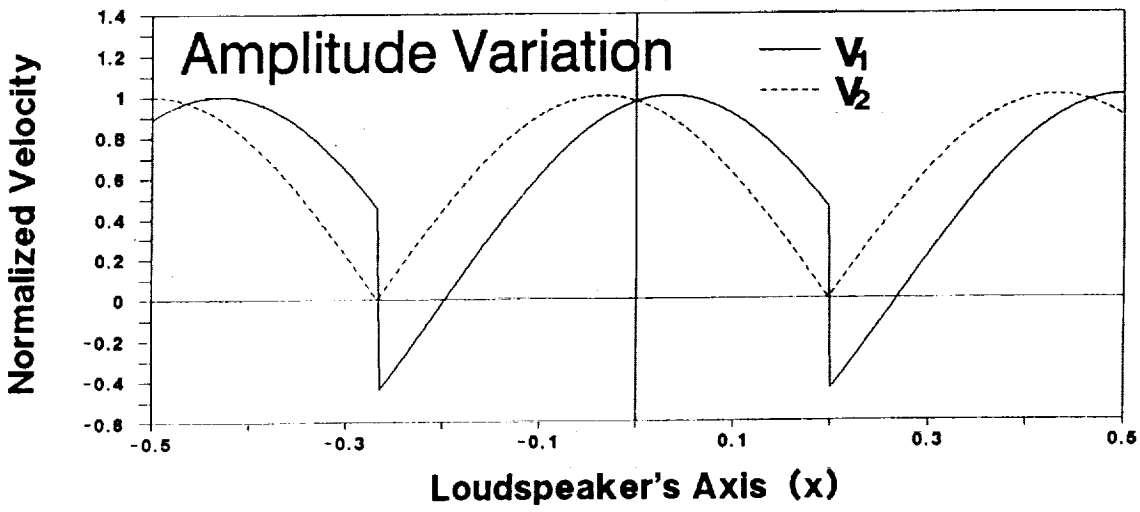

The next figure shows the magnitude of the acoustic pressure in the PCCE tube obtained using Equation 8.9, and for a pressure minimum at $x_0 = -\frac{3}{10} L$. From the previous figure, the normalized diaphragm velocity of the two loudspeakers required for a pressure minimum at x_0 are: $v_1 = 0.637$ and $v_2 = 0.218$.

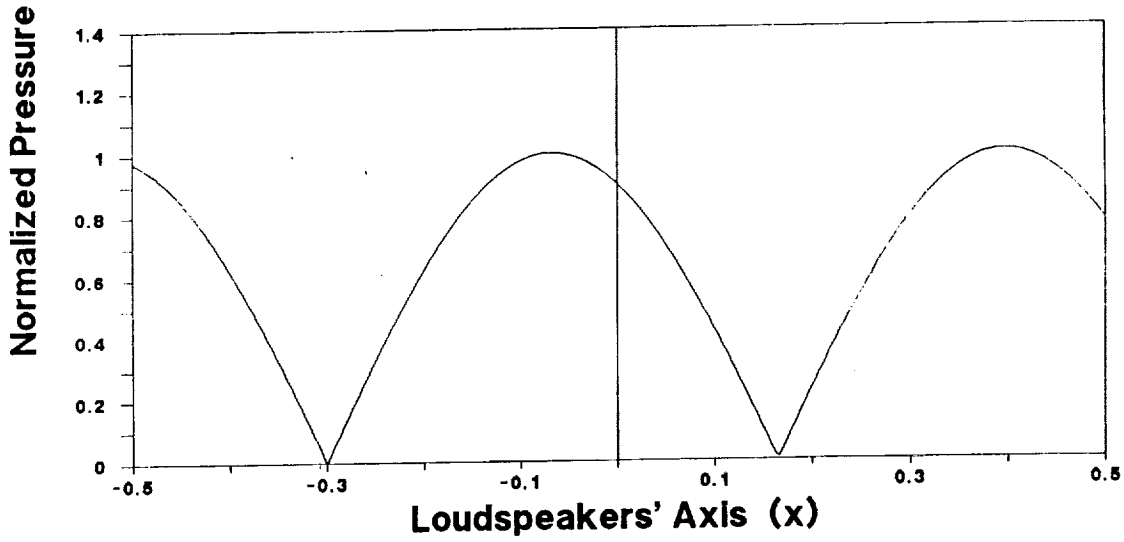

5.8.2.3. **Resonances**

Resonance occurs in the tube when the pressure magnitude β (Equation 8.9) goes to infinity. The resonance frequencies depend on the relative phase angle and amplitude between loudspeakers.

5.8.2.3.1. $\phi = 0$ **and** $v = v_1 = v_2$

The pressure magnitude β simplifies to:

$$\beta = v\rho_0 c \left| \frac{\sin(kx)}{\cos(kL/2)} \right| \tag{8.15}$$

Therefore, in this case, resonance occurs when the length of the pipe is equal to an odd number of half-wavelengths:

$$L = (2n + 1)\frac{\lambda}{2} \tag{8.16}$$

or

$$f_r(n) = (2n + 1)\frac{c}{2L} \tag{8.17}$$

The frequency interval between resonances is twice the frequency interval obtained in the case of one loudspeaker in a closed or open-ended tube (see Equations 4.6 and 5.5).

5.8.2.3.2. $\phi = \pi$ **and** $v = v_1 = v_2$

The pressure magnitude β reduces to:

$$\beta = v\rho_0 c \left| \frac{\cos(kx)}{\sin(kL/2)} \right| \tag{8.18}$$

Resonances occur when the length of the pipe is equal to an integer number of wavelengths:

$$L = n\lambda \tag{8.19}$$

or

$$f_r(n) = n\frac{c}{L} \tag{8.20}$$

The resonance frequencies when $\phi = \pi$ correspond to the antiresonance frequencies when $\phi = 0$.

5.8.2.3.3. $\phi \neq 0$ and $v_1 \neq v_2$

In this more general case, resonances occur when the denominator in Equation 8.9 is equal to zero, i.e., when the length of the pipe is equal to an integer number of half-wavelengths:

$$L = n\frac{\lambda}{2} \tag{8.21}$$

or

$$f_r(n) = n\frac{c}{2L} \tag{8.22}$$

The frequency interval between resonances is the same as the frequency interval obtained in the case of one loudspeaker in a closed or open-ended tube.

5.8.2.4. Conclusions

Again, as mentioned in the introduction, this analysis assumes that each loudspeaker diaphragm has the same area as the tube cross section and that the diaphragms' motions are unaffected by the acoustic field in the tube. This represents ideal velocity sources such as two rigid pistons in a tube, as in the figure below.

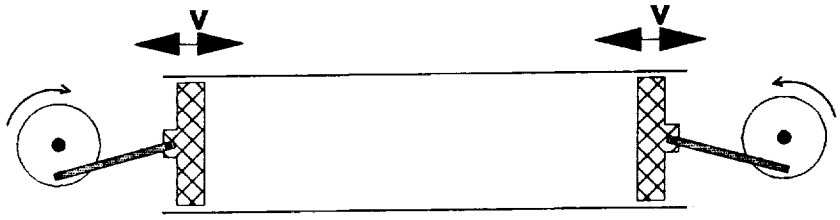

Here the motion of the pistons is unaffected by the fluid motion inside the tube. At resonance, the acoustic impedance of the fluid at the face of each piston is very large and the pistons require more energy to keep the faces moving at a constant velocity. This can be illustrated by replacing the air inside the tube by a medium having a higher acoustic impedance in order to simulate resonance. For instance, if the air in the tube were replaced with water, which has a characteristic impedance 3566 times the characteristic impedance of air, it is obvious that the pistons would require an increase in power in order for the faces to maintain the same velocity as they would if the working fluid were air. Moreover, the stresses in the pistons' faces will be very high due to the high pressure in the fluid.

Loudspeakers used in PCCE experiments have a finite impedance and do not act as rigid pistons at resonance. However, the analysis above should be accurate for frequencies slightly away from the system resonance frequency. Around the resonance frequency, a more accurate model can be obtained by replacing the constant velocity boundary condition at the loudspeakers' diaphragms by a complex impedance boundary condition. This complex impedance can be measured or calculated using loudspeaker modeling techniques.

6. Axial Resonances for PCCE Combustors

Due to the rigid terminations of the PCCE tube, axial resonances are present which affect the mixing process. These resonances occur whether plane waves or higher-order modes are excited. In this section, the frequencies for which resonances occur are calculated in the case of plane waves and higher-order modes. It is shown that the axial resonance frequencies are very close to each other just above the cut-off frequency of the first spinning mode.

6.1. Axial Resonances for Plane Waves

Below the cut-off frequency of the first higher-order mode, only plane waves propagate in the tube. Resonances occur when the pipe length L is an integer multiple n of half the sound wavelength λ, i.e.,

$$L = n\frac{\lambda}{2} \tag{1}$$

or

$$f_r(n) = \frac{nc}{2L} \tag{2}$$

where $f_r(n)$ is the n^{th} resonance frequency and c is the speed of sound. The resonance frequencies are separated by:

$$\Delta f_r(n) = f_r(n+1) - f_r(n) = \frac{c}{2L} \tag{3}$$

For a 33.5-inch long tube, $\Delta f_r(n) = 200$ Hz ($c = 340$ m/s).

6.2. Axial Resonances for the First Spinning Mode

Axial resonances also occur in the tube when higher-order modes are excited. However, these resonances do not occur at regular frequency intervals (as in the plane wave) due to the constant variation of the axial wave number k_z.

When a higher-order mode is excited, the axial wave number is given by:

$$k_z = \sqrt{k^2 - k_r^2} \tag{4}$$

where k is the wave number and k_r is the radial wave number. In a tube, k_r is such that:

$$k_r R = \gamma_{mn} \tag{5}$$

where R is the PCCE tube radius ($R = 2.5\,\text{cm}$), and γ_{mn} is the root of the derivative of the Bessel function. In the case of the PCCE tube, only the first spinning mode (mode 1,0) is excited. For this mode, $\gamma_{10} = 1.84$. Therefore,

$$k_r = \frac{1.84}{R} \tag{6}$$

Thus,

$$k_z = \sqrt{\left(\frac{2\pi f}{c}\right)^2 - \left(\frac{1.84}{R}\right)^2}$$

$$= \sqrt{3.415 \times 10^{-4} f^2 - 5248} \tag{7}$$

The following figure displays k and k_z for the first spinning mode of the PCCE combustor, illustrating the nonlinear variation of k_z with frequency.

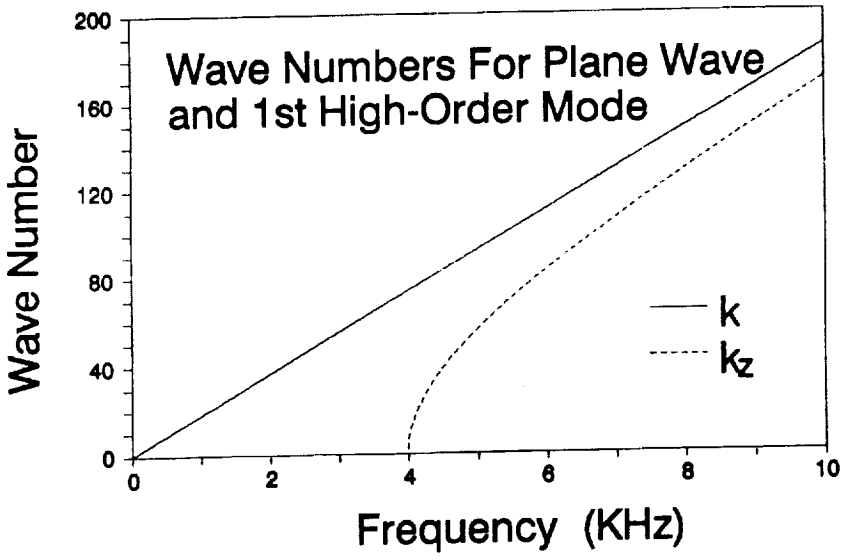

The cut-off frequency of the first mode occurs for $k_z = 0$, or

$$f_c = \sqrt{\frac{5248}{3.415 \times 10^{-4}}} = 3920 \text{ Hz} \tag{8}$$

As the frequency increases above f_c, the axial wavenumber increases nonlinearly from 0 when $f = f_c$, to k when $f \to \infty$.

The resonance condition is the same as in the plane wave case: resonance occurs when the pipe length L is an integer multiple n of half the sound axial wavelength λ_z, i.e.,

$$L = n\frac{\lambda_z}{2} \tag{9}$$

replacing the axial wavelength λ_z by the axial wavenumber k_z, we get:

$$k_z = \frac{n\pi}{L} \tag{10}$$

Thus using Equation 7, axial resonances occur when:

$$\frac{n\pi}{L} = \sqrt{\left(\frac{2\pi f_r(n)}{c}\right)^2 - \left(\frac{1.84}{R}\right)^2} \tag{11}$$

or

$$f_r(n) = \frac{c}{2\pi}\sqrt{\left(\frac{n\pi}{L}\right)^2 + \left(\frac{1.84}{R}\right)^2}$$

$$= 54.11\sqrt{13.63\,n^2 + 5248} \tag{12}$$

The following table lists the resonance frequencies $f_r(n)$, the frequency interval between each resonance $\Delta f_r(n)$, the axial wavelength λ_z, and the wavelength λ as a function of n

n	$f_r(n)$ Hz	$\Delta f_r(n)$ Hz	λ_z inches	λ inches
1	3925	15	67.00	3.41
2	3940	25	33.50	3.40
3	3965	36	22.33	3.38
4	4001	44	16.75	3.35
5	4045		13.40	3.31
10	4400	94	6.70	3.04
11	4494		6.09	2.98
20	5597	144	3.35	2.39
21	5741		3.19	2.33
50	10730	186	1.34	1.25
51	10916	187	1.31	1.23
52	11103		1.29	1.21

As the frequency increases, the frequency interval $\Delta f_r(n)$ between resonance frequencies increases up to the plane wave value 200 Hz. At frequencies just above the cut-off frequency of the first spinning mode, the frequency interval between resonances is very small.

A quick experimental check was carried out by measuring the frequency response of the PCCE combustor.

The sound pressure level in the PCCE combustor was measured with two microphones mounted flush with the combustor wall. A radial microphone probe was used to identify the modal characteristics of the sound field inside the tube, and an axial microphone probe was used to check the axial homogeneity of the sound field. The frequency response of the combustor was checked by sweeping the frequency from 3500 Hz to 4100 Hz and recording the output signals from the wall-mounted microphones. The sound pressure levels at the microphones are fairly low below the cut-off frequency of the first spinning mode (plane waves

only) except when axial resonances are excited (every 200 Hz). Above the cut-off frequency of the first spinning mode, the sound pressure levels are much higher (10 dB to 15 dB higher) due to the nonuniform pressure distribution in the tube cross-section. Several peaks in the frequency response appear at small frequency intervals and right after the cut-off frequency, corresponding to the axial resonance frequencies obtained with Equation 12, thus confirming the theoretical results.

7. Conclusions and Recommendations

1. Combined operation of axial and quadrature speakers promises greatly enhanced mixing compared to mixing by either mode alone. This prediction is confirmed both experimentally and theoretically. A program of drop tower tests is certainly justified.
2. Complete mixing in a sphere by steady streaming does not seem to be possible except under extremely carefully controlled conditions. Satisfactory mixing in a hemisphere is certainly possible. If mixing in the entire sphere is required, it is recommended that the speaker be operated in transient bursts. Of course, this mixing procedure can only be effective in micro-gravity.
3. Purely radial modes produce no secondary motion. Operation of the speakers at the corresponding frequencies will be completely ineffective.
4. The following topics are suggested for possible further study. They are listed in order of presumed complexity.
   a. Solve the boundary value problem of a sphere driven by two arbitrarily spaced and phased speakers. This would lead to an identification of the nodal plane for spinning modes in a sphere.
   b. Compute streaming, incorporating the small viscous corrections to the compressibility and frequencies. This will make possible an exact satisfaction of the no-slip boundary conditions.
   c. Investigate more carefully the possibility of radial nodes in the cylinder and sphere secondary flows. Could vorticity be generated internally by shearing motions in the first order acoustic fields?
   d. Study the interaction of first order axial and spinning modes.

e. Investigate the effects of radiation pressure much more thoroughly. What are the effects of multiple scattering on radiation pressure in a dense particle field? What is the nature of the motion of particles through the fluid due to radiation pressure? Is mixing influenced by particle density? This last question may be quite important.

References

[1.] Kundt, Ann. Physik, Vol. 127, pp. 497, 1866; Vol. 128, pp. 337, 1866.

[2.] Tyndall, J., *The Science of Sound*, Philosophical Library, Inc., pp. 244-253, 1964.

[3.] Koenig, W., Ann. Physik, Vol. 42, pp. 353 and pp. 549, 1891; Vol. 43, pp. 443, 1891.

[4.] Rayleigh, J. W. S., *The Theory of Sound*, Sec. 253b, Dover Publications, 1945.

[5.] Robinson, J., "Dust Figures," Proc. Lond. Phys. Soc., Vol. 25, pp. 256–263, 1913.

[6.] Thomas, G., Ann. Physik, (4), Vol. 42, pp. 1079, 1913.

[7.] Cook, S. H., "On the Distribution of Pressure around Spheres in a Viscous Fluid," Phil. Mag., Vol. 6, pp. 424–436, 1903.

[8.] Cook, S. H., Phil. Mag., Vol. 3, pp. 471, 1902.

[9.] Irons, E. J., "Studies in the Formation of Kundt's Tube Dust Figures," Phil. Mag., Vol. 7, pp. 523–537, 1929.

[10.] Andrade, E. N. , "On the Circulations Caused by the Vibration of Air in a Tube," Proc. Roy. Soc., A, Vol. 134, pp. 445–470, 1931.

[11.] Andrade, E. N. , "On the Groupings and General Behavior of Solid Particles Under the Influence of Air Vibrations in Tubes," Phil. Trans., A, Vol. 230, pp. 413–445, 1931.

[12.] Andrade, E. N. , "The Coagulation of Smoke by Supersonic Vibrations", pp. 1111–1125.

[13.] Andrade, E. N., "Sound Smoke Light on Old Problems," Royal Institution Library of Science-Physical Sciences. Edited by W. L. Bragg and G. Porter

[14.] St. Clair, H. W., "Agglomeration of Smoke, Fog, or Dust Particles by Sonic Waves," Industrial and Engineering Chemistry, Vol. 41, No. 11, pp. 2434–2438, 1949.

[15.] Mednikov, E. P., *Acoustic Coagulation and Precipitation of Aerosols*, Translated from Russian, Consultant Bureau Enterprise, Inc., 1965.

[16.] Faraday, M., Phil. Tran. Rev. Soc. (London) 121, 229, 1831. .

[17.] Rozenberg, L. D., *High-Intensity Ultrasonic Fields*, Plenum Press, 1971.

[18.] Goldberg, Z. A., "On the Propagation of Plane Waves of Finite Amplitude," Soviet Physics Acoustics, Vol. 3, pp. 340–347, 1957.

[19.] Eckart, C., "Vortices and Streams Caused by Sound Waves," Physical Review, Vol. 73, No. 1, pp. 68–76, 1948.

[20.] Ivanovskii, A. I., "Theoretical and Experimental Investigation of Sonically Induced Streaming," Gidrometeoizdat, 1959.

[21.] Statnikov, Y. G., "Streaming Induced by Finite-Amplitude Sound," Akust. Zh., Vol. 13 (1), pp. 146, 1967.

[22.] Rudenko, O. V., and Soluyan, S. I., *Theoretical Fundations of Nonlinear Acoustics*, Plenum, New York, 1977.

[23.] Fay, R. D., "Plane Sound Waves of Finite-Amplitude," The Journal of The Acoustical Society of America, Vol. 3, pp. 222–241, 1931.

[24.] Borisov, Y. Y., and Statnikov, Y. G., "Flow Currents Generated in an Acoustic Standing Wave," Akust. Zh., Vol. 11 (1), pp. 35, 1965.

[25.] Schlichting. H., Boundary-Layer Theory, McGraw-Hill, 1955.

[26.] Holzmark, J., Johnsen, I., Sikkeland, T., and Skavlem, S., "Boundary-Layer Flow Near a Cylindrical Obstacle in an Oscillating Incompressible Fluid," The Journal of the Acoustical Society of America, Vol. 26, No. 1, pp. 26, 1954.

[27.] Raney, W. P., Corelli, J. C., and Westervelt, P. J., "Acoustic Streaming in the Vicinity of a Cylinder", The Journal of the Acoustical Society of America, Vol. 26, No. 6, pp. 1006, 1954.

[28.] Lane, C. M. A., "Acoustical Streaming in the Vicinity of a Sphere," The Journal of the Acoustical Society of America, Vol. 27, No. 6, pp. 1123, 1953.

[29.] Andres, J. M., and Ingard, U., "Acoustic Streaming at High Reynolds Numbers," The Journal of the Acoustical Society of America, Vol. 25, No. 5, pp. 928, 1953.

[30.] Andres, J. M., and Ingard, U., "Acoustic Streaming at Low Reynolds Numbers," The Journal of the Acoustical Society of America, Vol. 25, No. 5, pp. 932, 1953.

[31.] Nyborg, W. M., "Acoustic Streaming", *Physical Acoustics*, Vol. 2, Part B., pp. 265–330, 1965

[32.] King, L. V.. Proc. Roy. Soc., A147, pp. 212, 1934.

[33.] Seifert, H. S., "A Miniature Kundt Tube," American Journal of Physics, Vol. 7, pp. 421–422, 1939.

[34.] Baker, R. A., "A Variation of Kundt's Method for the Speed of Sound," American Journal of Physics, Vol. 7, pp. 423–424, 1939.

[35.] Parsons, K. A., "Exciting a Kundt's Tube with a Siren," American Journal of Physics, Vol. 21, No. 5, pp. 392, 1953.

[36.] Baez, A. V., "Kundt's Tube Projection Demonstration," American Journal of Physics, Vol. 21, No. 1, pp. 64, 1953.

[37.] Hammond, H. E., "Exciting a Kundt's Tube with a Siren," American Journal of Physics, Vol. 21, pp. 475, 1953.

[38.] Carman, R. A., "Kundt Tube Dust Striations," American Journal of Physics, Vol. 23, pp. 505–507, 1955.

[39.] Hastings, R. B. and Yung-Yao Shih, "Experiments with an Electrically Operated Kundt Tube," American Journal of Physics, Vol. 30, pp. 512–516, 1962 (Hastings).

[40.] Piersa, H., "Fixing of Dust Figures in a Kundt's Tube," The Journal of The Acoustical Society of America, Vol. 37, pp. 533–535, 1965.

[41.] Hastings, R. B., "Thermistor Explorations in a Kundt Tube," American Journal of Physics, Vol. 37, No. 7, pp. 709–712, 1969.

[42.] Medwin, H., and Rudnick, I. J., The Journal of The Acoustical Society of America, Vol. 25, pp. 538, 1953.

[43.] Rayleigh, J. W. S., *The Theory of Sound*, Sec. 352, Dover Publications, 1945.

[44.] Slater, S. B., and Frank, Q. X., *Electromagnetism*, McGraw Hill, 1953.

[45.] Morse, P. M., and Ingard, U., *Theoretical Acoustics*, McGraw Hill, 1968.

[46.] Abramowitz, M., and Stegun, I., *Tables of Mathematical Functions*, National Bureau of Standards, 1960.

[47.] Maslen, S. H., and Moore, F. K., Journal of Aero Sciences, Vol. 14, pp. 583, 1956.

[33.] Seifert, H. S., "A Miniature Kundt Tube," American Journal of Physics, Vol. 7, pp. 421–422, 1939.

[34.] Baker, R. A., "A Variation of Kundt's Method for the Speed of Sound," American Journal of Physics, Vol. 7, pp. 423–424, 1939.

[35.] Parsons, K. A., "Exciting a Kundt's Tube with a Siren," American Journal of Physics, Vol. 21, No. 5, pp. 392, 1953.

[36.] Baez, A. V., "Kundt's Tube Projection Demonstration," American Journal of Physics, Vol. 21, No. 1, pp. 64, 1953.

[37.] Hammond, H. E., "Exciting a Kundt's Tube with a Siren," American Journal of Physics, Vol. 21, pp. 475, 1953.

[38.] Carman, R. A., "Kundt Tube Dust Striations," American Journal of Physics, Vol. 23, pp. 505–507, 1955.

[39.] Hastings, R. B. and Yung-Yao Shih, "Experiments with an Electrically Operated Kundt Tube," American Journal of Physics, Vol. 30, pp. 512–516, 1962 (Hastings).

[40.] Piersa, H., "Fixing of Dust Figures in a Kundt's Tube," The Journal of The Acoustical Society of America, Vol. 37, pp. 533–535, 1965.

[41.] Hastings, R. B., "Thermistor Explorations in a Kundt Tube," American Journal of Physics, Vol. 37, No. 7, pp. 709–712, 1969.

[42.] Medwin, H., and Rudnick, I. J., The Journal of The Acoustical Society of America, Vol. 25, pp. 538, 1953.

[43.] Rayleigh, J. W. S., *The Theory of Sound*, Sec. 352, Dover Publications, 1945.

[44.] Slater, S. B., and Frank, N. H., *Electromagnetism*, McGraw Hill, 1953.

[45.] Morse, P. M., and Ingard, U., *Theoretical Acoustics*, McGraw Hill, 1968.

[46.] Abramowitz, M., and Stegun, I., *Tables of Mathematical Functions*, National Bureau of Standards, 1960.

[47.] Maslen, S. H., and Moore, F. K., Journal of Aero Sciences, Vol. 14, pp. 583, 1956.

NASA
National Aeronautics and Space Administration

Report Documentation Page

1. Report No.	2. Government Accession No.	3. Recipient's Catalog No.
NASA CR-185159		

4. Title and Subtitle	5. Report Date
Microgravity Acoustic Mixing for Particle Cloud Combustors	March 1990
	6. Performing Organization Code

7. Author(s)	8. Performing Organization Report No.
Frederic Pla and Robert Rubinstein	None (E-5347)
	10. Work Unit No.
	694-24-00

9. Performing Organization Name and Address	11. Contract or Grant No.
Sverdrup Technology, Inc. NASA Lewis Research Center Group Cleveland, Ohio 44135	NAS3-25266
	13. Type of Report and Period Covered Contractor Report Final
12. Sponsoring Agency Name and Address	14. Sponsoring Agency Code
National Aeronautics and Space Administration Lewis Research Center Cleveland, Ohio 44135-3191	

15. Supplementary Notes

Project Manager, Bradford S. Linscott, Structural Systems Division, NASA Lewis Research Center.

16. Abstract

This report describes experimental and theoretical investigations of acoustic mixing procedures designed to uniformly distribute fuel particles in a combustion tube for application in the proposed Particle Cloud Combustion Experiment (PCCE). Two acoustic mixing methods are investigated: mixing in a cylindrical tube using high frequency spinning modes generated by suitably phased, or "quadrature" speakers, and acoustic premixing in a sphere. Quadrature mixing leads to rapid circumferential circulation of the powder around the tube. Good mixing is observed in the circulating regions. However, because axial inhomogeneities are necessarily present in the acoustic field, this circulation does not extend throughout the tube. Simultaneous operation of the quadrature-speaker set and the axial-speaker was observed to produce considerably enhanced mixing compared to operation of the quadrature-speaker set alone. Mixing experiments using both types of speakers were free of the longitudinal powder drift observed using axial-speakers alone. Vigorous powder mixing was obtained in the sphere for many normal modes; however, in no case was the powder observed to fill the sphere entirely. Theoretical analysis indicated that mixing under steady conditions cannot fill more than a hemisphere except under very unusual conditions. Premixing in a hemisphere may be satisfactory; otherwise, complete mixing in microgravity might be possible by operating the speaker in short bursts. A general conclusion is that acoustic transients are more likely to produce good mixing than steady state conditions. The reason is that in steady conditions, flow structures like nodal planes are possible and often even unavoidable. These tend to separate the mixing region into cells across which powder cannot be transferred. In contrast, transients not only are free of such structures, they also have the characteristics, desirable for mixing, of randomness and disorder. This conclusion is corroborated by mixing experiments using axial waves.

17. Key Words (Suggested by Author(s))	18. Distribution Statement
Acoustic streaming; Acoustic mixing; Particle mixing; Particle clouds; Particle combustion; Particle mixture	Unclassified – Unlimited Subject Category 71

19. Security Classif. (of this report)	20. Security Classif. (of this page)	21. No. of pages	22. Price*
Unclassified	Unclassified	154	A04

*For sale by the National Technical Information Service, Springfield, Virginia 22161